To the Graduate Council:

I am submitting herewith a thesis written by Thomas Wyatt Dobson, Jr. entitled "Discrete Frequency Acoustics Correlation for Rectangular Cavities Exposed to High Speed Flows." I have examined the final copy of this thesis for form and content and recommend that it be accepted in partial fulfillment of the requirements for the degree of Master of Science, with a major in Mechanical Engineering.

John E. Caruthers

John E. Caruthers, Major Professor

We have read this thesis
and recommend its acceptance:

Accepted for the Council:

Vice Provost
and Dean of The Graduate School

STATEMENT OF PERMISSION TO USE

In presenting this thesis in partial fulfillment of the requirements for a Master's degree at The University of Tennessee, Knoxville, I agree that the Library shall make it available to borrowers under rules of the Library. Brief quotations from this thesis are allowable without special permission, provided that accurate acknowledgment of the source is made.

Permission for extensive quotation from or reproduction of this thesis may be granted by my major professor, or in his absence, by the Head of Interlibrary Services when, in the opinion of either, the proposed use of the material is for scholarly purposes. Any copying or use of the material in this thesis for financial gain shall not be allowed without my written permission.

Signature Thomas Wyatt Dobson Jr.

Date December 1990

DISCRETE FREQUENCY ACOUSTICS CORRELATION FOR RECTANGULAR CAVITIES EXPOSED TO HIGH SPEED FLOWS

A Thesis

Presented for the

Master of Science

Degree

The University of Tennessee, Knoxville

Thomas Wyatt Dobson, Jr.

December 1990

ACKNOWLEDGMENTS

The author wishes to thank the many people who gave advice, time, and support in the preparation of this thesis. In particular, he wishes to thank his wife, Leigh Ann, for her encouragement.

ABSTRACT

Engineers and scientists at the Arnold Engineering Development Center (AEDC), National Aeronautics and Space Administration (NASA), Wright-Patterson Air Force Base, the Royal Aircraft Establishment, and others have been studying flow-induced pressure oscillations in cavities (for more than four decades) to establish a basis for an analytical frequency prediction technique. In the present study, a variable-depth rectangular cavity was exposed to a tangential flow over the cavity in the Mach number range from 0.6 to 5.0. Spectral data were studied at various locations within the cavity to gain insight on broadband and resonant response characteristics of the cavity. Based on the data, the Rossiter scheme for predicting resonant frequencies was modified and extended to the higher Mach number of this study to enhance the prediction technique. Potential problems arise when the assumptions used in the cavity flow model are invalidated by physical phenomena such as a coupling of the cavity multidimensional modes and cavity edge tones.

TABLE OF CONTENTS

CHAPTER		PAGE
I	INTRODUCTION	1
II.	THEORETICAL BACKGROUND	4
	Historical Review	4
	Rossiter's Model	11
III.	EQUIPMENT AND PROCEDURES	17
IV.	RESULTS	24
	Boundary Layer Assessment	24
	Cavity Modal Frequencies	24
	Error Analysis	44
V.	CONCLUSIONS AND RECOMMENDATIONS	53
LIST OF REFERENCES		55
APPENDICES		58
A.	CAVITY RESPONSE PLOTS FOR A LENGTH-TO-DEPTH RATIO OF 4.5	59
B.	CAVITY RESPONSE PLOTS FOR A LENGTH-TO-DEPTH RATIO OF 9.0	79
VITA		99

LIST OF FIGURES

FIGURE		PAGE
1.	Rossiter's Frequency of Periodic Fluctuations That Lie on a Family of Curves [3]	5
2.	Rossiter's Simplified Model of Flow Over a Cavity [3]	8
3.	Schematic of a Cavity Oscillation Cycle [6]	12
4.	Comparison of Measured and Predicted Modal Frequencies [13]	13
5.	Nondimensional Resonant Frequencies as a Function of Mach Number - Implementation of Modified Rossiter Equation [5]	15
6.	Nondimensional Resonant Frequencies as a Function of Mach Number with Additional Data Added	16
7.	Generic Flat-Plate Cavity Model [13]	20
8.	Pressure Transducer Locations	21
9.	Characteristic Centerline Acoustic Spectra [13]	23
10.	Nondimensional Resonant Frequencies as a Function of Mach Number for the Length-to-Depth Ratio of 4.5	30
11.	Nondimensional Resonant Frequencies as a Function of Mach Number for the Length-to-Depth Ratio of 9.0	34
12.	Rossiter's α Term as a Function of Length-to-Depth Ratio [13]	41

FIGURE PAGE

13. Nondimensional Resonant Frequencies as a Function of Mach Number - For an Optimum α 42

14. Error Band for the Current Data 45

NOMENCLATURE

a	Free-stream stagnation speed of sound (Eq. 4)
c	Mean speed of sound in cavity, ft/s
D	Depth of the cavity (feet)
f	Frequency (Hz)
Ki	Kulite®
k	Fraction of free-stream speed U at which vortices travel over the cavity (Eq. 3)
k_v	Vortex velocity/free-stream velocity (Eq. 5)
L	Length of the cavity (feet)
ℓ	Length of the model leading edge to the cavity lip (feet)
L/D	Nondimensional length-to-depth cavity ratio
M	Mach number in the free stream
m	Integer mode number (= $m_a + m_v$)
m_a	Number of complete wavelengths of acoustic radiation involved in the generation of cavity oscillation, Equation (4)
m_v	Number of complete wavelengths of the vortex motion involved in the generation of cavity oscillation, Equation (3)
MRE	Modified Rossiter Equation
P_{rms}	Root mean square pressure, psi, (Eq. 6)
P_{ref}	Reference pressure, 2.9×10^{-9}, psi, (Eq. 6)
PSD	Power spectral density
PT	Total pressure, psi
Q-INF	Free-stream dynamic pressure, psi
Re	Reynolds number, per foot
SPL	Sound pressure level, db, referenced to 2.9×10^{-9}, psi

St	Strouhal number (fL/U)
TT	Total temperature, °R
t'	Time at which the acoustic wave reaches forward bulkhead, sec
U,V-INF	Free-stream velocity, ft/sec
W	Width of the cavity, feet
W/L	Nondimensional width-to-length cavity ratio
X	Distance from the leading edge of the cavity opening, feet
x	Distance from the leading edge of the plate, ft, (Eq. 7)
z_j	Variable, $z_j = St_j - m\,\Psi_j$, (Eq. 10)
α	Phase delay parameter
δ	Turbulent boundary-layer thickness, in.
$\varepsilon(\ )$	Uncertainty measurement
γ	Ratio of specific heats = 1.4, (Eq. 5)
Ψ_j	Variable $\Psi_i = \dfrac{1}{\left[\dfrac{M}{\left(1 + \frac{\gamma-1}{2} M^2\right)} + 1.75\right]}$, (Eq. 8)

CHAPTER I

INTRODUCTION

It is generally accepted that increases in aircraft performance can be realized through internal carriage of stores. However, when doors are opened in flight to expose the storage cavity, an aeroacoustic environment is created that can raise additional concerns. For instance, cavity aeroacoustics may stimulate adverse aircraft/store structural responses, and might also influence crew performance. During the past forty years, a number of investigators have studied the aeroacoustic phenomena associated with pressure oscillations excited by air flowing over open cavities [1-13][1]. Considerable information has been compiled about the aeroacoustic phenomena in cavities, but it is not completely understood because of the complex nature of the problem.

Unsteady flow characteristics over open cavities depend primarily on cavity geometry, the approaching boundary layer, and aerodynamic parameters [2, 3, 4, 5, 12, and 13]. Clearly the magnitude and the frequency of the cavity pressure fluctuations are influenced by a balance between the available energy in the free stream, the energy dissipated within the cavity, and the acoustic radiation from the cavity. Specifically, the frequencies associated with the cavity acoustics are a function of the cavity geometry (L/D and W/D), the approaching

---

[1]Numbers in brackets refer to similarly numbered references in the List of References.

boundary layer (δ/L), flow speed (M), the location in the cavity (X/L) [12], and Reynolds number, although only slightly.

Most of the investigations to date have been concerned with understanding the aeroacoustic phenomena and the mechanisms which control them. Heller, Holmes, and Covert [5] give a brief description of the various investigations and flow models, but no single approach provided a satisfactory correlation of all geometric and measured aerodynamic parameters. Rossiter's model has been generally accepted because it was able to predict modal frequencies with acceptable accuracy for a Mach number range of 0.4 to 1.2 [3]. Plumblee's model offered a prediction scheme for modal frequencies which produced fair results [2]. East [4] verified Rossiter's model with experimental data for the same Mach number range, and in addition using Plumblee's and Rossiter's results offered a unified view of the physical mechanisms involved in cavity tone generation [4,12]. Heller, Holmes, and Covert [5] suggested the modified Rossiter model to extend the frequency prediction method out to Mach numbers 2 and 3 which produced acceptable results for the data.

Some challenges exist in formulating an inclusive math model that will predict both the response of a cavity at the higher Mach numbers ($M > 2.0$) as pointed out by Dix [13] and the response of a deep or shallow cavity as pointed out by Heller, Holmes, and Covert [5], and Smith and Shaw [7]. The purpose of the study is to further test the validity of the Rossiter frequency prediction model, particularly at high Mach numbers, and to add to the current Mach number data base to

include the Mach numbers 2.75, 3.50, and 5.00 for cavity L/D's of 4.5 and 9.0.

CHAPTER II

THEORETICAL BACKGROUND

I. HISTORICAL REVIEW

It was suggested by Plumblee [2] that the forcing function mechanism causing the acoustic response of deep cavities (L/D < 2) was the upstream turbulent boundary layer. A problem occurs with Plumblee's model in that a laminar boundary layer is sometimes capable of initiating cavity responses more powerful than a turbulent boundary layer (Krishnamurty [1]). It was also suggested by Plumblee that cavity volume was important in determining the modal frequencies of the cavity acoustic response. Finally, Plumblee offers a three-dimensional prediction scheme for the frequencies excited by the oncoming flow, but the scheme provides fair correlation with his data and is somewhat cumbersome to use.

Rossiter [3] used experimental data to derive a model for a frequency-prediction scheme for deep cavities (L/D < 4) based on the amplitude spectra. From the data, a dominant frequency exists (called the fundamental frequency) which changes with Mach number. In addition to the fundamental frequency there exist two or three additional frequencies that are not harmonics of the fundamental frequency. When plotted as a function of Mach number the fundamental and additional frequencies lie on a family of curves as shown in Figure 1 [3]. Rossiter's experimental investigation thus led to the following conclusions concerning the principle characteristics of the periodic

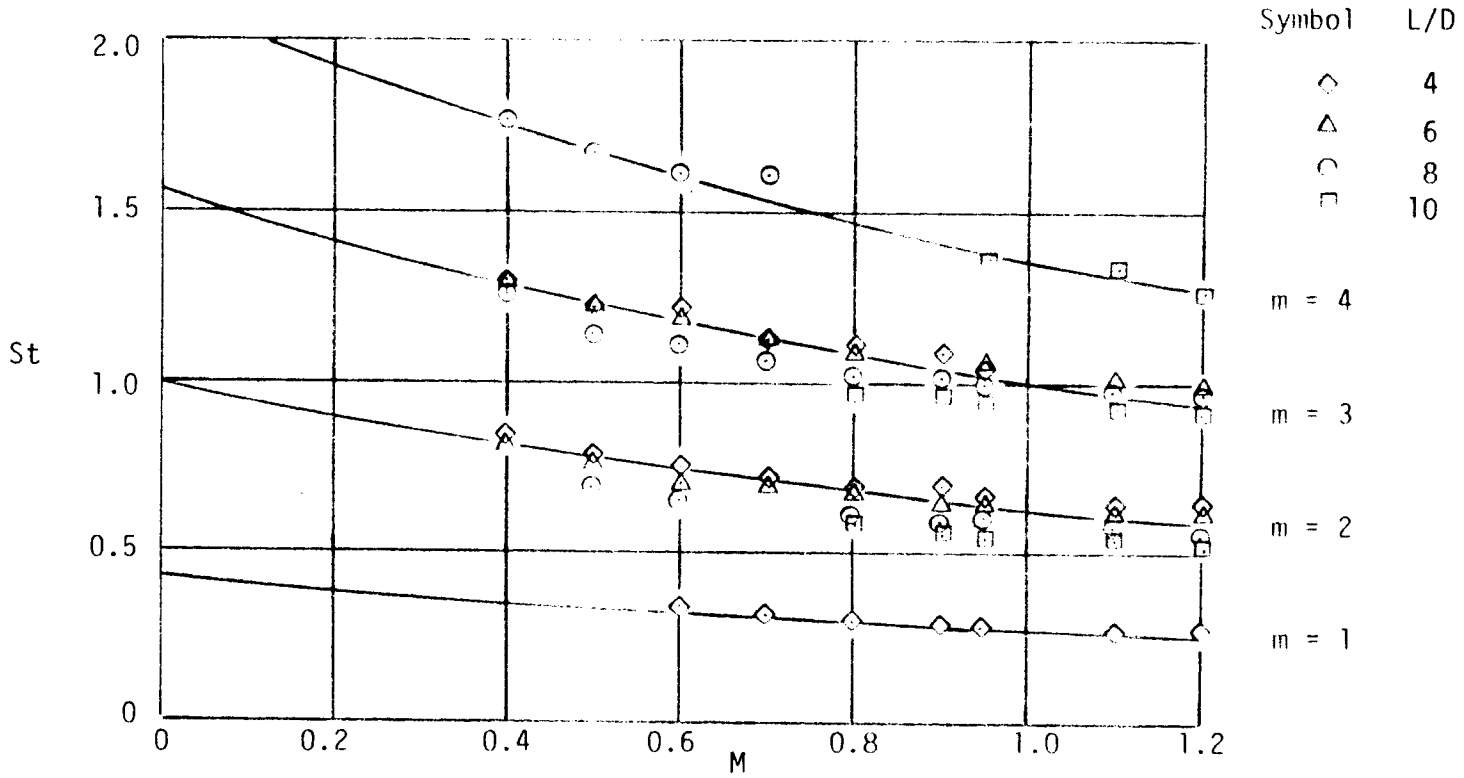


Figure 1. Rossiter's Frequency of Periodic Fluctuations That Lie on a Family of Curves [3]

pressure fluctuations which occur in the cavities: 1) there is a periodic shedding of vortices from the leading edge of the cavity that causes acoustic radiation from the cavity; 2) because of acoustic resonance, a standing wave pattern will sometimes appear in the cavity; 3) pressure fluctuations may contain a number of periodic components, with frequencies in a sequence of

$$(m - a) \tag{1}$$

for the cavity; 4) the frequency of any component is defined by the following equation

$$f\frac{L}{U} = f(M, Re) \tag{2}$$

for a fixed cavity geometry and a fixed boundary layer. Based on these principles, Rossiter envisioned a physical model of the flow phenomena similar to the phenomena producing edge tones, i.e., periodic shedding of vortices from the leading edge of the cavity and an acoustic source at the rear bulkhead. Shedding of the vortices and the acoustic generation produce a number of periodic pressure fluctuations with frequencies in the sequence of Equation (1). Rossiter noted the importance of the cavity geometry (specifically L/D) as a parameter in defining the cavity-response frequencies. Observing that the regular shedding of vortices found in the flow over a cavity seemed to be coupled with the acoustic radiation, Rossiter suggested an inter-dependent, or feedback phenomenon: vortex shedding could be initiated

by acoustic radiation, which in turn could be generated by the passage of the vortex over the downstream bulkhead lip. Rossiter's concept is illustrated in Figure 2 [3]. The average speed of the vortices was thought to be some fraction of the free-stream velocity (k). Assuming that the temperature of the fluid in the cavity was the same as the free-stream static temperature, Rossiter's model is simply derived by equating the arrival time of the acoustic signal to the instant of vortex generation at the leading edge. This implies that

$$m_v \lambda_v = L + \alpha_v \lambda_v + kUt' \tag{3}$$

and since

$$L = m_a a_a + ct'. \tag{4}$$

Rearranging yields

$$St = \frac{fL}{U} = \frac{(m - \alpha)}{\left(\frac{1}{k} + M\right)}. \tag{5}$$

The constant α was the phase difference assumed to exist between the arrival of the acoustic wave at the upstream bulkhead and the subsequent shedding of the vortex at the leading edge. Rossiter assumed the phase difference was a function of the cavity L/D. Rossiter's values for α are listed in Table 1.

East [4] followed Plumblee's work and observed for deep cavities at low subsonic Mach numbers that resonant conditions exist when the dominant frequency of the acoustic response of the cavity equals the

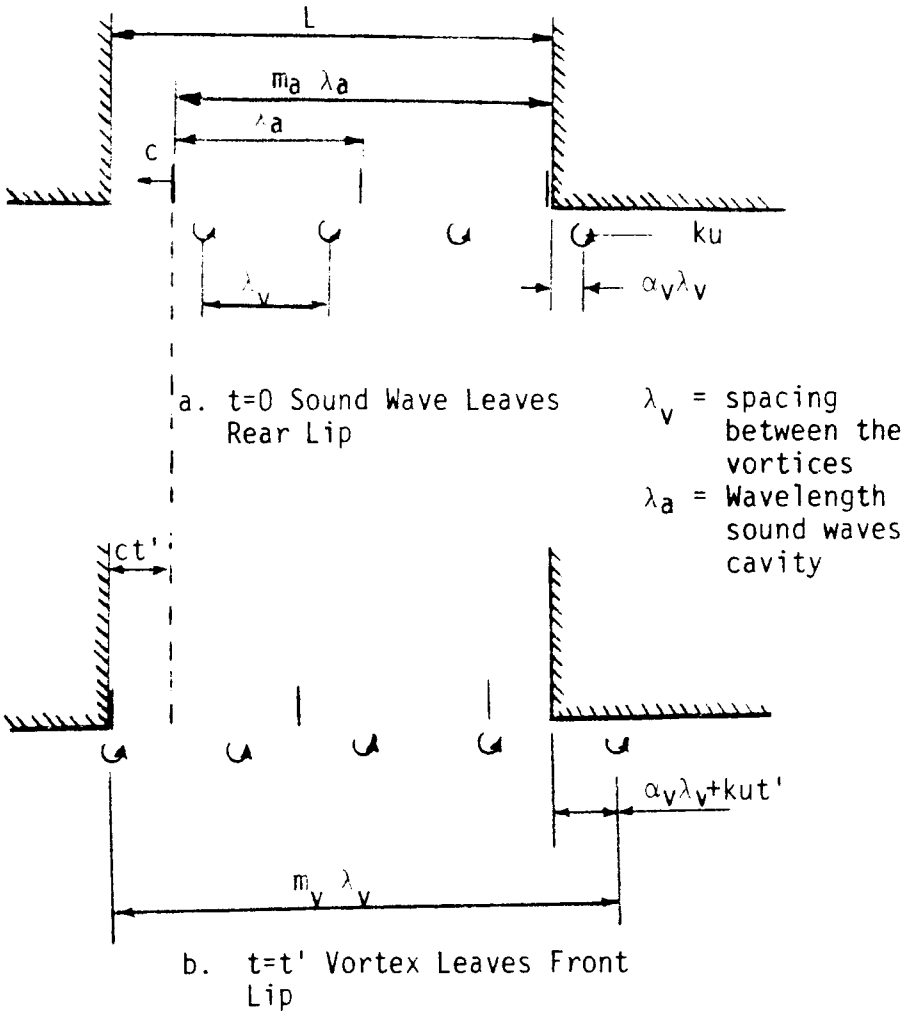


Figure 2. Rossiter's Simplified Model of Flow Over a Cavity [3]

Table 1. Rossiter's Values for α Averaged Over the Speed Range

L/D	α
4	0.25
6	0.38
8	0.54
10	0.58

dominant frequency of the shear layer feedback system. East calls this feedback system a "doubly-tuned amplification" and presents an empirical relationship for resonant conditions,

$$\frac{fL}{a} = \frac{0.25}{\left[1 + 0.65\,(L/D)^{0.75}\right]}, \tag{6}$$

East, aware of Rossiter's suggestion of an acoustic feedback mechanism, proceeded in confirming Rossiter's model, East observed that the cavity excitation frequency was indeed related to the vortex shedding (East's "vortex convection speed"), but further, that the frequency of the vortex shedding speed was affected by the thickness of the approaching boundary layer. Based on Equation (6), East determined the unknown streamwise vortex-convection speed to range from thirty-five to sixty percent of the free-stream velocity. East looked at the first mode assuming a long pipe closed at one end which allows L/D to approach zero resulting in the Strouhal number equal to 0.25 which is the classical organ pipe effect.

Heller and Bliss [6] demonstrated that the expansion of an approaching supersonic flow into the cavity generated pressure waves that travel to the downstream bulkhead and reflect. At the downstream bulkhead, fluid is forced from the cavity by the increase in pressure, and the lip shock detaches. When the pressure is reduced by the reflection and mass ejection, the lip shock reattaches. The reflection wave propagates forward and forces the shear layer away from the

cavity. Expansion occurs at the leading edge of the cavity and the cycle repeats. The process is illustrated in Figure 3 [6].

II. ROSSITER'S MODEL

Rossiter's data and correlation are illustrated in Figure 1, page 5. The correlation is good for the experimental data, which were recorded in the range of Mach numbers from 0.4 to 1.20. Dix [13] points out that for Mach numbers greater than 1.2, Rossiter's model does not provide a good frequency prediction, Figure 4. Rossiter's model fails in the assumption that the fluid temperature in the cavity is the same as the free-stream static temperature, i.e., a recovery factor of zero. Heller, Holmes, and Covert [6] suggest a modified Rossiter equation (MRE):

$$St = \frac{fL}{U} = \frac{(m - \alpha)}{\left[\frac{M}{\left(1 + \frac{\gamma - 1}{2} M^2\right)^{1/2}} + \frac{1}{k_v} \right]} \qquad (7)$$

based on an observation that the temperature of the fluid in the cavity approaches the free-stream stagnation temperature. This becomes more important as Mach number increases. Smith and Shaw [7] compare flight data and experimental data that verify the Heller, Holmes, and Covert suggestion. The consequence of Rossiter's assumption of zero recovery factor is that the speed of sound in the cavity is assumed equal to the speed of sound in the free stream. Clearly, the error involved in

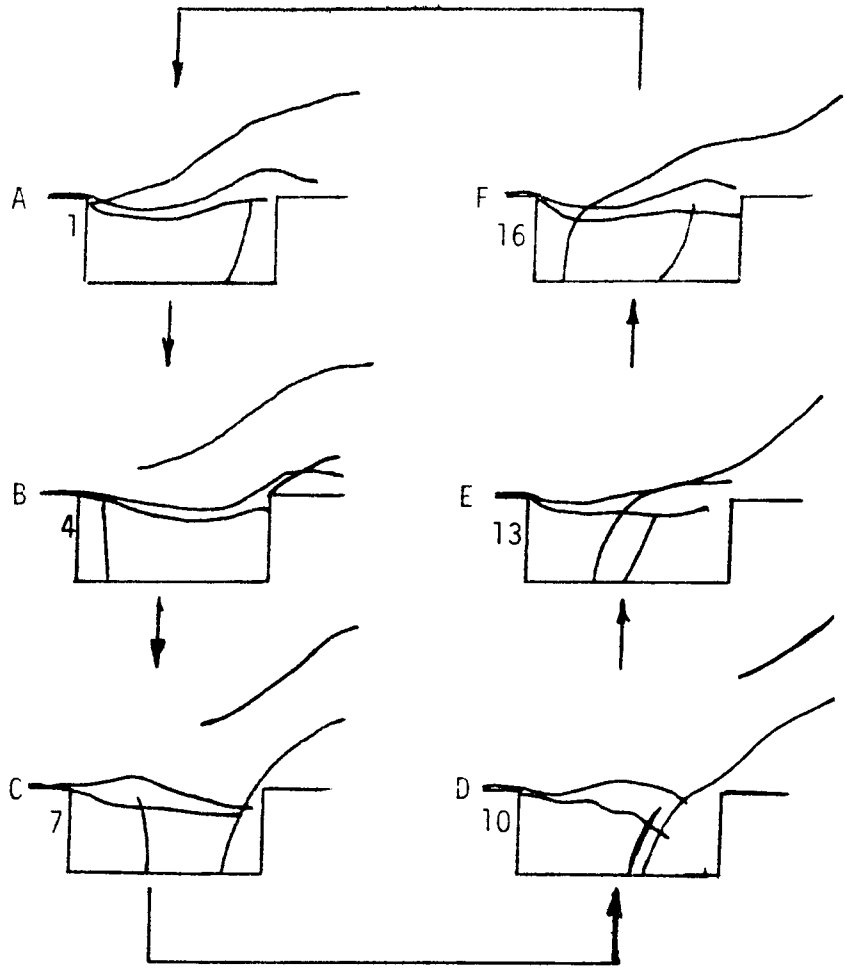
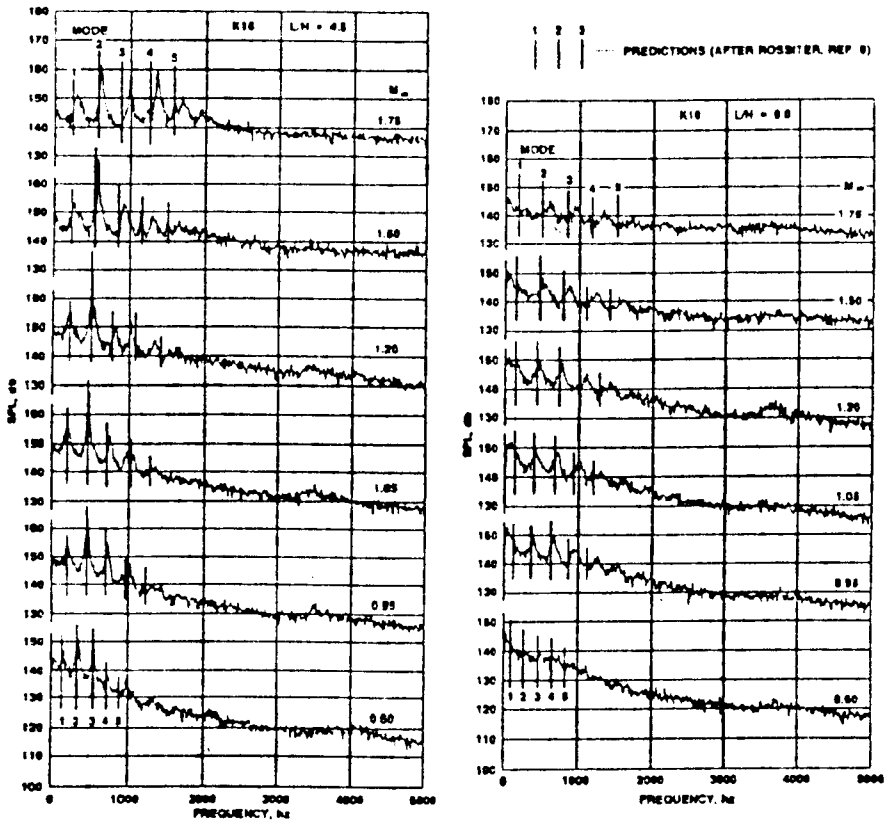


Figure 3. Schematic of a Cavity Oscillation Cycle [6]



a. Cavity L/H = 4.5, transducer K16

b. Cavity L/H = 9.0, transducer K16

(For transducer K16 location, refer to Figure 8)

Figure 4. Comparison of Measured and Predicted Modal Frequencies [13]

assuming the wrong temperature increases with Mach number. Illustrated in Figure 5 [5] are data compiled by Heller, Holmes, and Covert using the MRE with $\alpha = 0.25$ and $k_V = 0.57$. Note that data for Mach numbers 2 and 3 have been added to support the stagnation temperature suggestion. The MRE appears to represent an appropriate model of the discrete frequency response in the deep cavity. When the data for Mach numbers of 2.75, 3.51, and 5.04 are included, as shown in Figure 6, however, the MRE, Equation (5), does not appear to represent a satisfactory correlation.

Summarizing, it is clear that improvements or extensions should be made to the method currently in favor for predicting modal frequency in cavities, i.e., the MRE Equation (5). Specifically, ranges of cavity geometry and Mach number wider than included in the original data base are not correlated well by MRE. The current study addresses these concerns.

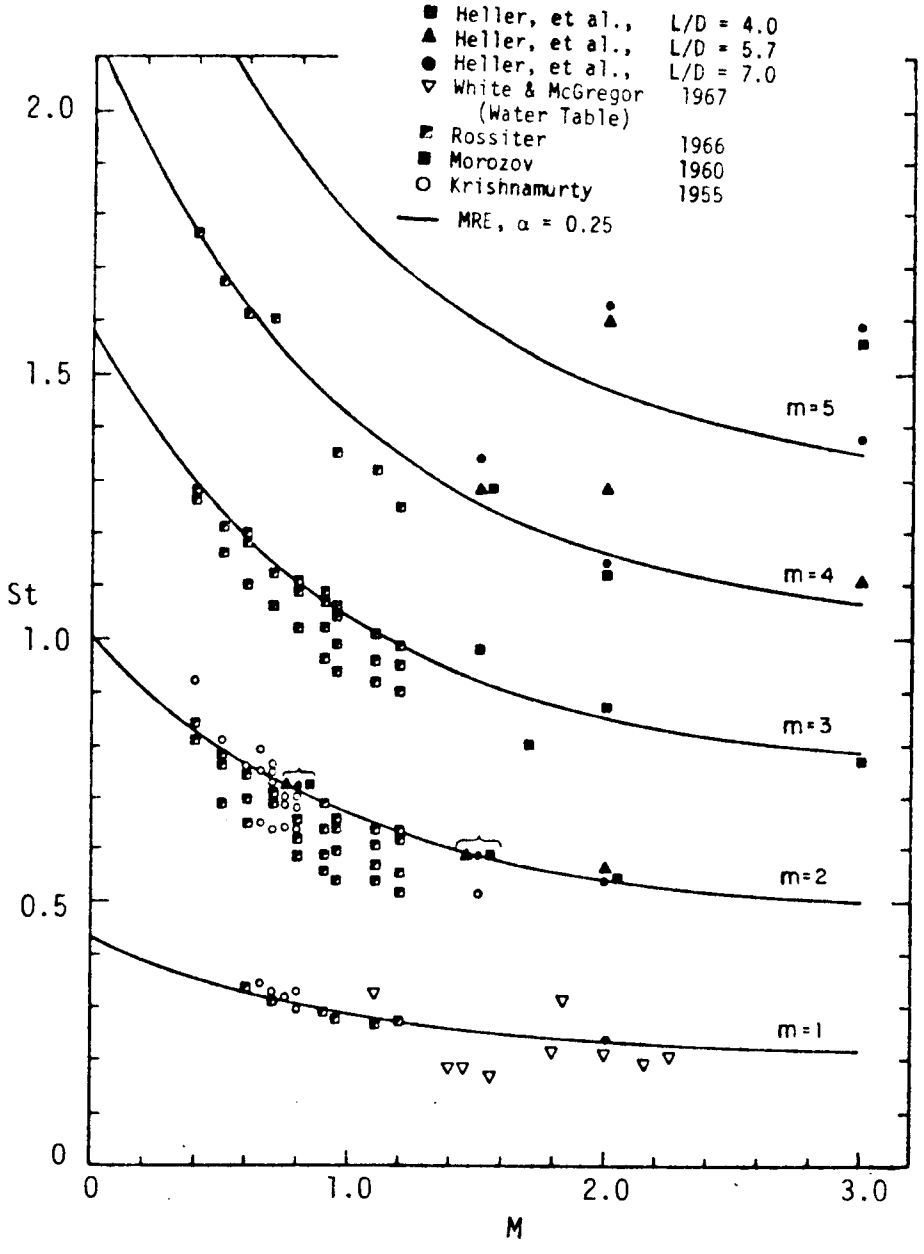


Figure 5. Nondimensional Resonant Frequencies as a Function of Mach Number-Implementation of Modified Rossiter Equation [5]

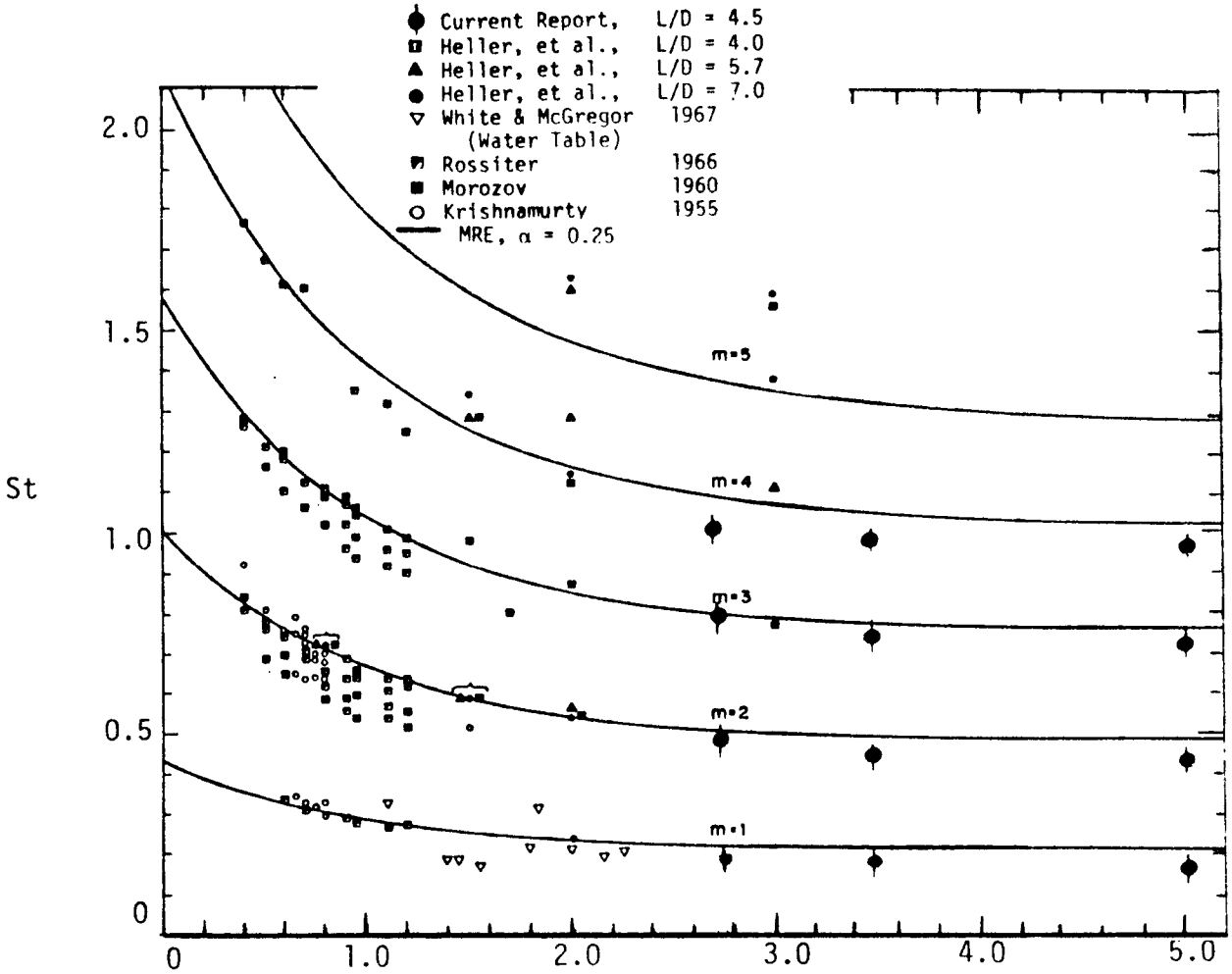


Figure 6. Nondimensional Resonant Frequencies as a Function of Mach Number with Additional Data Added

CHAPTER III

EQUIPMENT AND PROCEDURE

The experimental part of the current study was directed at extending the empty cavity data to higher Mach numbers using the current MRE. Listed in Table 2 are the experimental flow conditions for two different depths, L/D = 4.5 and 9.0, and Mach numbers from 0.6 to 5.00.

A schematic of the cavity model is shown in Figure 7. The cavity was eighteen inches long and four inches wide. The cavity floor could be moved up and down to provide various depths, but only two depths are considered herein, two inches and four inches. Dynamic pressure was measured with Kulite® differential transducers and forty-five locations, Figure 8. Each transducer was rated at ±5 psi, with a maximum allowable differential pressure of 15 psi. The reference pressure port was vented to the static pressure in the instrument housing on the backside of the flat plate, which was approximately equal to the free-stream static pressure. Cavity transducers were sampled simultaneously 10,000 times per second for five seconds. The corresponding time-ordered data were transformed into power spectral density (PSD) plots in the frequency domain using conventional fast Fourier Transform (FFT) techniques. The spectra are shown in Appendices A and B for cavity length-to-depth ratios of 4.5 and 9.0, respectively. Each PSD spectrum was produced by averaging twenty-five ensembles, where each ensemble consisted of 1024 pressure-time samples. All spectral data presented herein have been calculated using the Hanning window.

Table 2. Free-Stream Parameters as Function of Mach Number

a. L/D = 4.5

Mach	PT (psfa)	TT (°R)	Q(psfa)	Re/ft x 10-6
0.60	1895.1	553.7	374.1	3.01
0.75	1207.9	546.7	327.3	2.24
0.85	1199.7	546.7	378.4	2.37
0.90	1209.1	546.7	405.1	2.45
0.95	1466.0	547.7	520.2	3.02
1.00	1201.1	547.7	445.3	2.51
1.05	1443.7	552.7	556.0	3.02
1.10	1197.8	549.7	475.6	2.55
1.20	1399.3	550.7	582.0	2.99
1.30	1200.7	551.7	512.2	2.55
1.40	1216.0	553.7	524.3	2.54
1.50	987.8	556.7	423.8	2.01
1.60	1213.6	553.7	511.6	2.42
1.75	1211.3	552.7	487.5	2.31
1.90	1210.9	551.7	456.5	2.18
2.00	1874.2	581.7	670.7	3.01
2.75	2617.7	580.7	551.3	2.90
3.50	4005.8	580.7	446.3	2.97
5.04	9118.7	600.7	292.5	3.00

Table 2. Concluded

b. L/D = 9.0

Mach	PT (psfa)	TT (°R)	Q(psfa)	Re/ft x 10^{-6}
0.60	1243.6	553.7	245.6	1.97
0.75	1201.3	548.7	329.9	2.23
0.85	1188.7	547.7	375.0	2.34
0.90	1196.3	548.7	400.7	2.41
0.95	992.3	550.7	350.7	2.03
1.00	1184.5	549.7	440.5	2.47
1.05	1451.7	556.7	558.3	3.01
1.10	1201.7	550.7	476.9	2.54
1.15	1201.7	554.7	489.4	2.53
1.20	456.5	547.7	189.8	0.98
1.30	1196.4	553.7	511.3	2.52
1.50	1201.3	557.6	515.4	2.44
1.75	1199.1	556.6	483.0	2.26
2.00	1891.8	578.7	677.0	3.06
2.25	2110.8	580.7	646.9	3.02
2.50	2375.8	580.7	608.4	3.00
2.75	2613.8	579.7	550.4	2.90
3.50	4015.8	581.7	447.7	2.97
5.04	9156.4	603.7	293.7	2.99

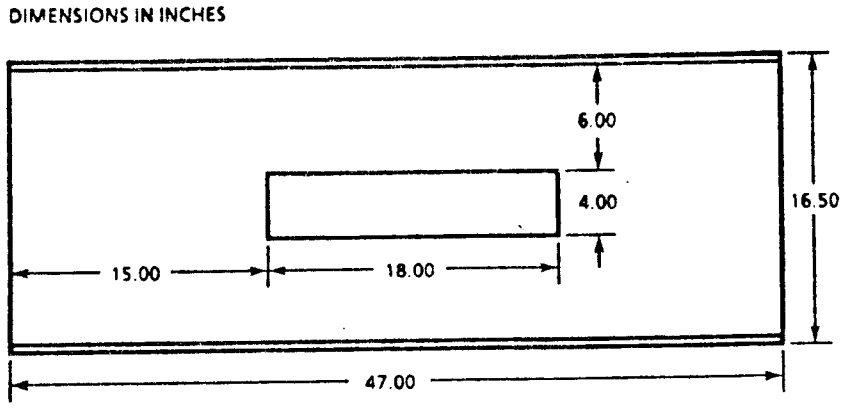


Figure 7. Generic Flat-Plate Cavity Model [13]

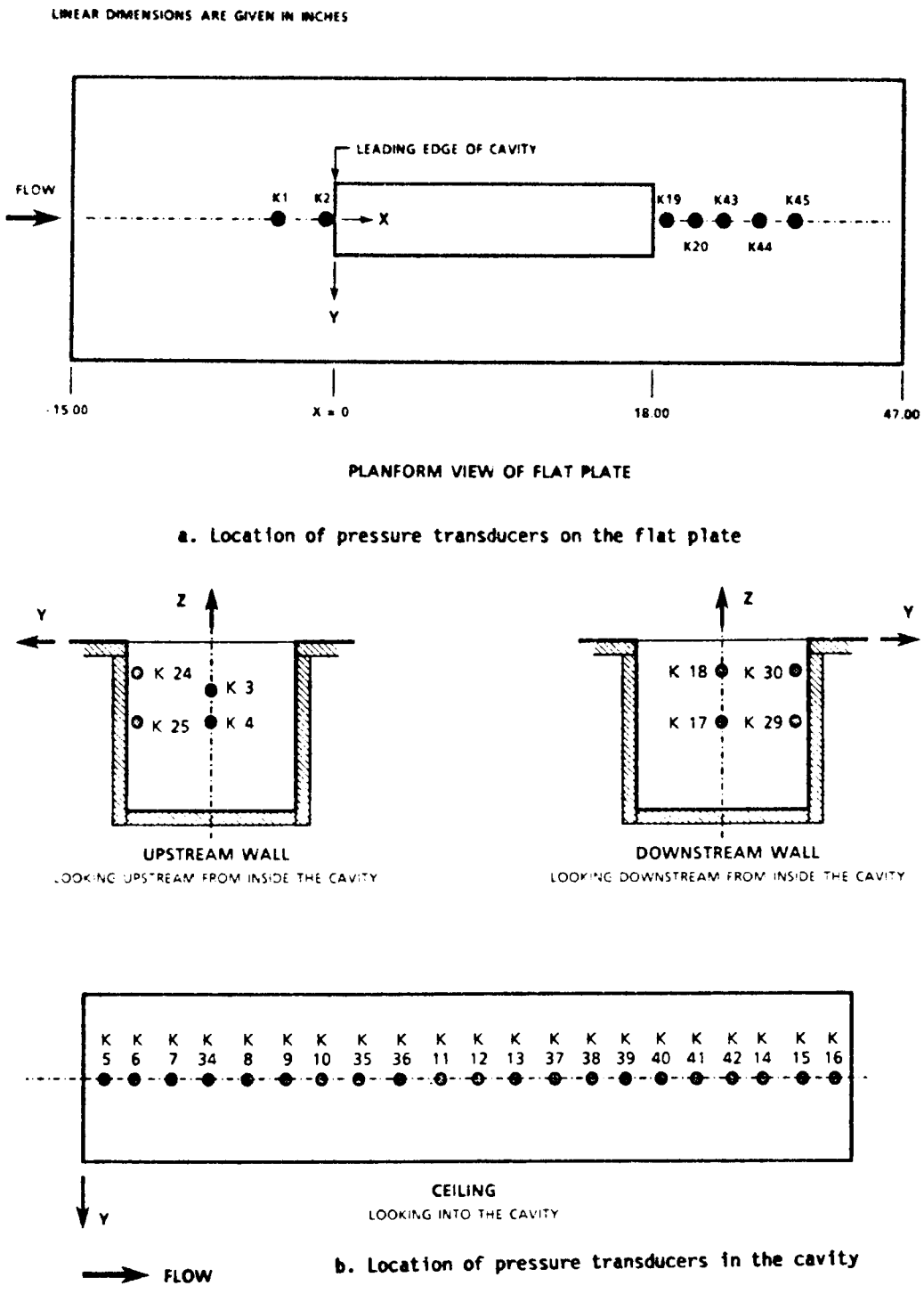


Figure 8. Pressure Transducer Locations

Sound pressure level (SPL) was calculated in the following manner:

$$SPL = 20\ log\left(\frac{P_{rms}}{P_{ref}}\right) \approx 20\ log\left(\frac{P_{rms}}{2.9 \times 10^{-9}}\right) \tag{8}$$

where the reference pressure, P_{ref}, was the international threshold of audibility. The output of transducer K16 was used throughout as a criterion. Transducer K16 was located in the region immediately upstream of the downstream bulkhead where the highest noise level in the cavity existed, as illustrated in Figure 9 [13].

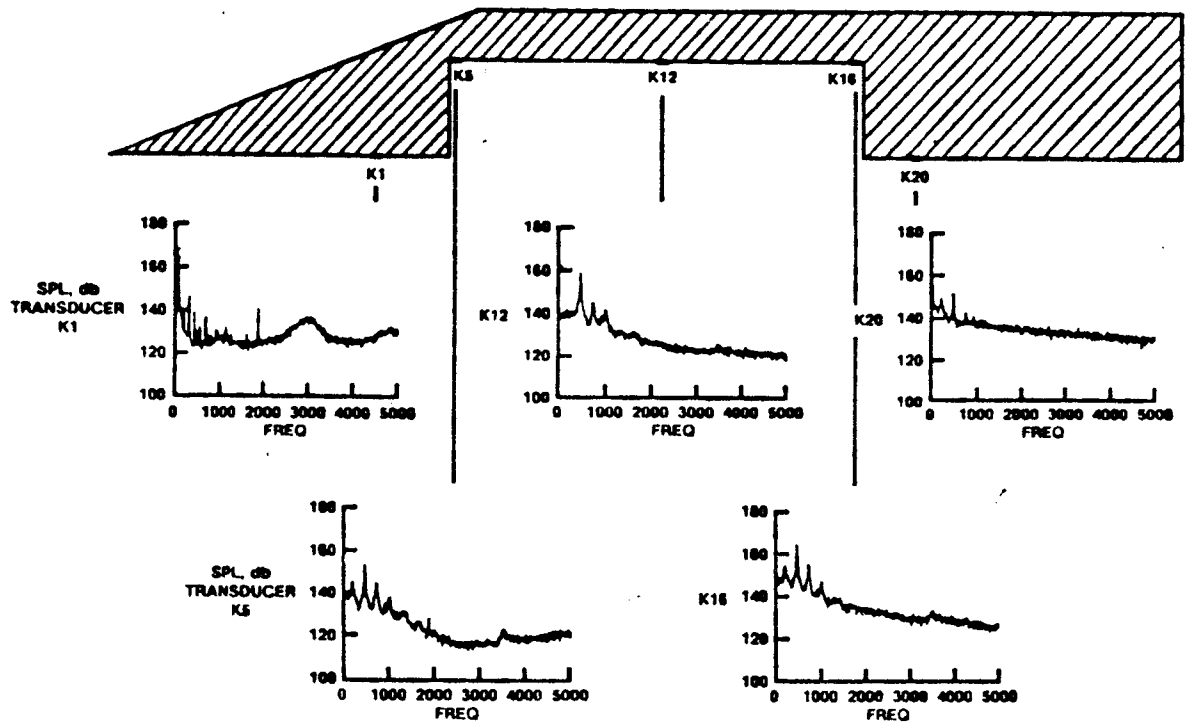


Figure 9. Characteristic Centerline Acoustic Spectra [13]

CHAPTER IV

RESULTS

I. BOUNDARY LAYER ASSESSMENT

Following the suggestions of Plumblee, Rossiter, East, Heller, Holmes, and Covert [2-5] that the boundary layer could be an important determinant of cavity aeroacoustic response, an assessment of boundary layer variation in the current experiment was made. Using the conventional one-seventh power law approximation for fully developed turbulent boundary layers [14]

$$\delta \approx 0.16\, x\, Re_x^{-1/7}, \tag{9}$$

only a ten-percent change in the boundary layer thickness existed within the current data base. Consequently, the effect of boundary layer variations on the cavity aeroacoustics of this study are considered to be small.

II. CAVITY MODAL FREQUENCIES

Data from the current study were substituted into the MRE in an attempt to expand the data of [1-5]. Discrete resonant frequencies were determined from the spectral data in Appendices A and B by picking the modal peaks (where possible) and reading the corresponding frequencies. The dashed lines on the plots in Appendices A and B correspond to the discrete frequencies for the first four modes and are listed in

Table 3. As previously mentioned in Chapter II, Section II, and illustrated in Figure 6, page 16, the additional Mach number data do not satisfactorily correlate. If the α term in the MRE is allowed to vary with mode number, much better correlation exists for the first four modes. The correlation can be seen in plots of Strouhal number as a function of Mach number for the two different cavities, L/D = 4.5 and 9.0, Figures 10 and 11, respectively. The constant k_v was held at 0.57 as suggested by Smith and Shaw [7]. From Figures 10 and 11, the current data are between the curves calculated using the MRE. A best-fit curve was determined to match the data to the predicted curves, and the corresponding α values are listed in Table 4. Also listed in Table 4 are Rossiter's α values which have been allowed to vary with mode number. There is excellent agreement between these variable Rossiter α values and the current study α values.

The best fit was determined using a regression analysis technique. From Equation (5) let:

$$\Psi = \frac{1}{\left[\frac{M}{\left(1 + \frac{\gamma - 1}{2} M^2\right)^{1/2}} + 1.75\right]} \tag{10}$$

$$E_i = St_i^m - St_i^p \tag{11}$$

Table 3. Nondimensional Resonant Frequencies for the First Four Modes

a. Mode 1

L/D = 4.5			L/D = 9.0		
M	Freq (Hz)	St	M	Freq (Hz)	St
0.60	146.484	0.331	0.60	---	---
0.75	165.781	0.305	0.75	---	---
0.85	175.313	0.289	0.85	---	---
0.90	185.547	0.291	0.90	---	---
0.95	185.547	0.278	0.95	---	---
1.00	195.313	0.279	1.00	---	---
1.05	200.200	0.275	1.05	---	---
1.10	205.078	0.271	1.10	---	---
1.20	214.844	0.269	1.15	---	---
1.30	224.375	0.261	1.20	---	---
1.40	243.906	0.267	1.30	---	---
1.50	244.141	0.253	1.50	---	---
1.60	248.203	0.240	1.75	---	---
1.75	257.465	0.243	2.00	---	---
1.90	273.203	0.246	2.25	---	---
2.00	282.969	0.240	2.50	---	---
2.75	300.859	0.220	2.75	---	---
3.50	302.734	0.204	3.50	---	---
5.04	315.141	0.193	5.04	---	---

Table 3. Continued

b. Mode 2

L/D = 4.5			L/D = 9.0		
M	Freq (Hz)	St	M	Freq (Hz)	St
0.60	341.797	0.771	0.60	297.969	0.658
0.75	396.141	0.729	0.75	---	---
0.85	419.922	0.691	0.85	364.720	0.600
0.90	439.219	0.689	0.90	380.859	0.596
0.95	448.984	0.674	0.95	390.625	0.582
1.00	468.516	0.669	1.00	410.156	0.583
1.05	478.546	0.658	1.05	410.156	0.564
1.10	490.047	0.648	1.10	430.859	0.569
1.20	507.578	0.628	1.15	433.156	0.555
1.30	527.109	0.613	1.20	439.453	0.543
1.40	546.875	0.599	1.30	468.750	0.540
1.50	576.172	0.598	1.50	488.047	0.508
1.60	595.703	0.576	1.75	495.703	0.561
1.75	605.234	0.571	2.00	562.528	0.480
1.90	615.000	0.553	2.25	---	---
2.00	644.063	0.547	2.50	---	---
2.75	686.442	0.502	2.75	---	---
3.50	712.656	0.480	3.50	---	---
5.04	744.690	0.455	5.04	---	---

Table 3. Continued

c. Mode 3

L/D = 4.5			L/D = 9.0		
M	Freq (Hz)	St	M	Freq (Hz)	St
0.60	546.875	1.234	0.60	498.047	1.119
0.75	644.531	1.187	0.75	582.701	1.061
0.85	683.594	1.126	0.85	634.766	1.044
0.90	693.359	1.087	0.90	652.717	1.022
0.95	732.422	1.099	0.95	673.828	1.006
1.00	751.953	1.074	1.00	693.359	0.986
1.05	771.797	1.061	1.05	703.125	0.967
1.10	791.016	1.046	1.10	732.422	0.967
1.20	830.078	1.027	1.15	748.817	0.951
1.30	859.375	1.000	1.20	771.484	0.954
1.40	888.438	0.973	1.30	791.016	0.012
1.50	927.734	0.963	1.50	859.375	0.894
1.60	957.266	0.926	1.75	907.734	0.843
1.75	976.234	0.922	2.00	---	---
1.90	1015.390	0.913	2.25	---	---
2.00	1034.450	0.880	2.50	---	---
2.75	1132.810	0.829	2.75	---	---
3.50	1171.881	0.789	3.50	---	---
5.04	1227.803	0.750	5.04	---	---

Table 3. Concluded

c. Mode 4

L/D = 4.5			L/D = 9.0		
M	Freq (Hz)	St	M	Freq (Hz)	St
0.60	751.953	1.696	0.60	751.953	1.690
0.75	869.563	1.600	0.75	781.250	1.423
0.85	947.563	1.560	0.85	869.141	1.430
0.90	976.563	1.531	0.90	947.266	1.483
0.95	1005.862	1.510	0.95	966.797	1.442
1.00	1015.161	1.436	1.00	986.328	1.402
1.05	1015.63	1.396	1.05	1005.86	1.384
1.10	1015.63	1.343	1.10	1015.63	1.341
1.20	1025.394	1.269	1.15	1025.39	1.302
1.30	1064.450	1.238	1.20	1074.22	1.328
1.40	1103.522	1.209	1.30	1142.58	1.318
1.50	1152.341	1.196	1.50	1142.58	1.189
1.60	1318.362	1.275	1.75	1210.94	1.140
1.75	1347.659	1.272	2.00	1328.13	1.133
1.90	1476.948	1.329	2.25	1015.63	0.813
2.00	1425.551	1.211	2.50	---	---
2.75	1503.909	1.100	2.75	---	---
3.50	1513.671	1.019	3.50	---	---
5.04	1552.733	0.948	5.04	---	---

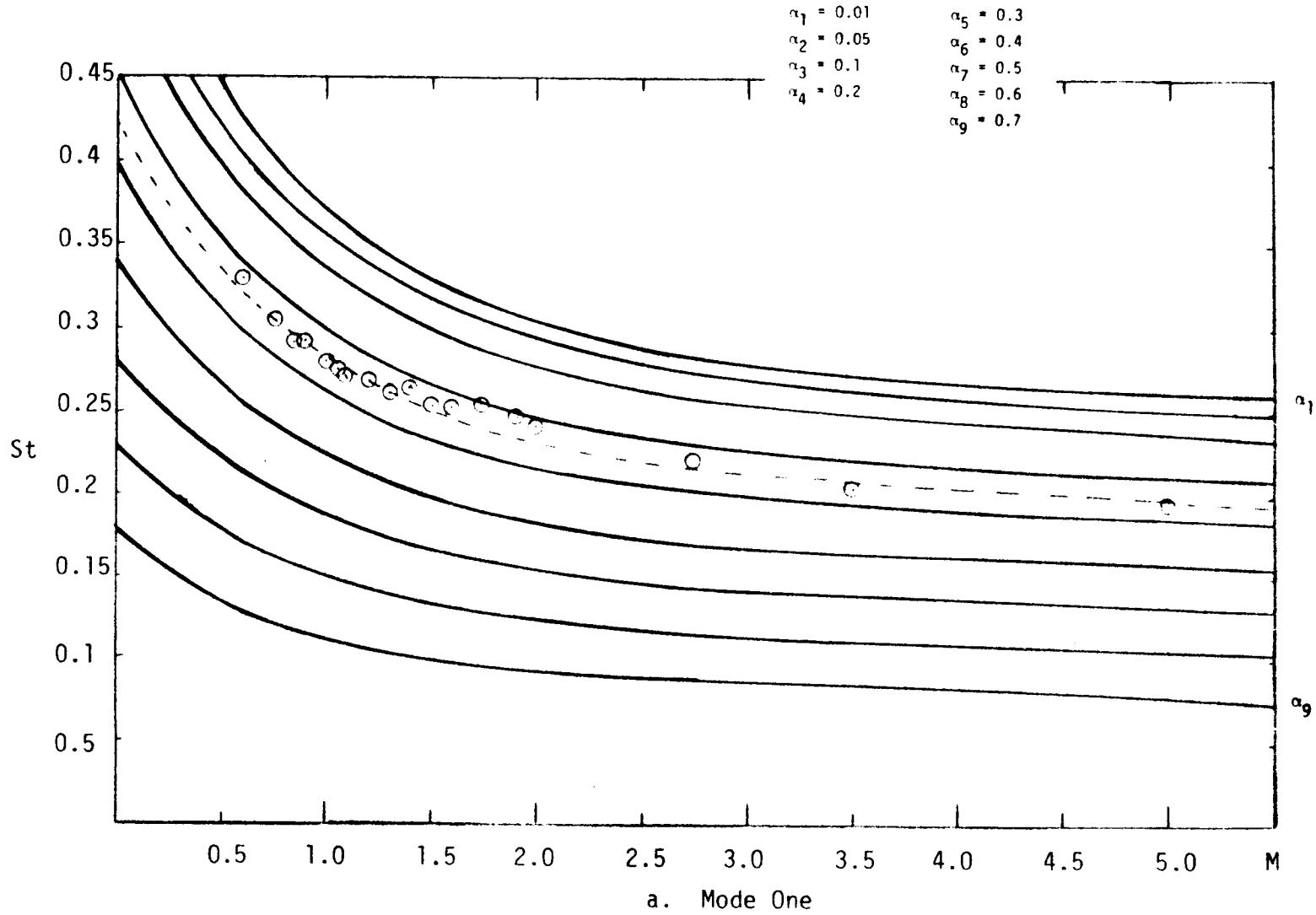
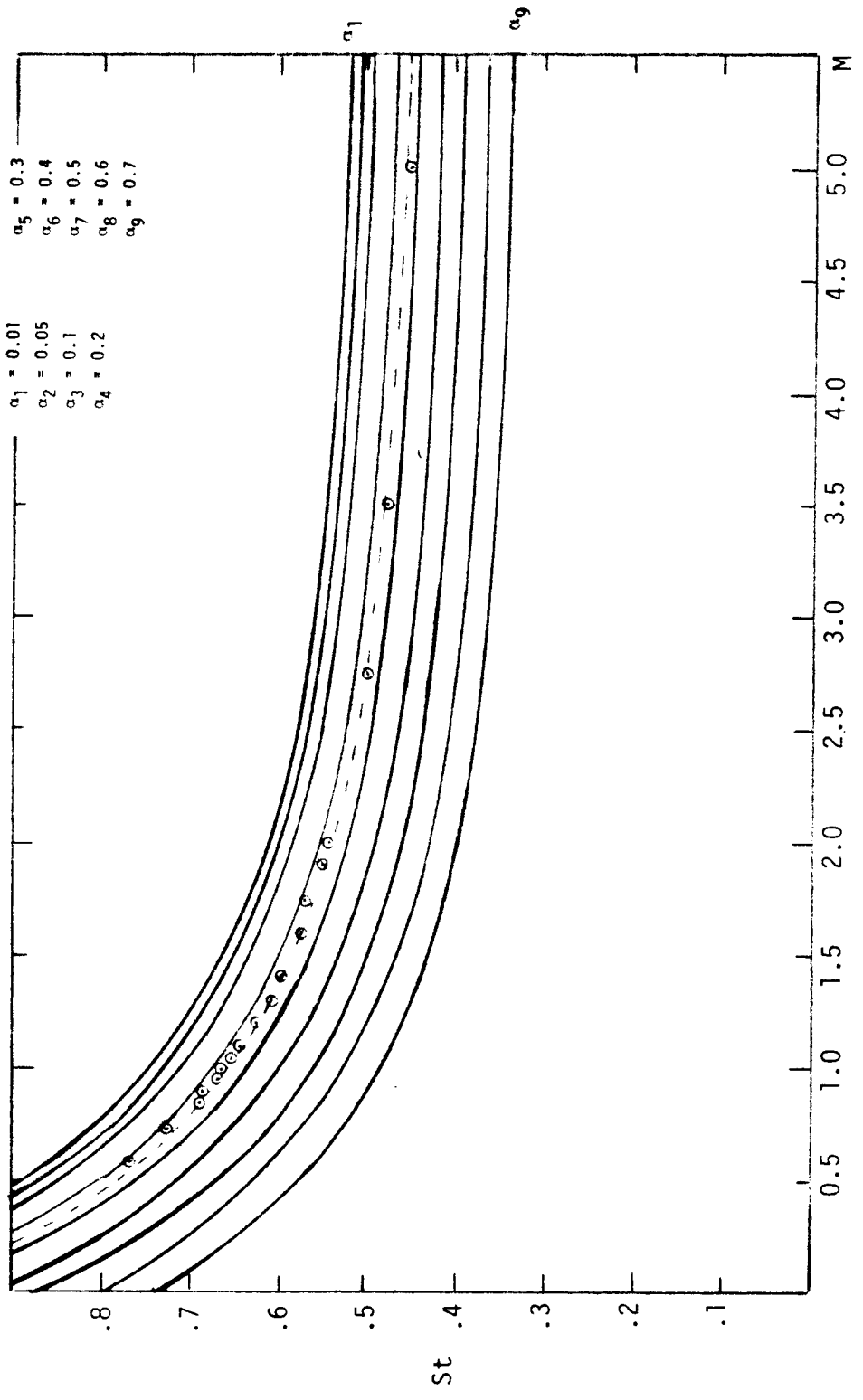
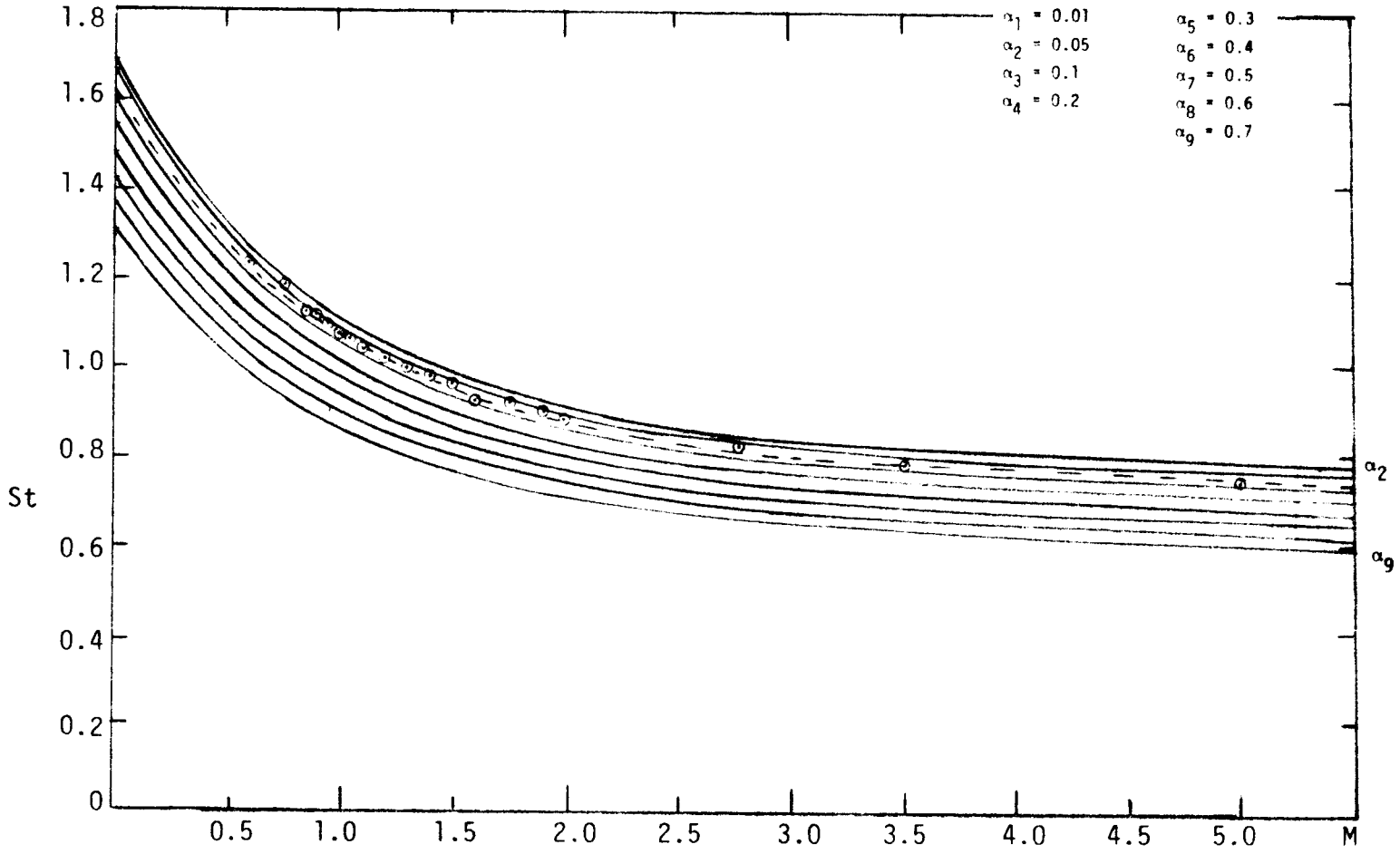


Figure 10. Nondimensional Resonant Frequencies as a Function of Mach Number for the Length-to-Depth Ratios of 4.5



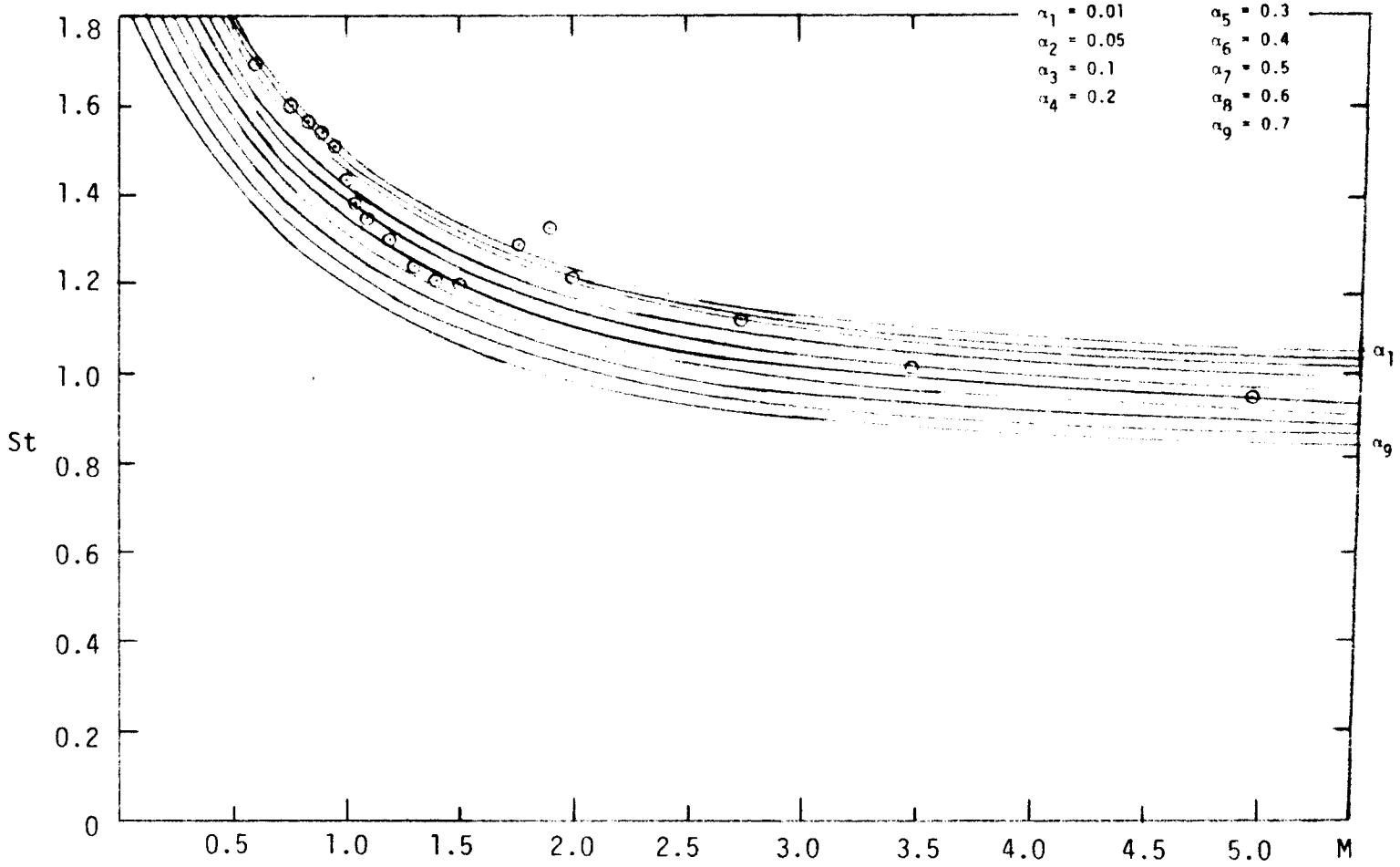
b. Mode Two

Figure 10. Continued



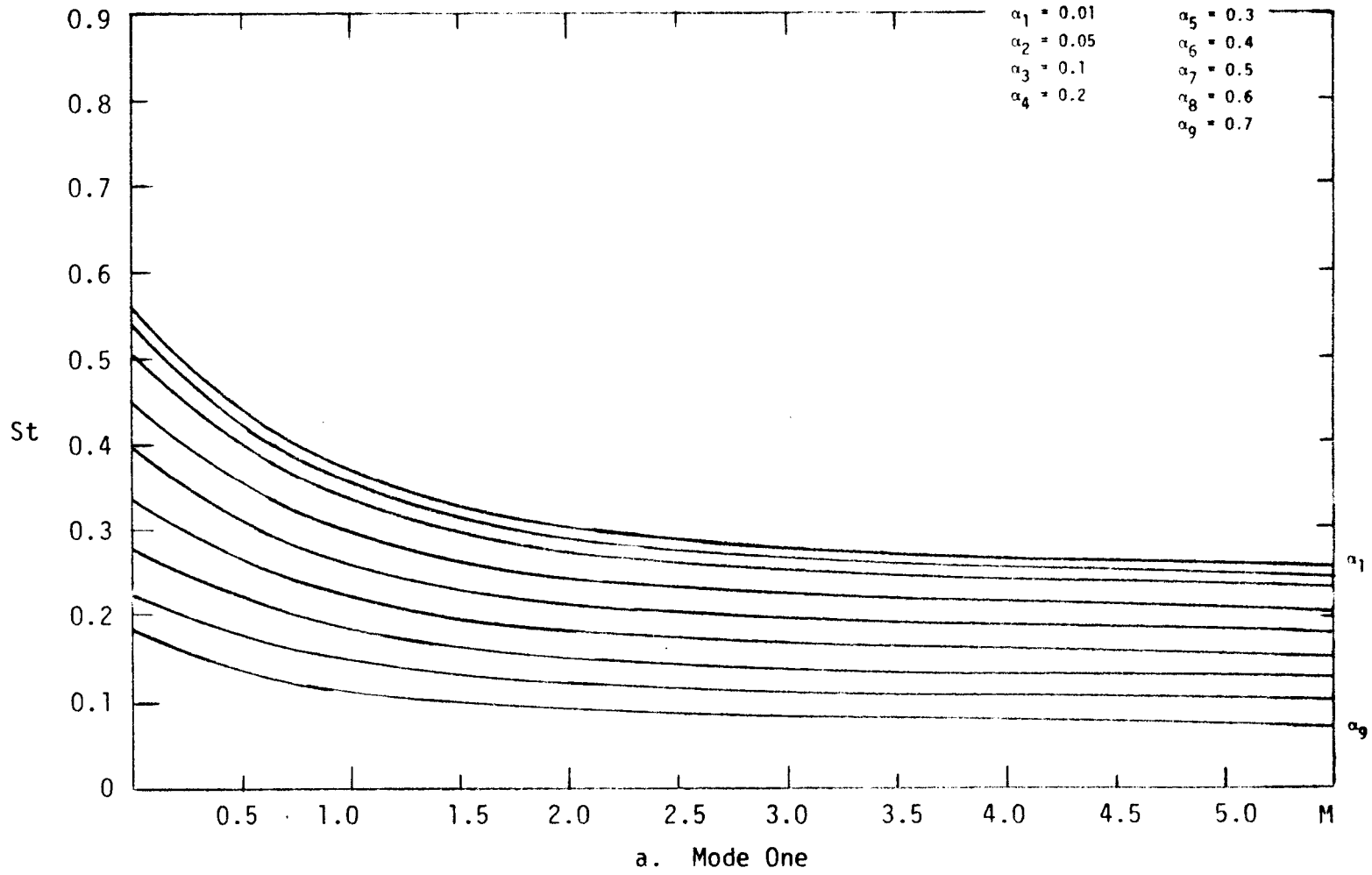
c. Mode Three

Figure 10. Continued



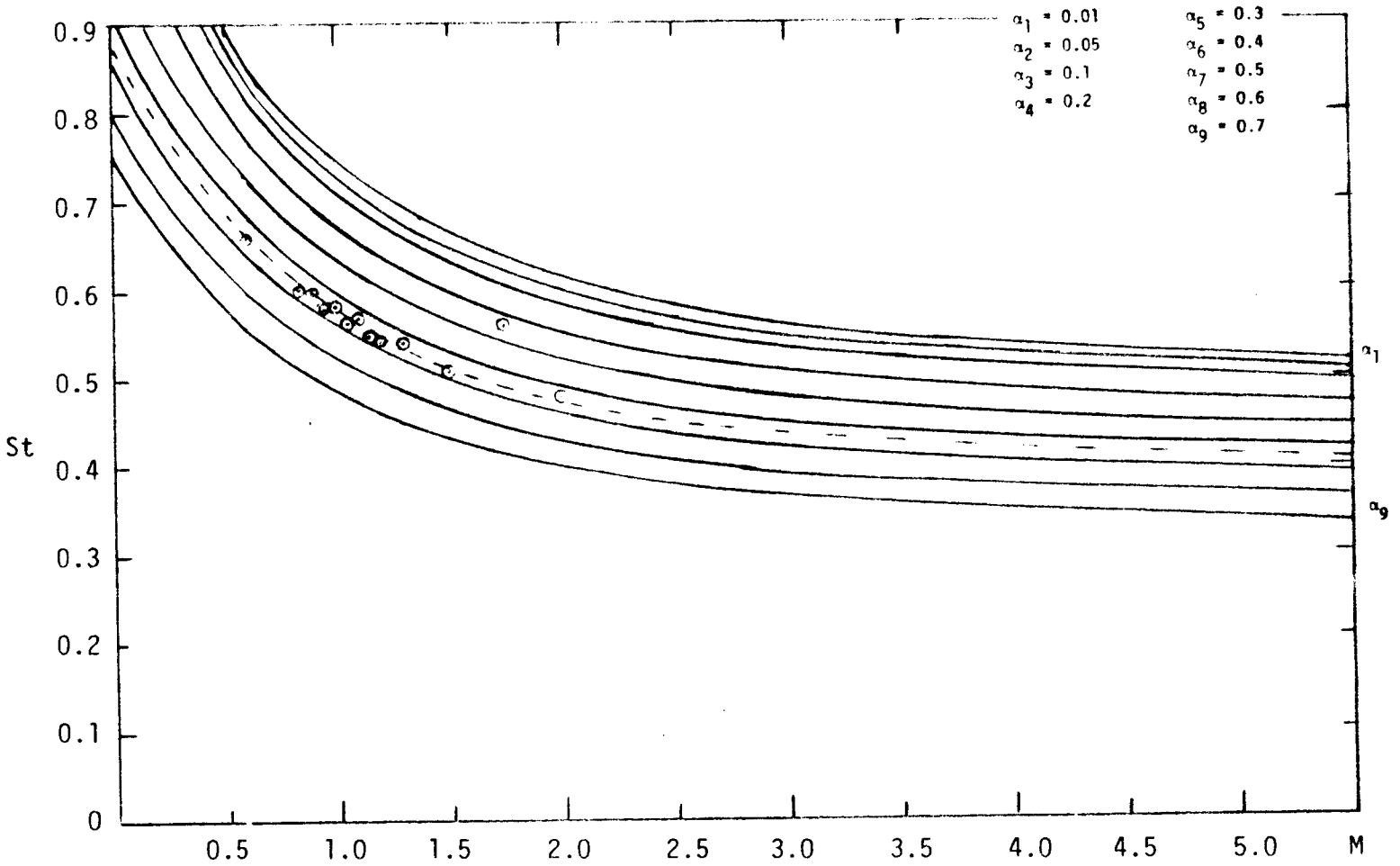
d. Mode Four

Figure 10. Concluded



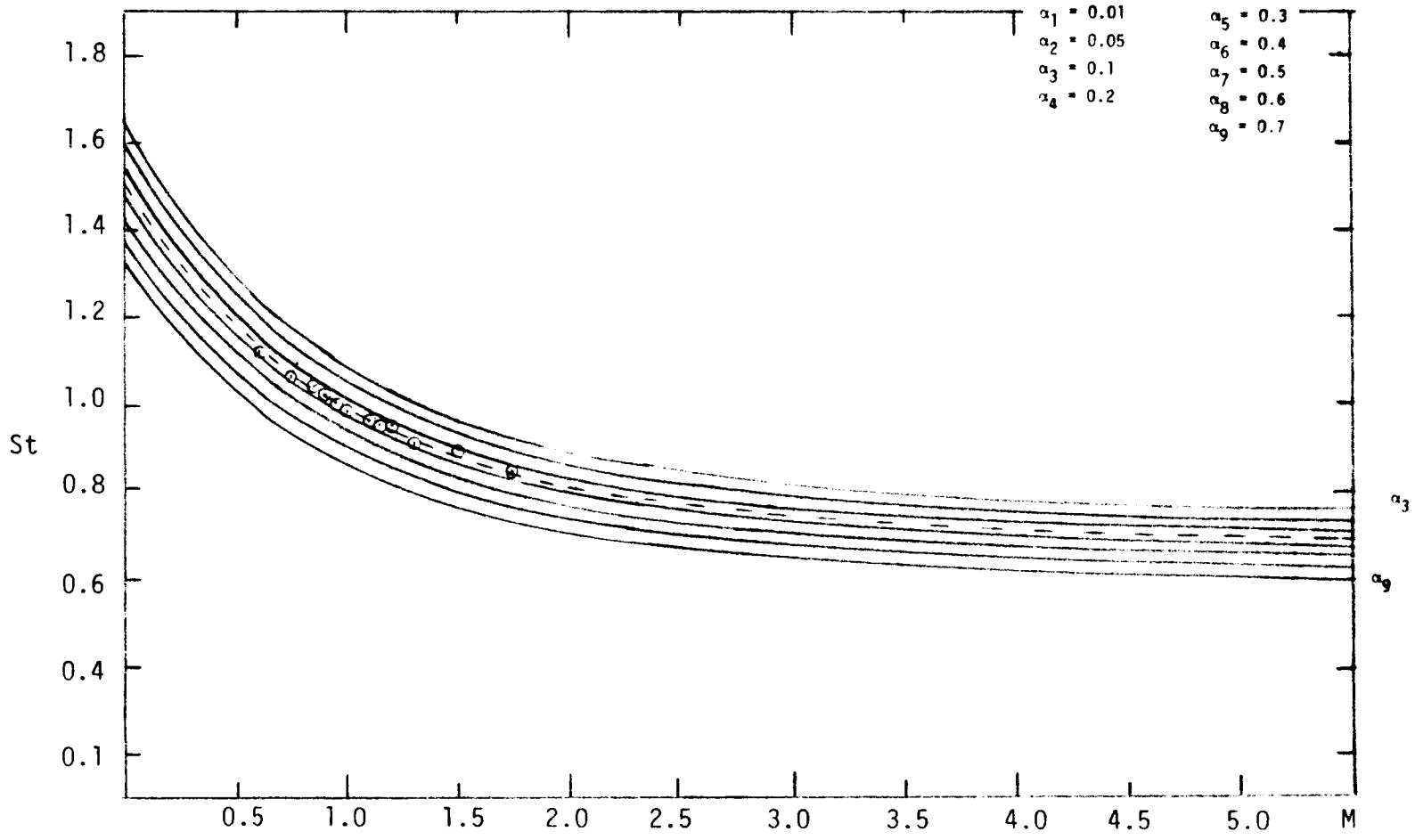
a. Mode One

Figure 11. Nondimensional Resonant Frequencies as a Function of Mach Number for the Length-to-Depth Ratio of 9.0



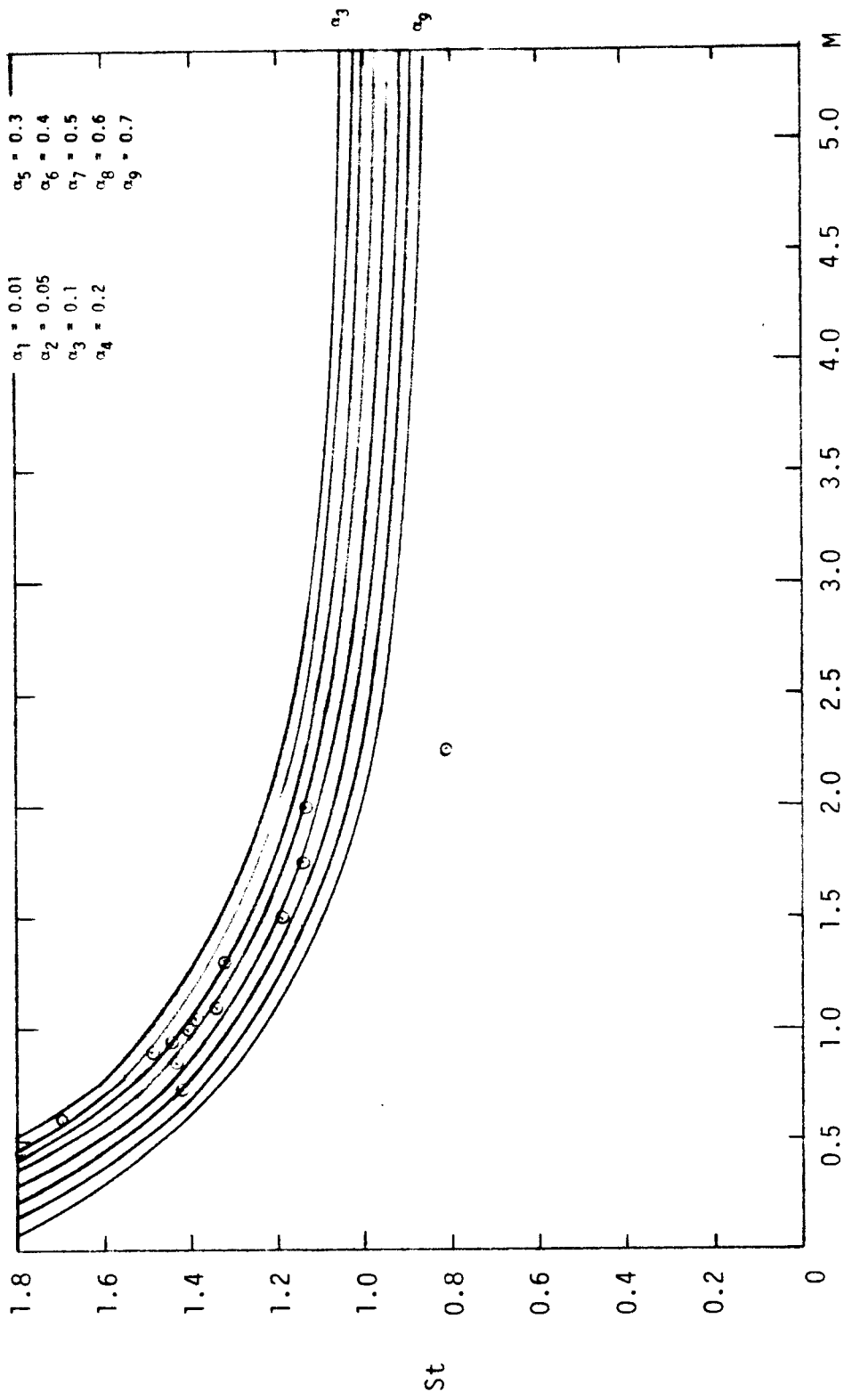
b. Mode Two

Figure 11. Continued



c. Mode Three

Figure 11. Continued



d. Mode Four

Figure 11. Concluded

Table 4. Best-Fit α Values Based on Equation 19

Mode No.	L/D	Current α	Rossiter's α
1	4.0	---	0.2526
2	4.0	---	0.2320
3	4.0	---	0.1407
4	4.0	---	---
1	4.5	0.2473	---
2	4.5	0.2281	---
3	4.5	0.1344	---
4	4.5	---	---
1	8.0	---	---
2	8.0	---	0.4143
3	8.0	---	0.3140
4	8.0	---	---
1	9.0	---	---
2	9.0	0.4510	---
3	9.0	0.3653	---
4	9.0	---	---
1	10.0	---	---
2	10.0	---	0.5161
3	10.0	---	0.4360
4	10.0	---	---

where

$$St_i^p = m\psi_i - a\psi_i \tag{12}$$

so that

$$E_i = St_i^m - m\psi_i + a\psi_i. \tag{13}$$

Defining z_i as

$$z_i = St_i^m - m\psi_i \tag{14}$$

$$E_i = a\psi_i - z_i \tag{15}$$

and

$$\sum_{i=1}^{N} E_i^2 = \sum_{i=1}^{N} (a\psi_i - z_i)^2 \tag{16}$$

For a minimum it is required that

$$\frac{\partial}{\partial a} \sum_{i=1}^{N} E_i^2 = 0 \tag{17}$$

where N is the number of data points. Then:

$$\frac{\partial}{\partial a} \sum_{i=1}^{N} \left(a\psi_i - z_i \right)^2 = 0 \tag{18}$$

resulting in the optimum a:

$$a = \frac{\sum_{i=1}^{N} \psi_i z_i}{\sum_{i=1}^{N} \psi_i^2}. \tag{19}$$

It can be inferred from Figures 10 and 11 that as the mode number increases, a decreases. Mode four data are highly scattered, most likely attributable to the coupling of the cavity multidimensional

modes and possibly edge tone effects. The results of the coupling produce what appear to be random tones as illustrated in Figures 10d and 11d.

It is interesting to note that the modal frequencies that can be tentatively identified as mode one for the L/D = 9.0 cavity (Appendix B), does not fit the Strouhal versus Mach number correlation of Figure 11a. The values of Strouhal number are in the range of approximately 0.48 to 0.66, considerably greater than expected. However, when the detected modes are considered to be the second mode, then the Strouhal-Mach number correlation is clear, Figure 11b. Furthermore, the same shift can be inferred for mode 3, Figure 11c. Just as for the L/D = 4.5 cavity, as the mode number increases, α decreases. Also, for the shallow cavity, L/D = 9.0, the optimum α was larger than for the L/D = 4.5 cavity, but not the same traditional values of α = 0.58 [3,7,9,13]. Dix [13] presents a plot, Figure 12, which indicates how α varies with L/D. In Figure 13, the first three modes are shown along with some of the data available in the literature using the optimum α values from the current study. It must be pointed out that the available data are for cavities of different length-to-depth ratios from the current cavity. Plumblee, Gibson, and Lassiter [2] data presented in Figure 13 do not correlate well with the curves. The MRE only models the longitudinal modes in deep cavities. Plumblee's data are for very deep cavities, L/D = 0.8, whereas the other data presented are for the deep cavity L/D ratios between two and seven. Plumblee indicates that for

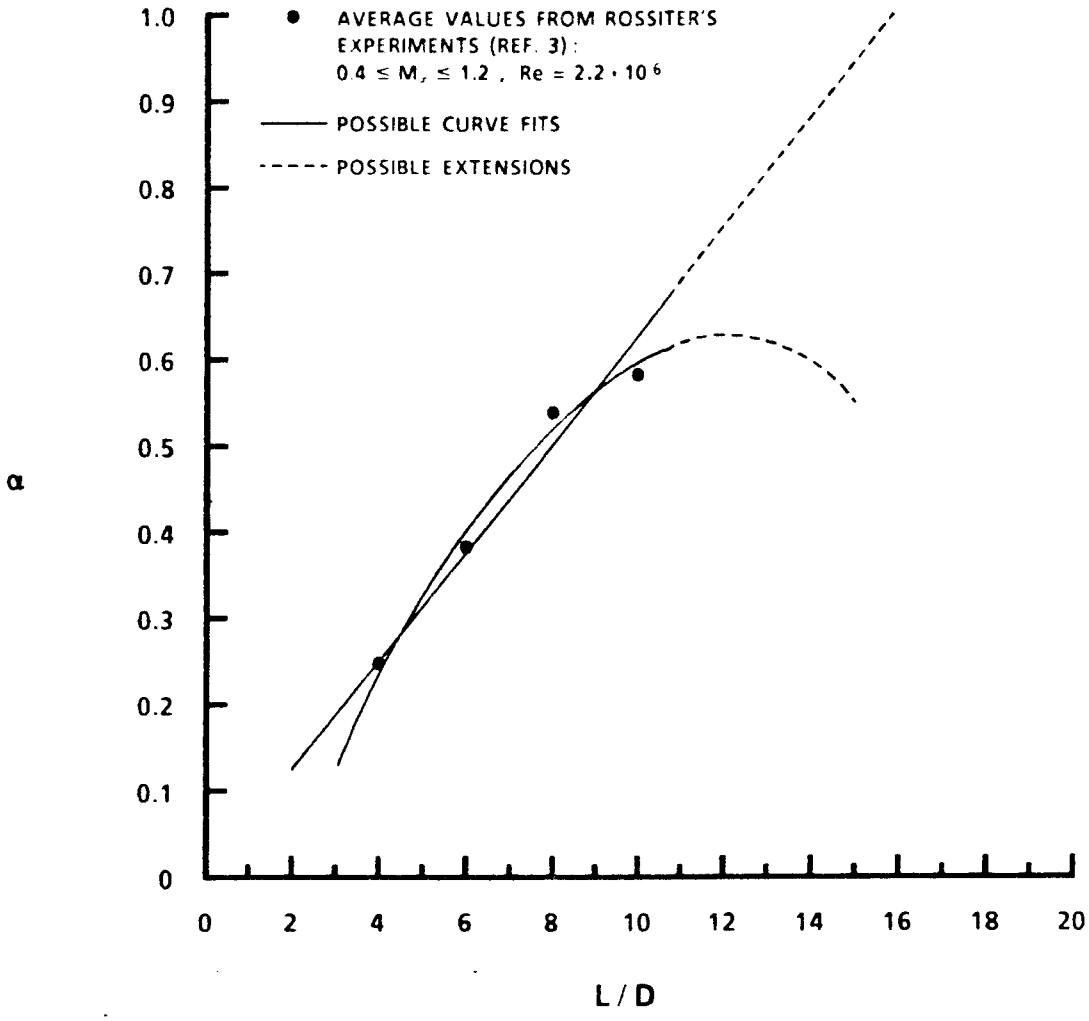


Figure 12. Rossiter's α Term as a Function of Length-to-Depth Ratio [13]

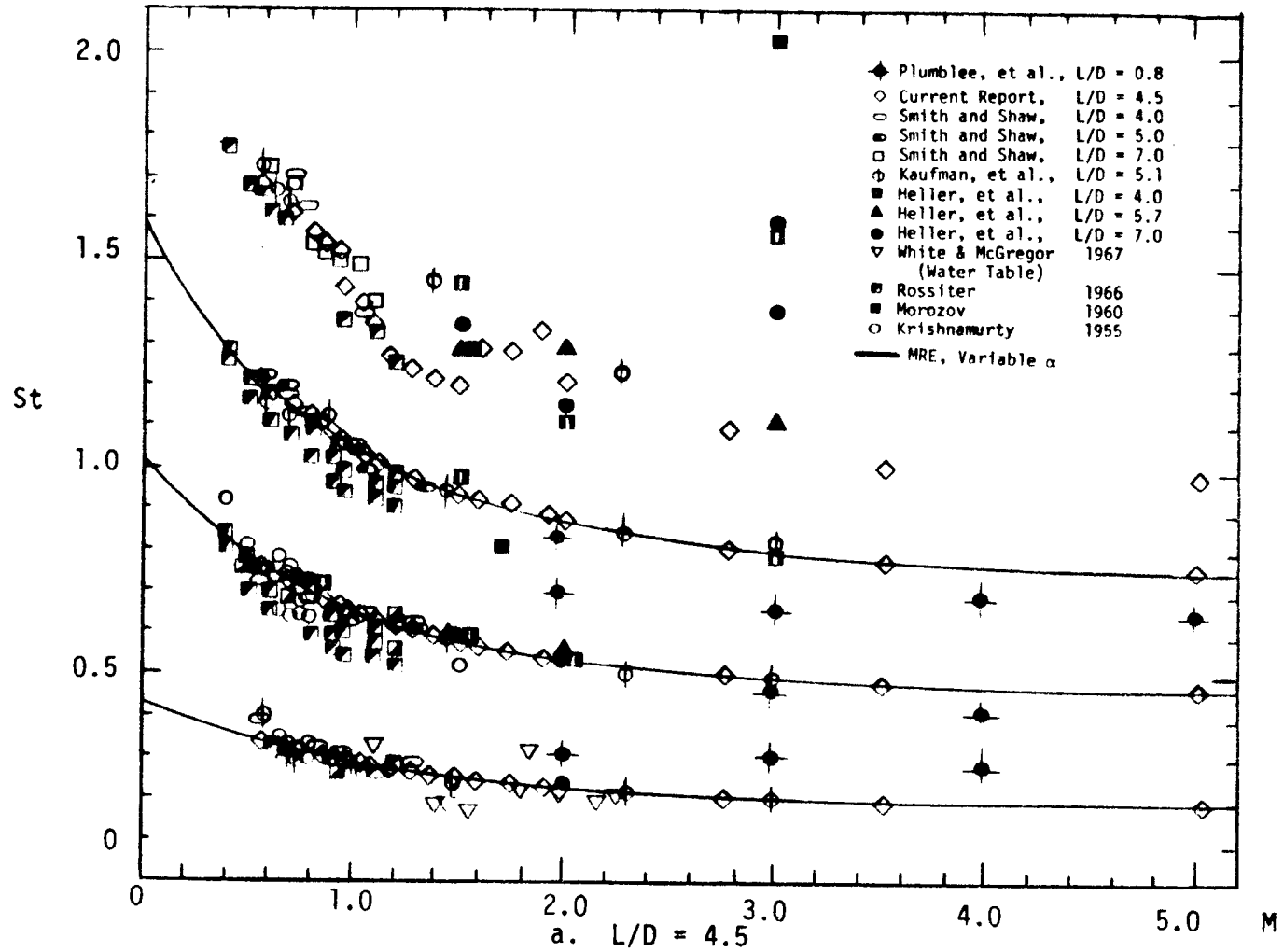
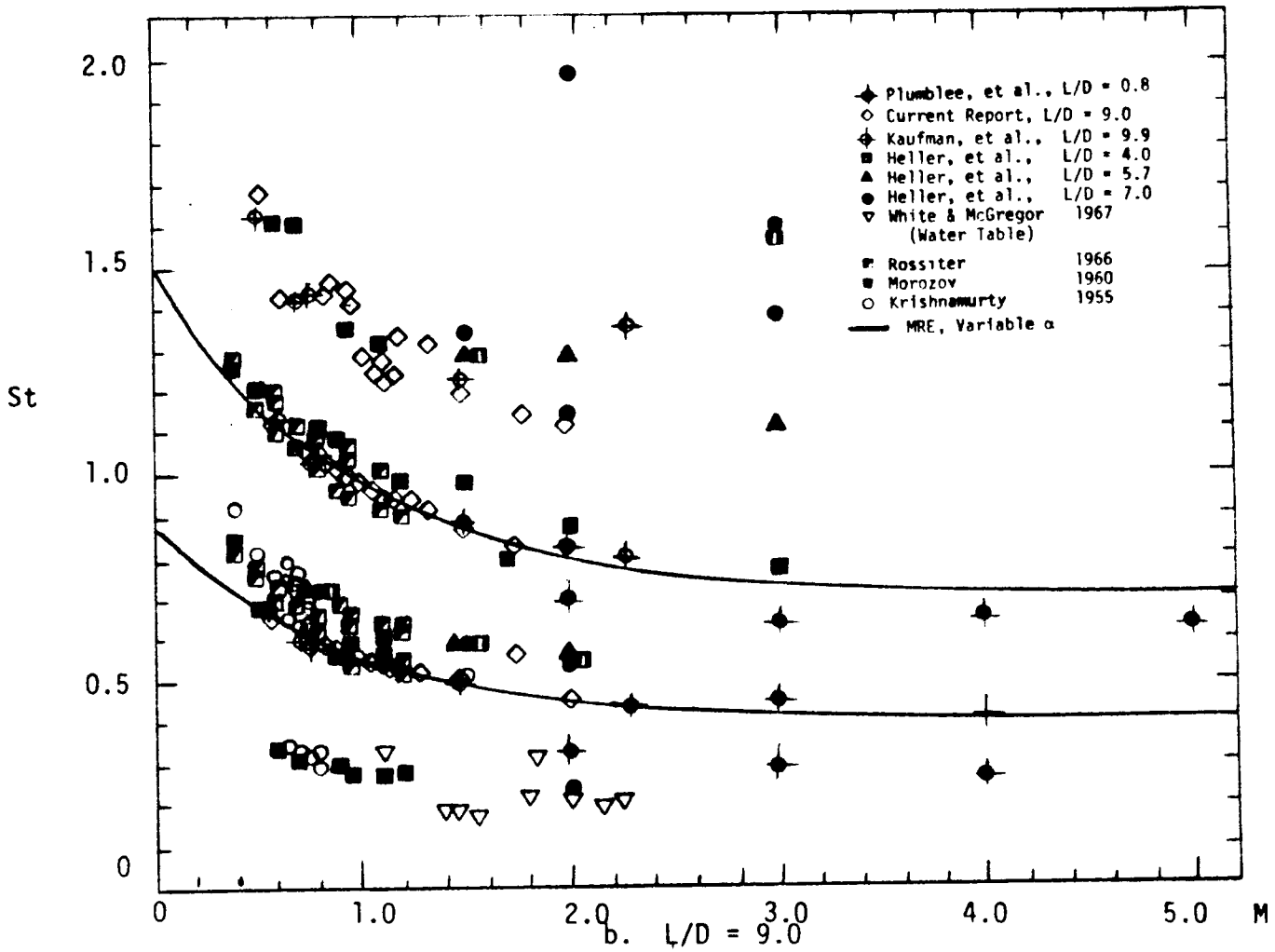


Figure 13. Nondimensional Resonant Frequencies as a Function of Mach Number - For an Optimum α



b. L/D = 9.0

Figure 13. Concluded

an L/D < 1 the cavity acoustics are dominated by depth modes and not longitudinal modes. It is this depth mode domination that contributes to the lack of data correlation. There is better agreement between the data and predicted values based on the MRE [5] and the optimum α values. Rossiter [3] pointed out and it was confirmed by Dix [13] that α is a function of L/D, but in addition α is a function of mode number. Dix [15] concurs with this result as indicated from the current data

$$\alpha = \alpha\,(L/D, m). \tag{20}$$

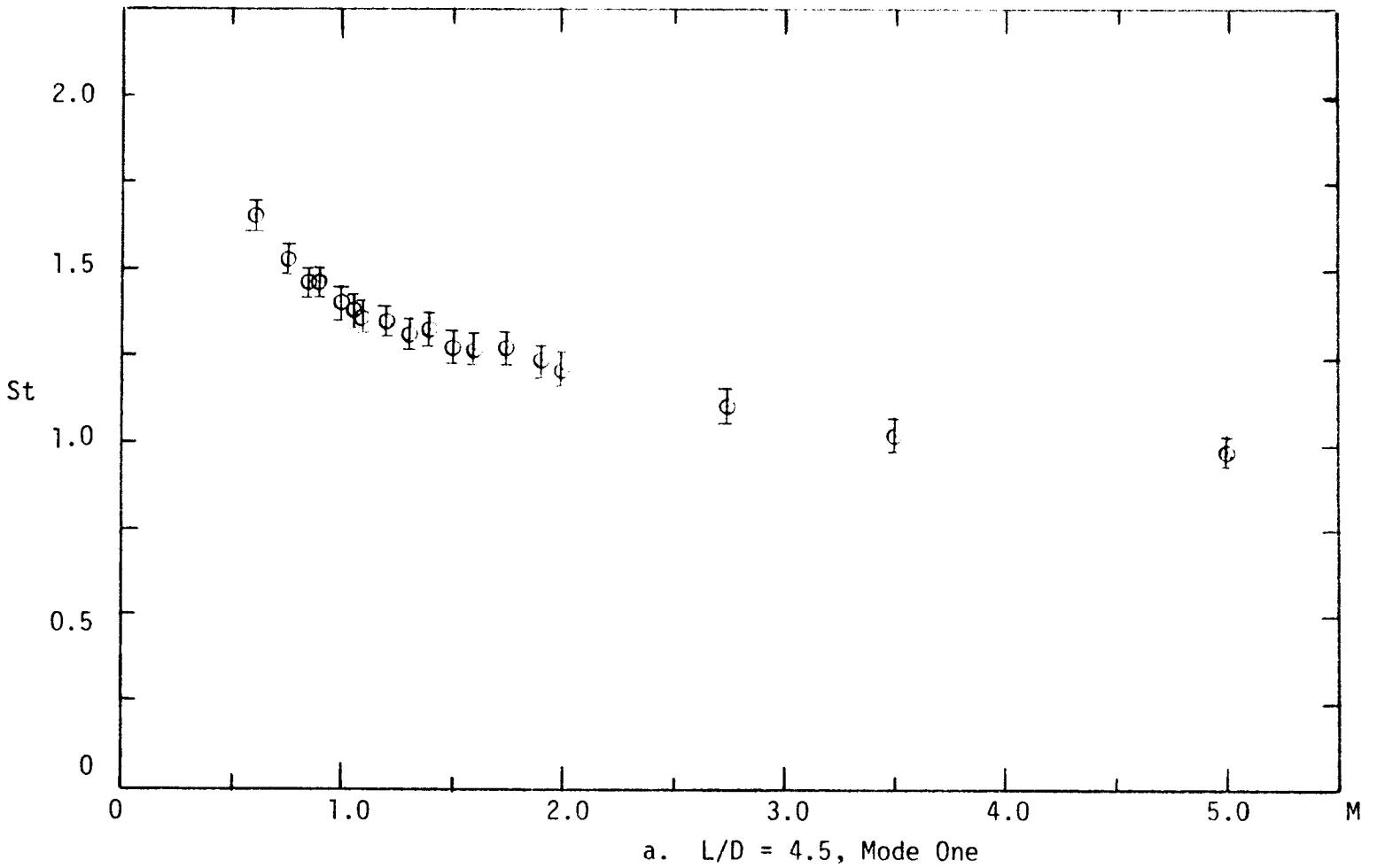
Summarizing, the MRE can be used to produce better predictions of the discrete-frequency response of a cavity if the α term is considered to be a variable as suggested in Equation (20).

III. ERROR ANALYSIS

An error analysis of the current data was accomplished, and is illustrated by error bands in Figure 14. There are two sources of error that significantly contribute to the reduced frequency data (Strouhal number): 1) an error attributable to the velocity measurement; and 2) an error attributable to the frequency. The error is determined by:

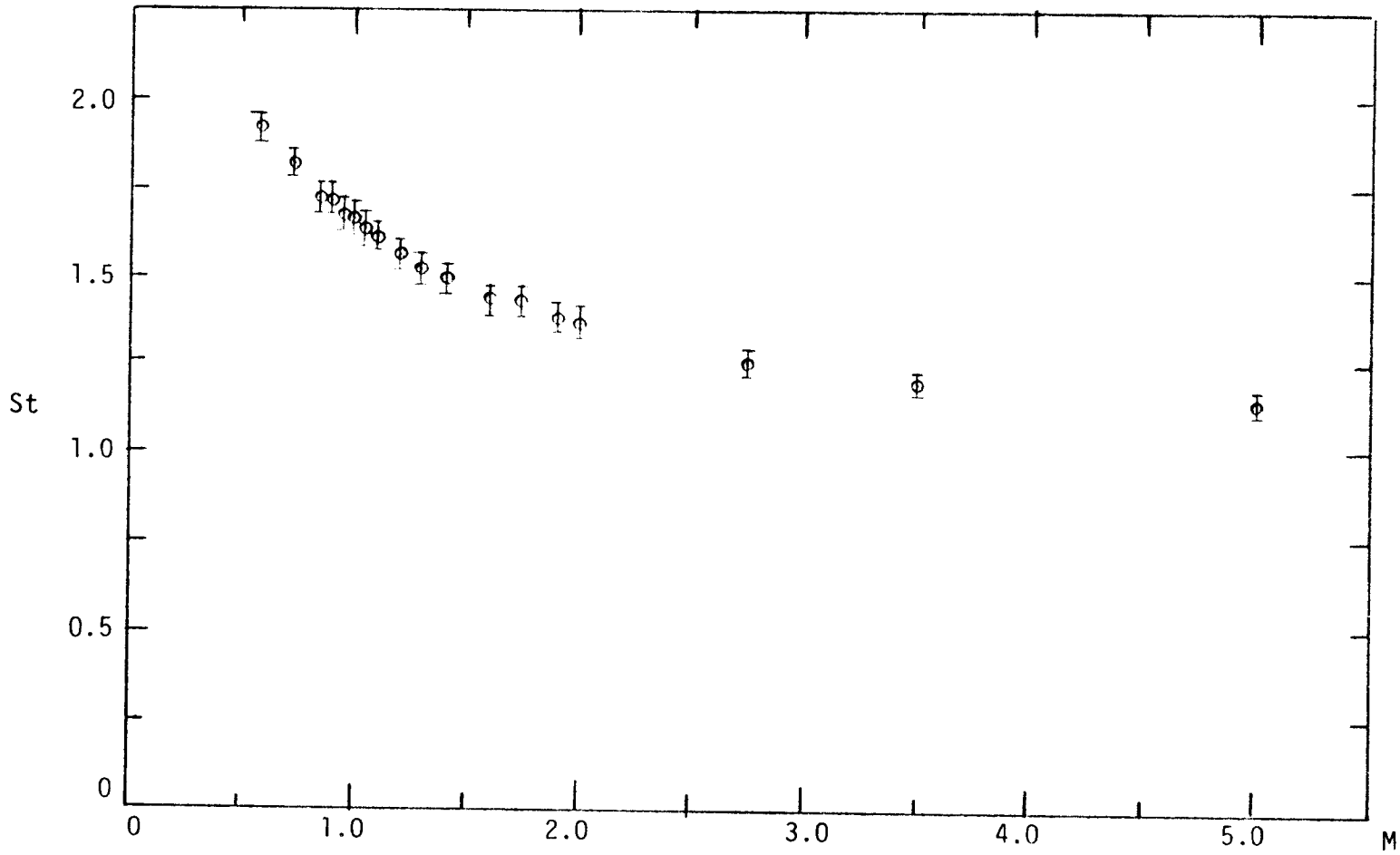
$$St = \frac{fL}{U} \tag{21}$$

$$\varepsilon^2(St) = \left[\frac{\partial St}{\partial f}\,\varepsilon(f)\right]^2 + \left[\frac{\partial St}{\partial L}\,\varepsilon(L)\right]^2 + \left[\frac{\partial St}{\partial U}\,\varepsilon(U)\right]^2 \tag{22}$$



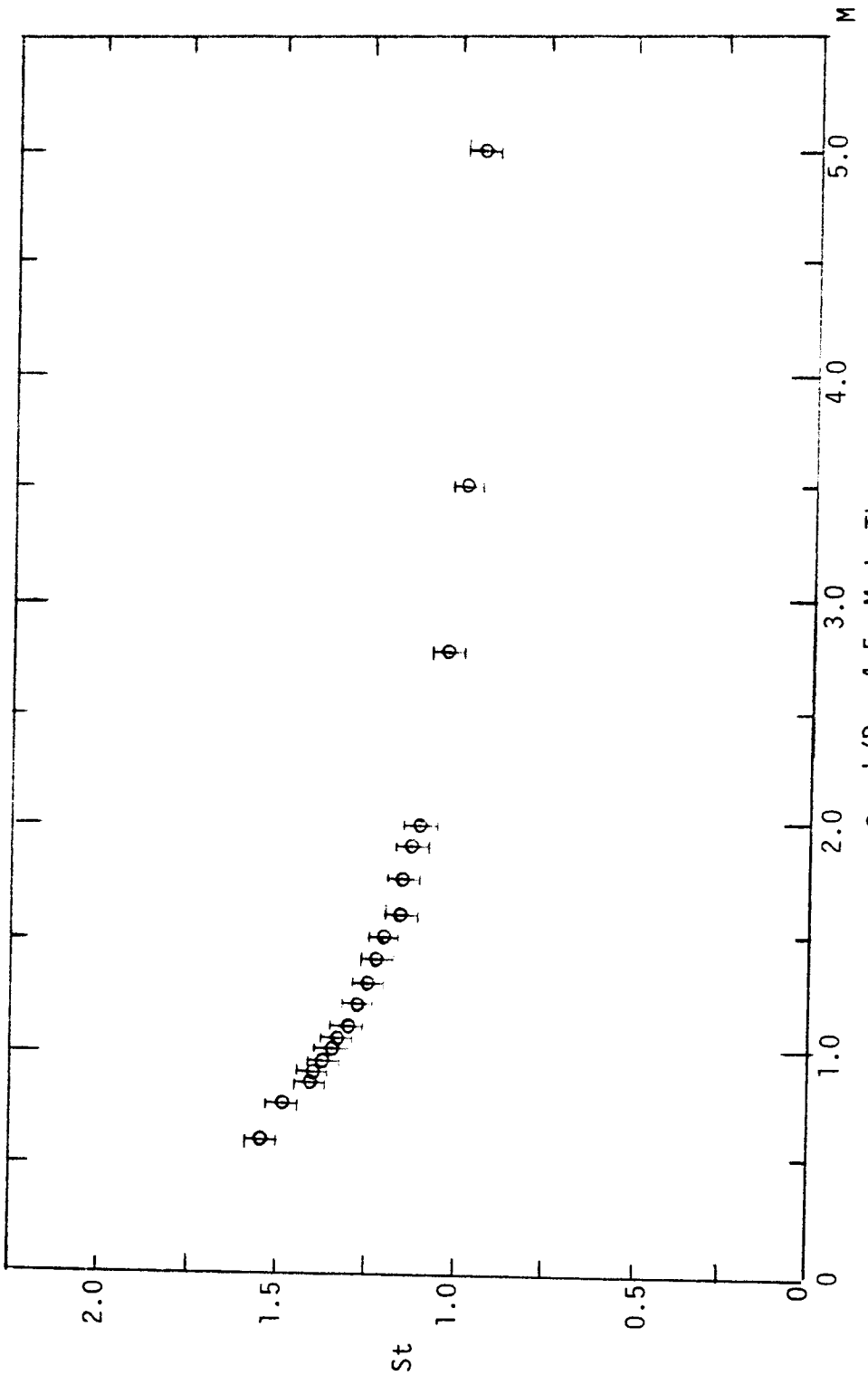
a. L/D = 4.5, Mode One

Figure 14. Error Band for the Current Data



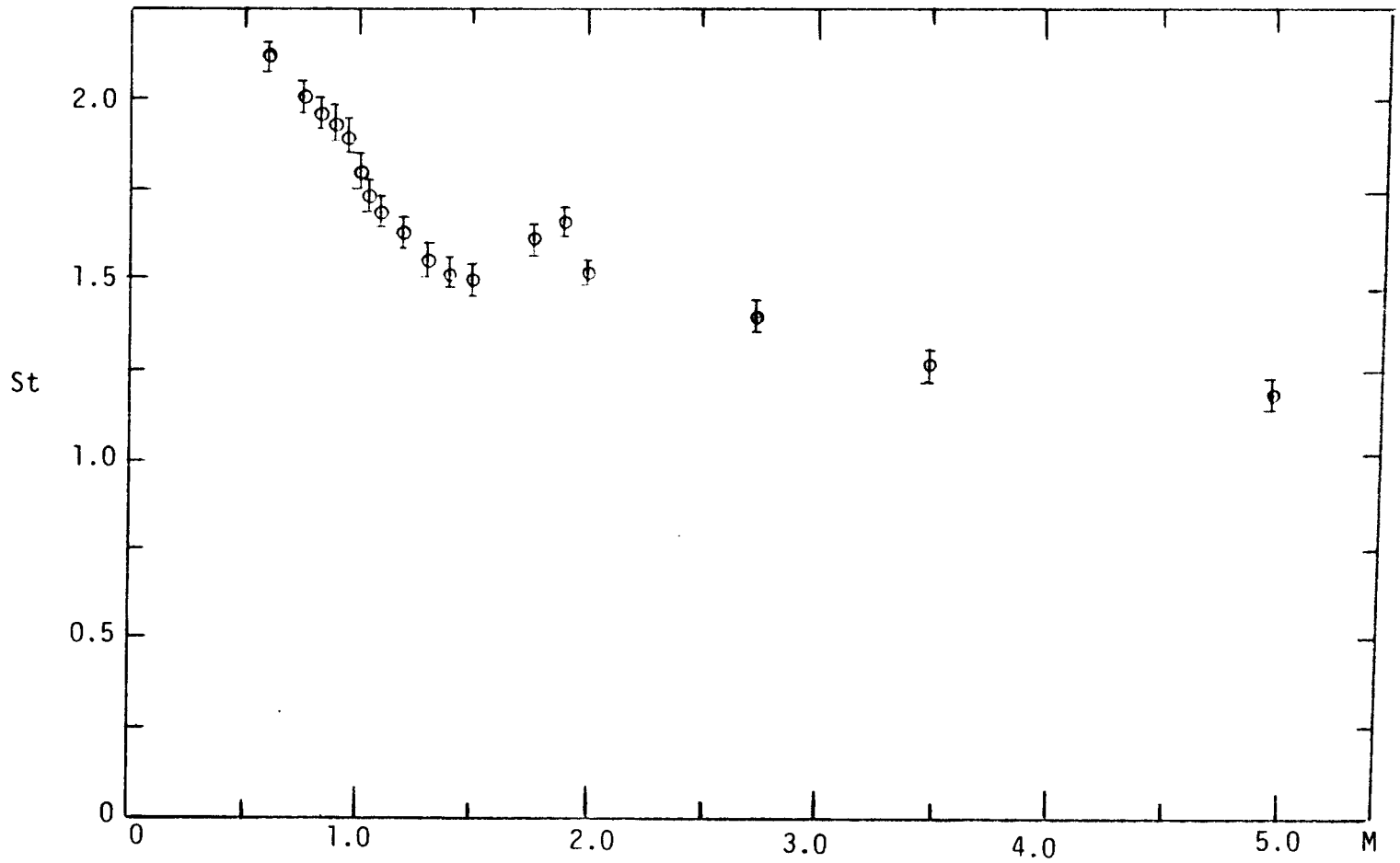
b. L/D = 4.5, Mode Two

Figure 14. Continued



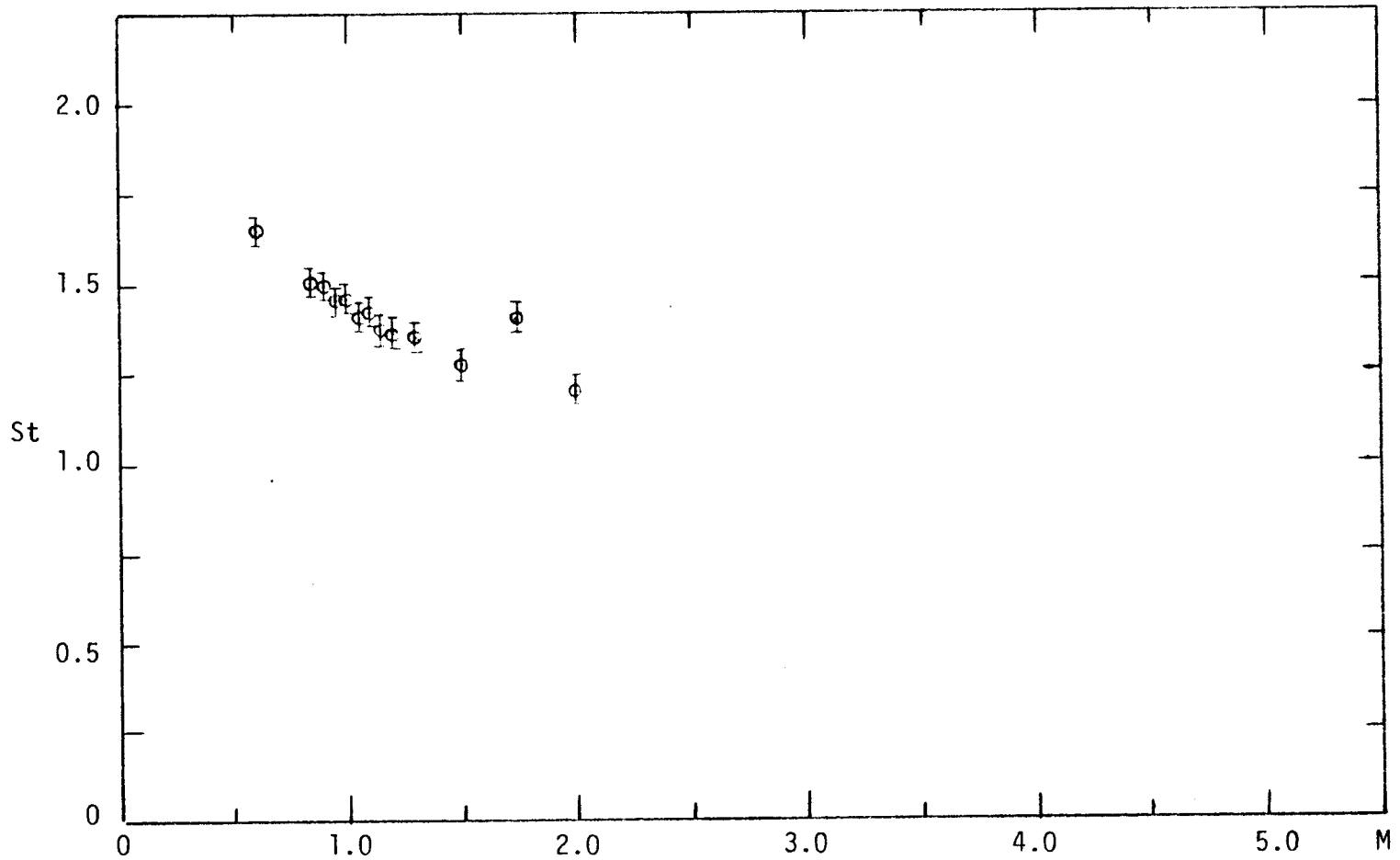
c. L/D = 4.5, Mode Three

Figure 14. Continued



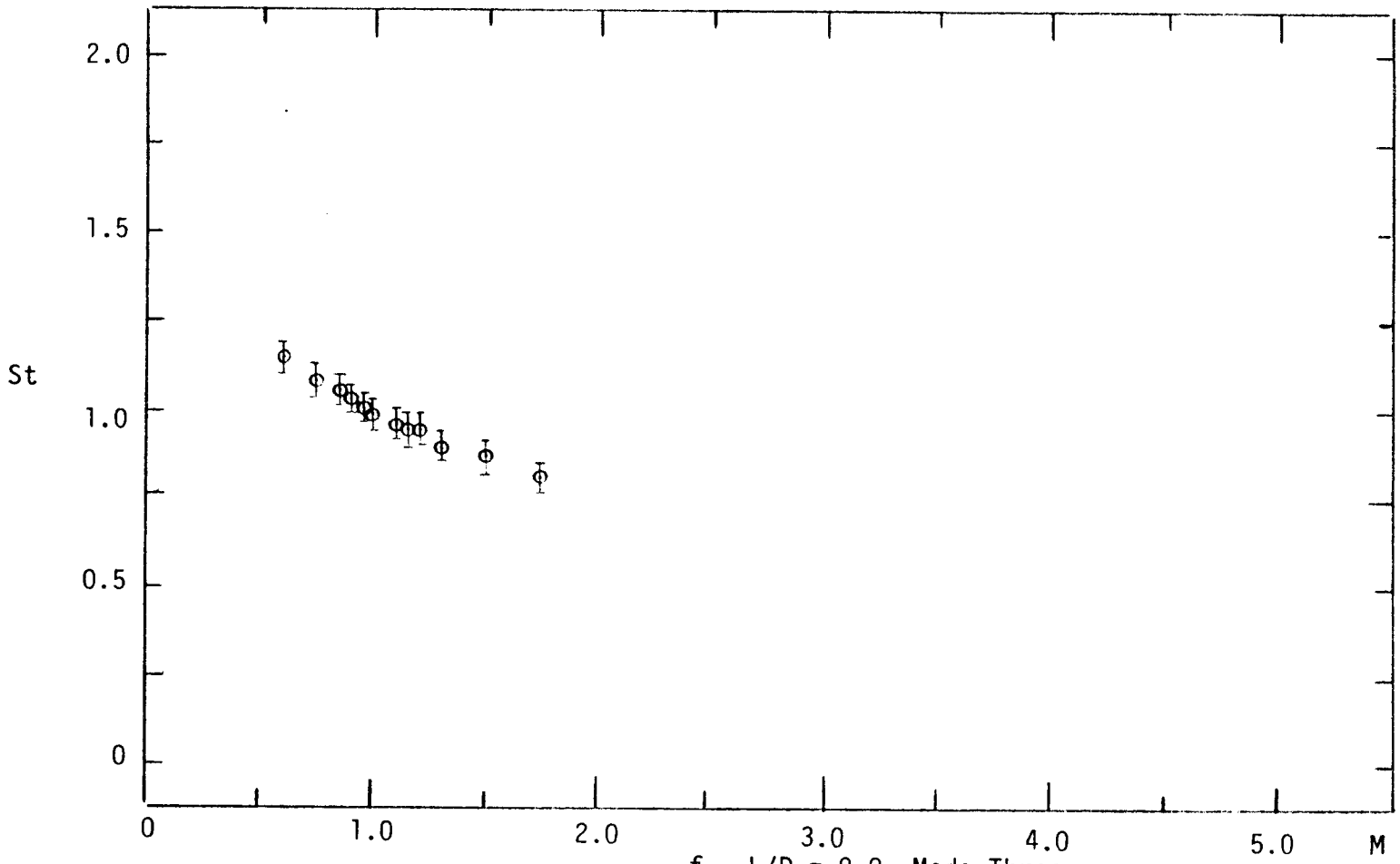
d. L/D = 4.5, Mode Four

Figure 14. Continued



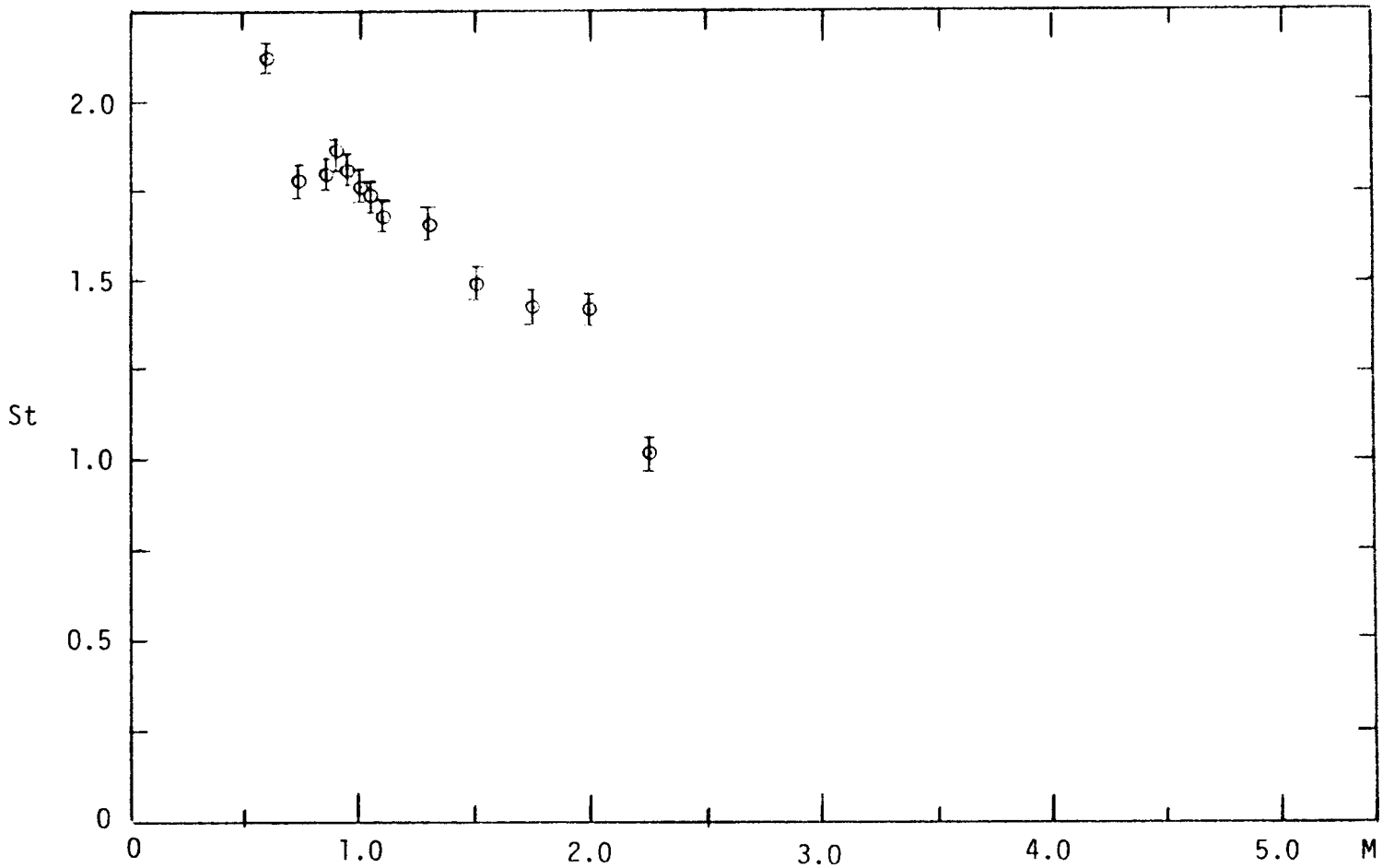
e. L/D = 9.0, Mode Two

Figure 14. Continued



f. L/D = 9.0, Mode Three

Figure 14. Continued



g. L/D = 9.0, Mode Four

Figure 14. Concluded

resulting in the error equation:

$$\varepsilon^2(St) = \frac{L^2}{U^2}\varepsilon^2(f) + \frac{f^2}{U^2}\varepsilon^2(L) + \frac{f^2L^2}{U^4}\varepsilon^2(U). \tag{23}$$

Thermal expansion of the model plate was determined to be 0.0001 ft at the maximum temperature and was assumed to be negligible. The contribution to the error in Strouhal number due to the length measurement errors at Mach numbers 0.6 and 5.04 are 0.000122 and 0.000071, respectively, where $\varepsilon(L) \approx 0.010$-in. The uncertainty in the velocity measurement is determined by:

$$\varepsilon(U) = \left[\left(\frac{\partial U}{\partial M}\right)^2 (dM)^2 + \left(\frac{\partial U}{\partial TT}\right)^2 (dTT)^2\right]^{1/2}. \tag{24}$$

The contribution to the error in Strouhal number due to the velocity measurement errors at Mach numbers 0.6 and 5.04 are 0.0101 and 0.0037, respectively. Considering the error in the frequency, it must be assumed that the data have a Gaussian distribution, where the modal frequency will vary within the bandwidth [16]. That is, the frequencies corresponding to the modal peaks from the plots in Appendix A and B should vary within the bandwidth of 9.76 Hz and the uncertainty is approximately ±5 Hz. Where the contribution to the error in the Strouhal number due to the frequency at Mach numbers 0.6 and 5.04 are 0.063 and 0.0173, respectively. Therefore, the error attributable to the measured length was negligible compared to the error in the velocity and frequency.

CHAPTER V

CONCLUSIONS AND RECOMMENDATIONS

Using the modified Rossiter equation (MRE) the previous frequency data base was extended to higher Mach numbers for an empty cavity. The observations summarized below are based on experimental results.

1. Possible cavity resonant frequencies can be predicted by the MRE. However, the predicted modal tones using the MRE may not necessarily be measurable.
2. The modal tones predicted using the MRE for the two cavities (L/D = 4.9 and 9.0) correlate well with the first three modes that were measured.
3. When plotted on a Strouhal versus Mach number plot, the discrete frequencies for the higher ordered measured modes (mode 4 and above) appear to be randomly distributed, and therefore do not correlate with the predicted modal tones using the MRE. This is possibly attributable to the complex coupling of the multidimensional modes and possible edge tone effects.
4. The prediction scheme was improved by considering α to be a function of mode number as well as the length-to-depth ratio.

It was revealed during the review of the literature listed in the Reference section that little data exist for rectangular cavities at Mach numbers above 3.0 and a systematic approach has not been taken to study the effects of the approaching boundary layer on the cavity

acoustics. Therefore, it is recommended that additional testing be done to study the effects of the boundary layer by holding the free-stream conditions constant and either changing the cavity lengths or extending the length of the model forward of the cavity to change the boundary layer thickness. In addition, testing at higher Mach numbers should be accomplished to add to the current data base.

LIST OF REFERENCES

LIST OF REFERENCES

1. Krishnamurty, K., "Acoustic Radiation from Two-Dimensional Rectangular Cutouts in Aerodynamic Surfaces," NACA TN 3487, August 1955.

2. Plumblee, H. E., Gibson, J. S., and Lassiter, L. W., "A Theoretical and Experimental Investigation of the Acoustic Response of Cavities in an Aerodynamic Flow," WADD-TR-61-75, (AD-277803), March 1962.

3. Rossiter, J. E., "Wind Tunnel Experiment on the Flow Over Rectangular Cavities at Subsonic and Transonic Speeds," Ministry of Aviation, Aeronautical Research Council, Reports and Memoranda No. 3438, October 1964.

4. East, L. F., "Aerodynamically Induced Resonance in Rectangular Cavities," Journal of Sound and Vibration, Vol. 3, No. 3, 1966, pp. 277-287.

5. Heller, H. H., Holmes, G., and Covert, "Flow Induced Pressure Oscillations in Shallow Cavities," AFFDL-TR-70-104, (AD-880496), December 1970.

6. Heller, H. H. and Bliss, D. B., "Aerodynamically Induced Pressure Oscillations in Cavities - Physical Mechanisms and Suppression Concepts," AFFDL-TR-74-133 (AD-B002701), August 1974.

7. Smith, D. L. and Shaw, L. L., "Prediction of the Pressure Oscillations in Cavities Exposed to Aerodynamic Flow," AFFDL-TR-75-34, (AD-A018518), October 1975.

8. Clark, Rodney L., "Evaluation of F-111 Weapon Bay Aeroacoustic and Weapon Separation Improvement Techniques," AFFDL-TR-79-3003, (AD-A070253), February 1979.

9. Bartel, H. W. and McAvory, J. M., "Cavity Oscillation in Cruise Missile Carrier Aircraft," AFWAL-TR-81-3036, (AD-A108610), June 1981.

10. Stallings, Robert L., Jr. and Wilcox, Floyd J., Jr., "Experimental Cavity Pressure Distributions at Supersonic Speeds," NASA Technical Paper 2683, June 1987.

11. Dix, Richard E., "On Simulation Techniques for the Separation of Stores from Internal Installations," SAE Technical Paper Series 871799, October 1987.

12. Caruthers, John E., "Rectangular Cavity Discrete Frequency Acoustics," The University of Tennessee Space Institute, Calspan Project Number F40600-85-C-0020, March 1990.

13. Dix, Richard E. and Butler, Carrol, "Cavity Aeroacoustics," Proceedings of the Royal Aeronautical Society Store Carriage, Integration, and Release Conference, April 1990.

14. White, Frank M., Fluid Mechanics. New York: McGraw-Hill Book Company, 1979.

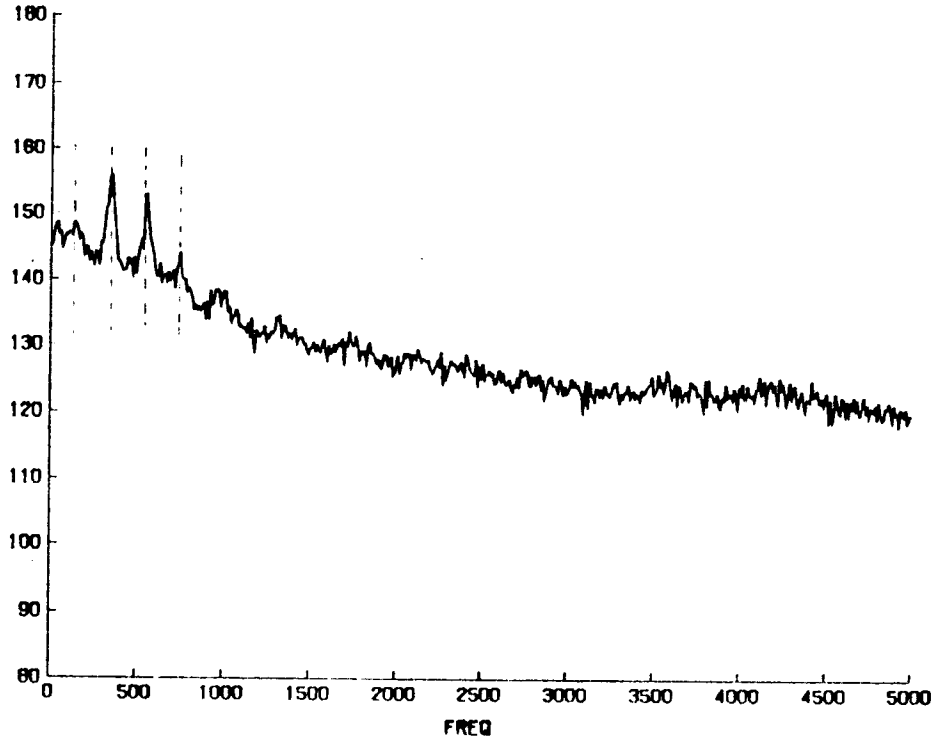
15. Discussion with AEDC/KE2 Richard E. Dix, Principal Engineer.

16. Otnes, Robert K. and Enochson, Loren, Digital Time Series Analysis. New York: John Wiley and Sons, Inc., 1972.

APPENDICES

APPENDIX A. CAVITY RESPONSE PLOTS FOR A LENGTH-TO-DEPTH RATIO OF 4.5

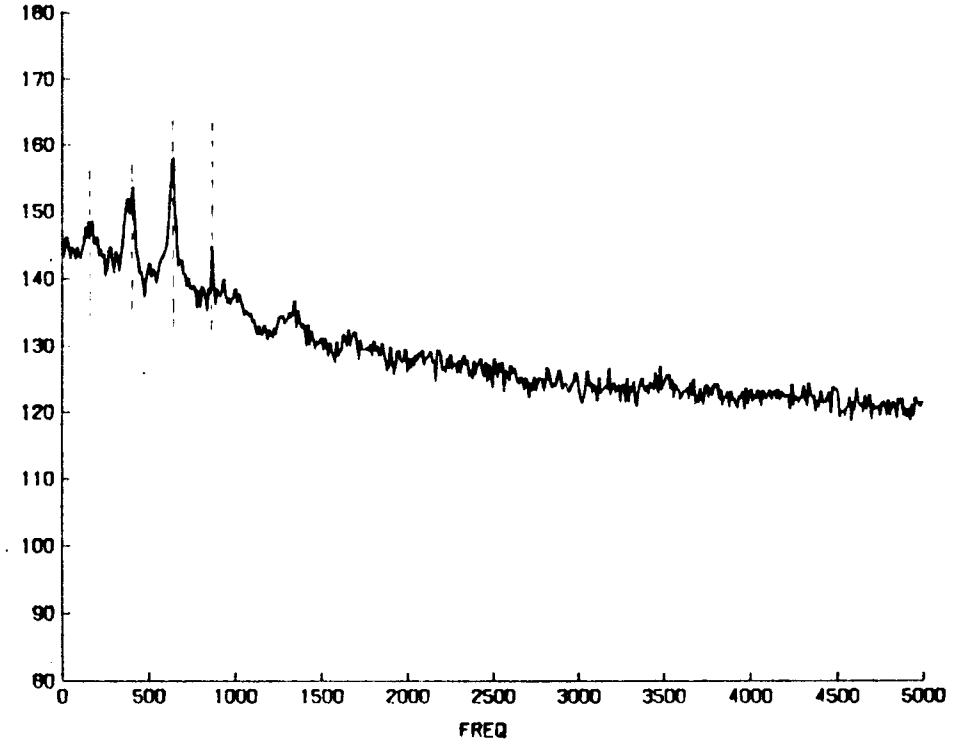
	MACH	UNIT RE. 1/FT.	V-INF	Q-INF	PT	TT
☐	0.60	3.01E+6	668.0	374.1	1895.1	553.7



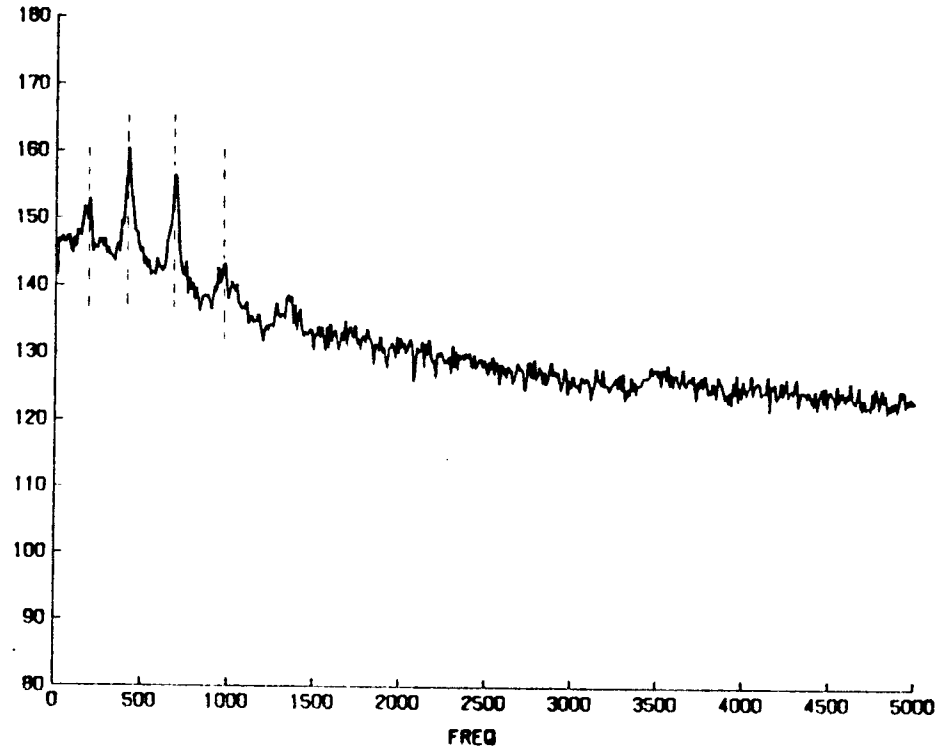
K16

09

	MACH	UNIT RE. 1/FT.	V-INF	Q-INF	PT	TT
◻	0.75	2.24E+6	814.7	327.3	1207.9	546.7

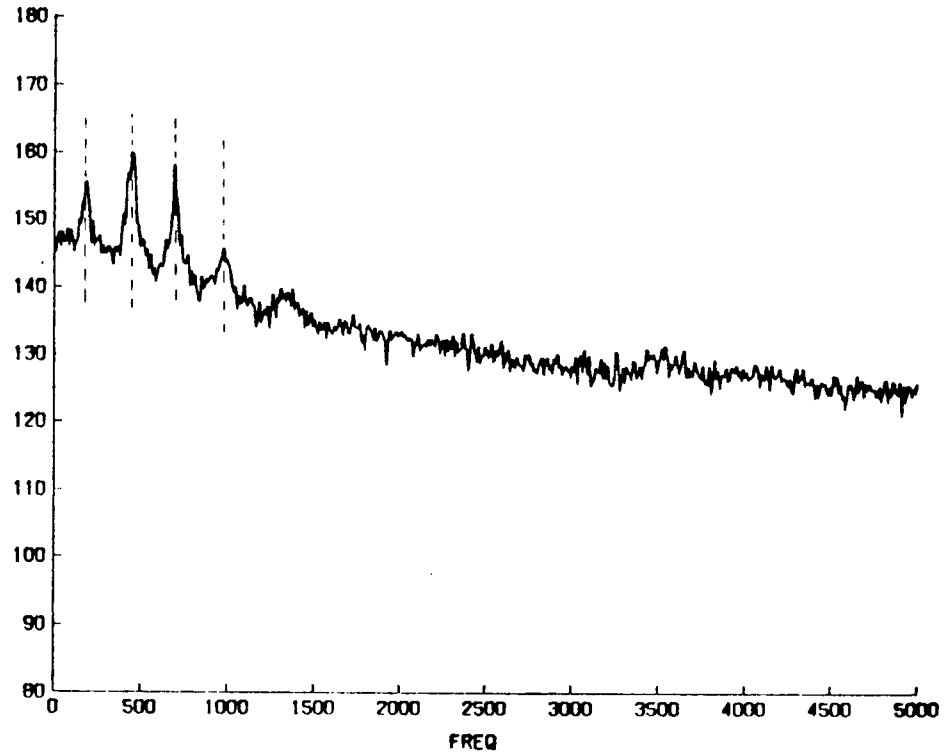


	MACH	UNIT RE, 1/FT.	V-INF	Q-INF	PT	TT
☐	0.85	2.37E+6	910.8	378.4	1199.7	546.7

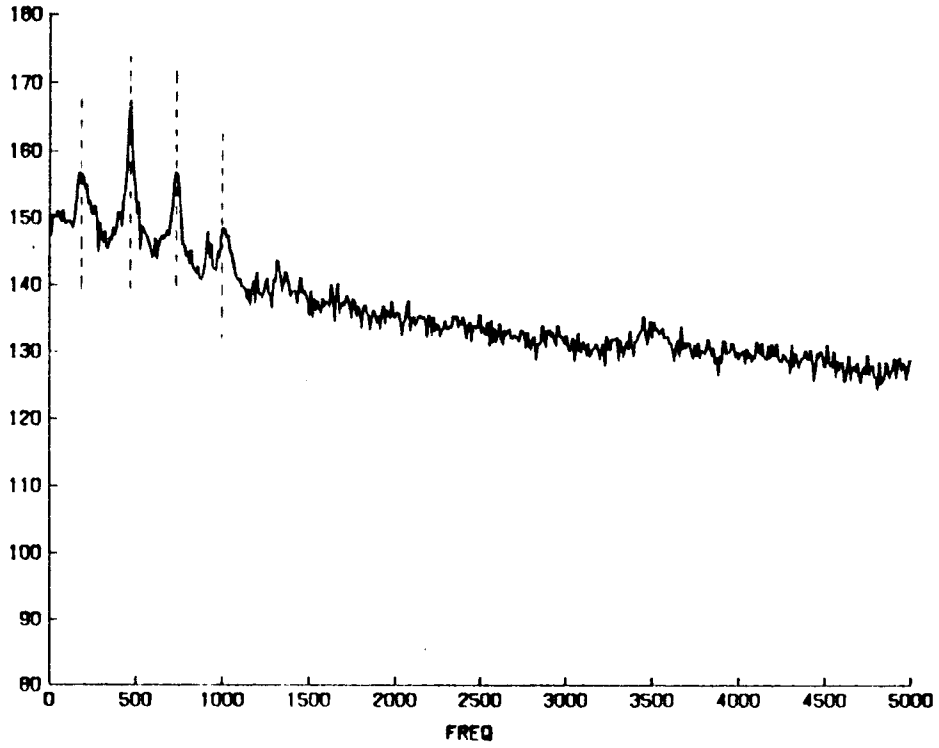


K16

	MACH	UNIT RE. 1/FT.	V-INF	Q-INF	PT	TT
☐	0.90	2.45E+6	956.5	405.1	1209.1	546.7

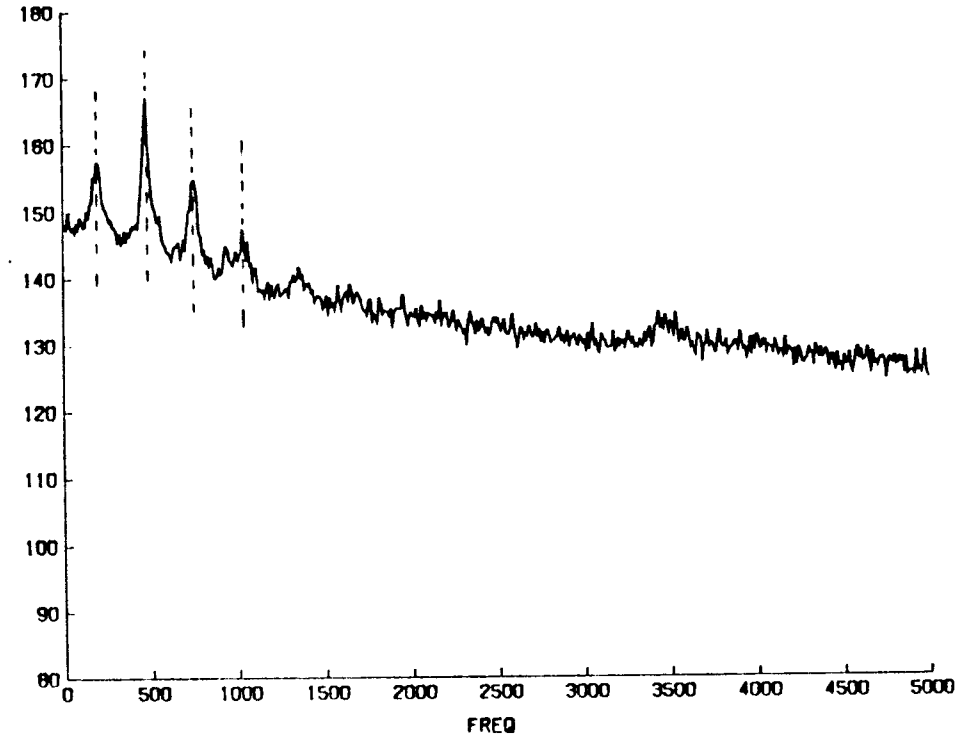


	MACH	UNIT RE, 1/FT.	V-INF	Q-INF	PT	TT
☐	0.95	3.02E+6	1006.7	520.2	1466.0	547.7



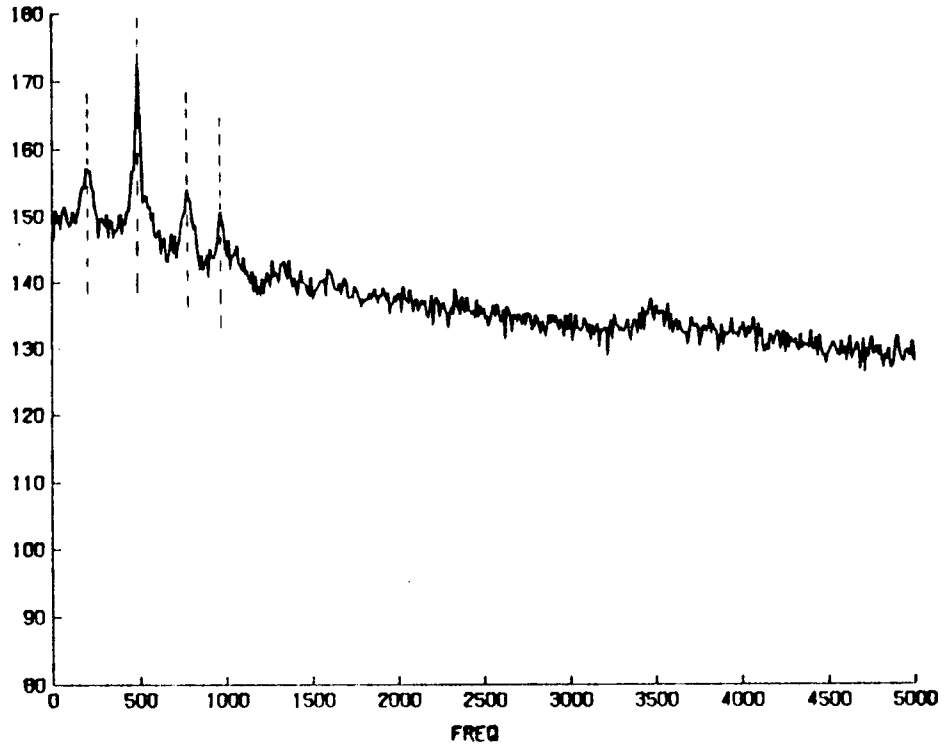
K16

	MACH	UNIT RE. 1/FT.	V-INF	Q-INF	PT	TT
◻	1.00	2.51E+6	1050.0	445.3	1201.1	547.7



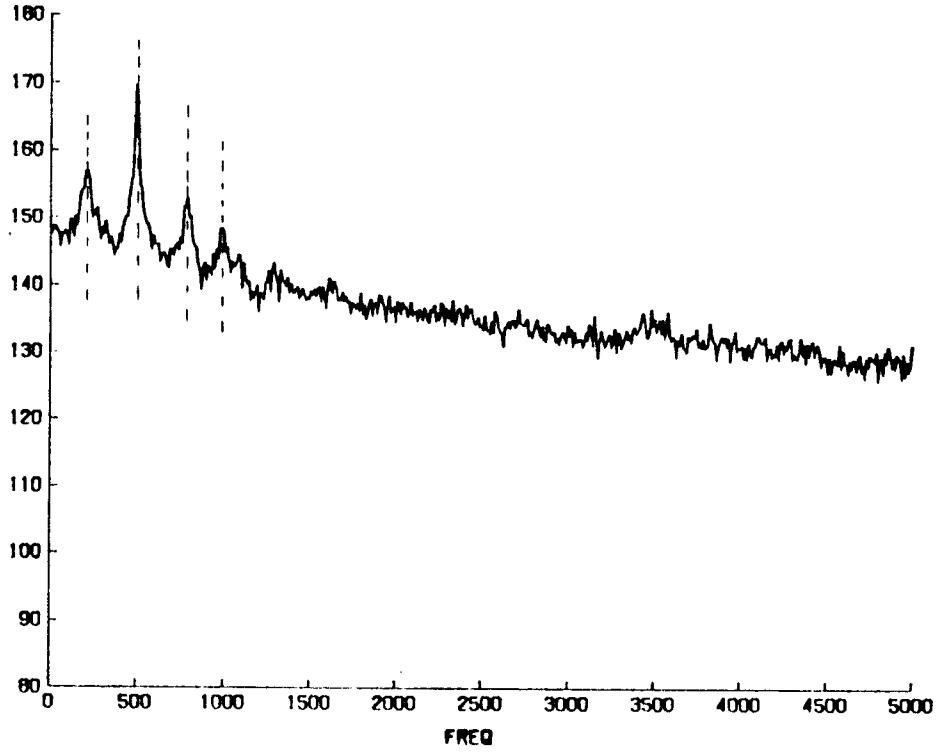
K16

	MACH	UNIT RE, 1/FT.	V-INF	Q-INF	PT	TT
☐	1.05	3.02E+6	1098.0	556.0	1443.7	552.7

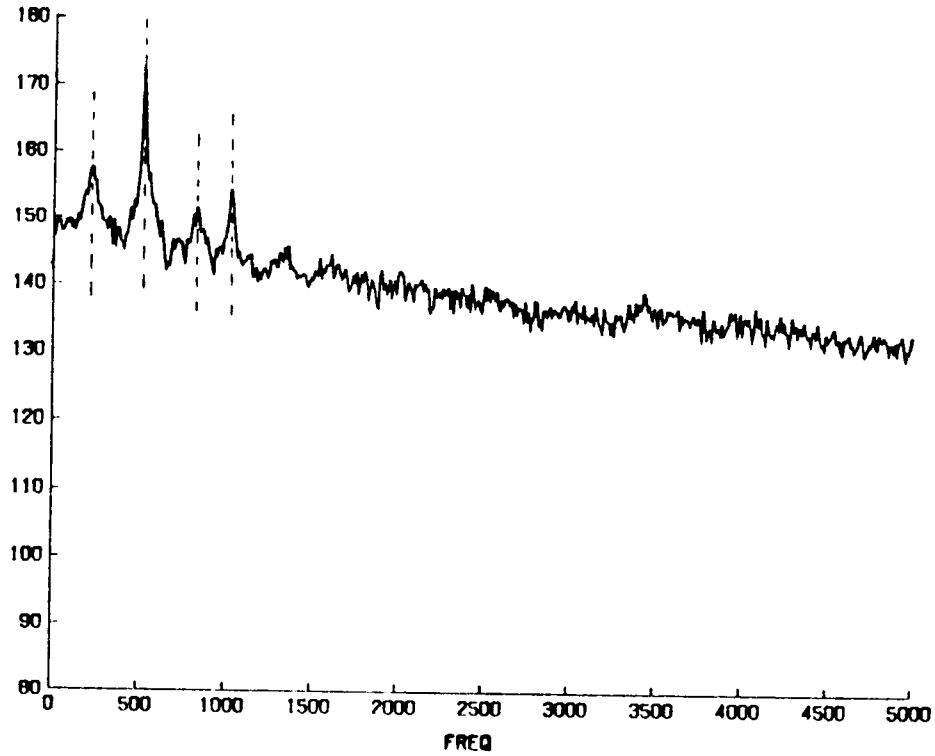


K18

	MACH	UNIT RE, 1/FT.	V-INF	Q-INF	PT	TT
☐	1.10	2.55E+6	1134.7	475.6	1197.8	549.7

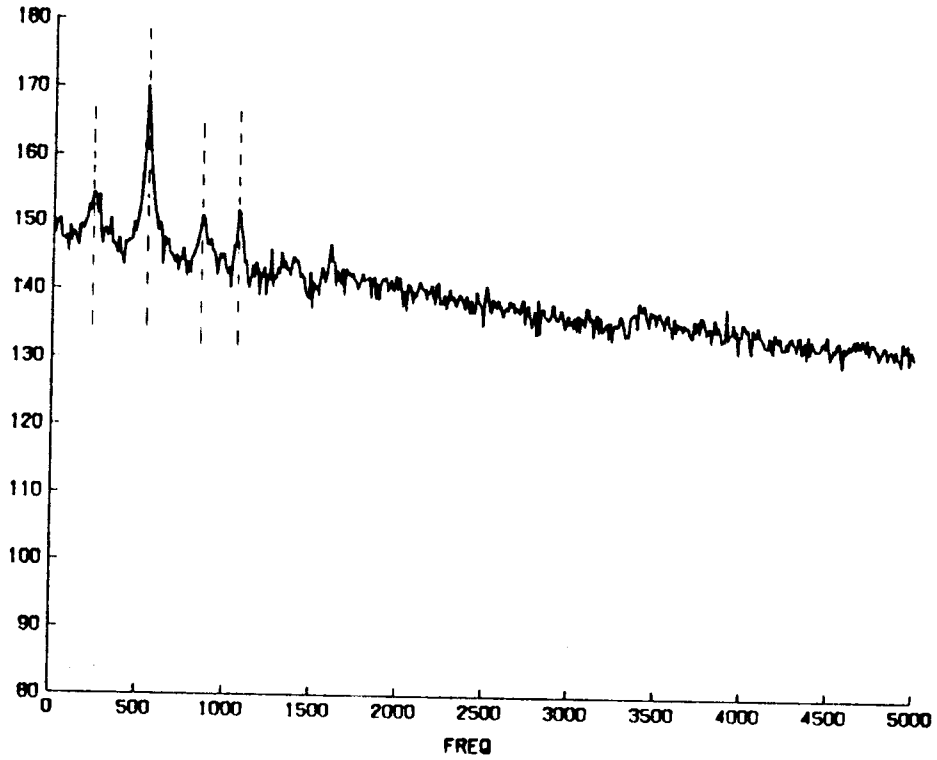


	MACH	UNIT RE. 1/FT.	V-INF	Q-INF	PT	TT
□	1.20	2.99E+6	1216.3	582.0	1399.3	550.7



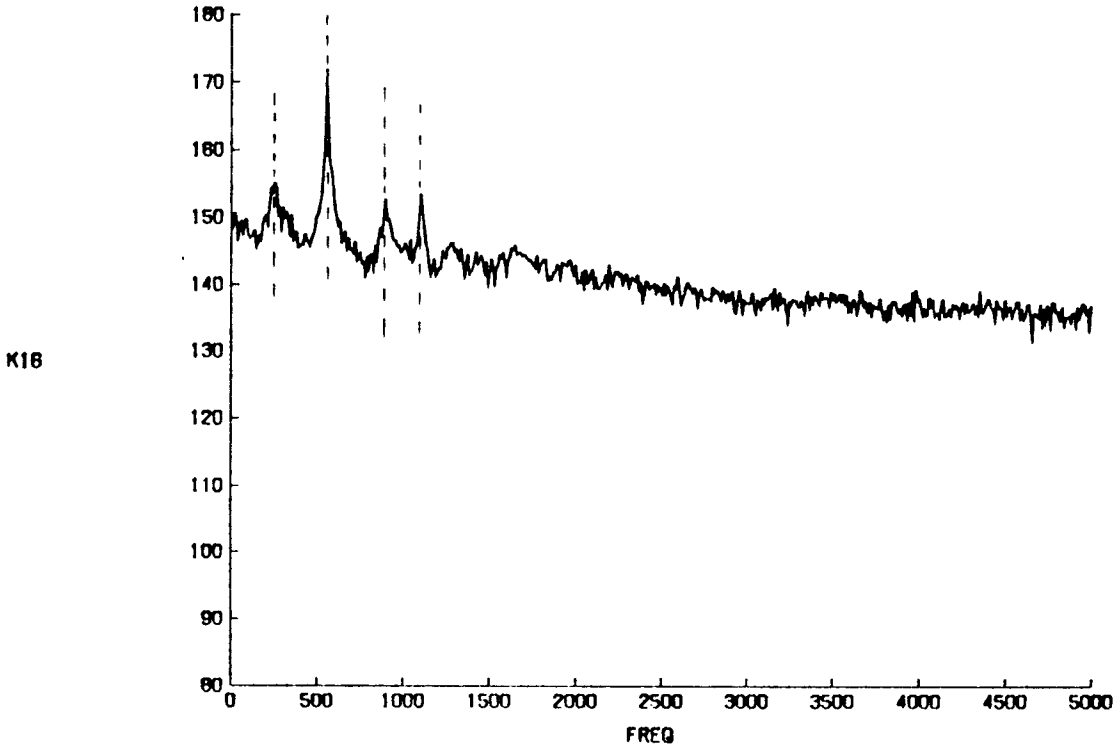
K16

	MACH	UNIT RE, 1/FT.	V-INF	Q-INF	PT	TT
☐	1.30	2.55E+6	1289.4	512.2	1200.7	551.7

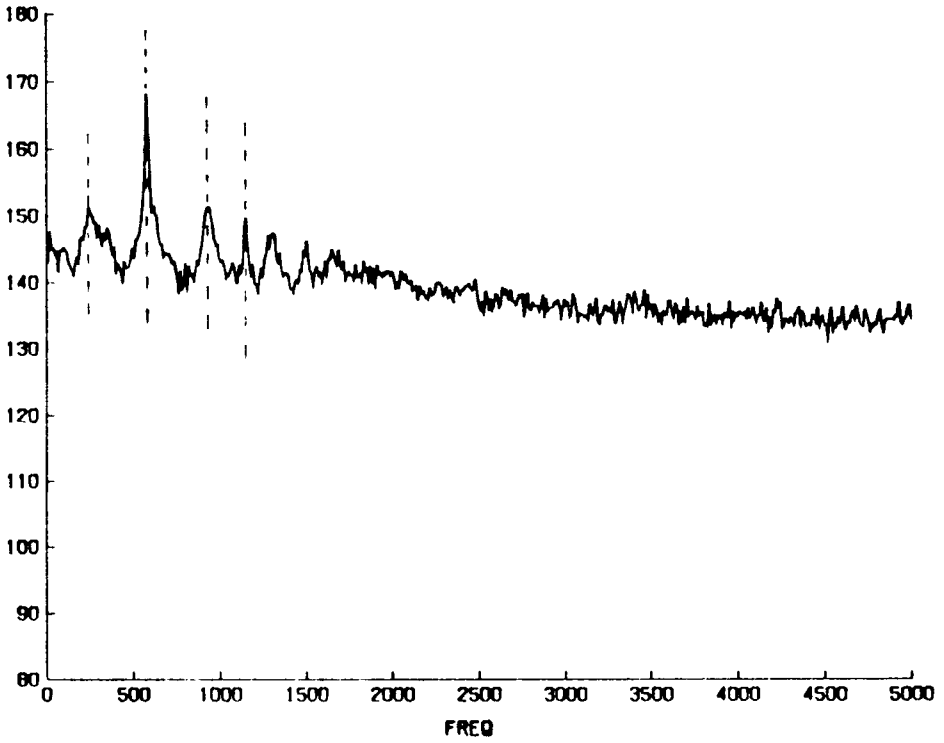


K16

	MACH	UNIT RE, 1/FT.	V-INF	Q-INF	PT	TT
☐	1.40	2.54E+6	1369.4	524.3	1216.0	553.7

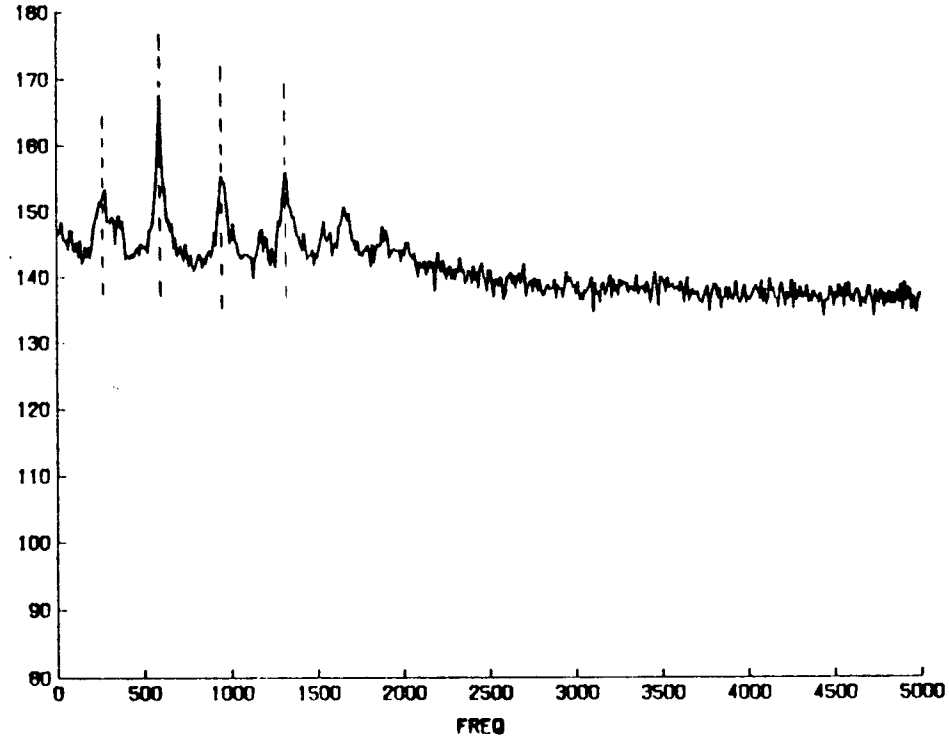


	MACH	UNIT RE. 1/FT.	V-INF	Q-INF	PT	TT
☐	1.50	2.01E+6	1441.3	423.8	987.8	556.7

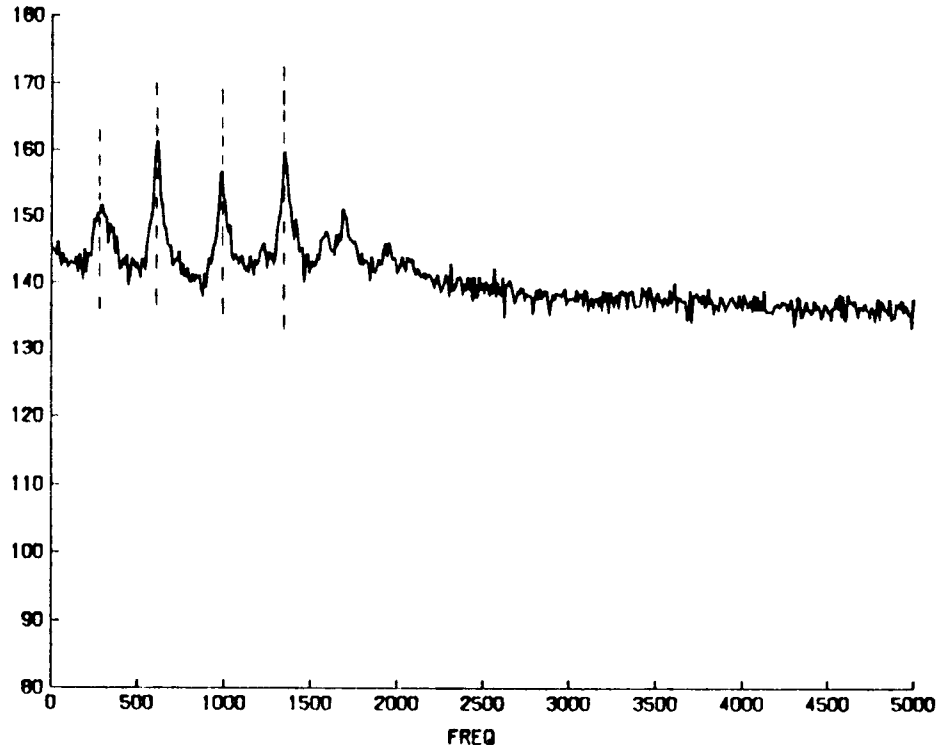


K16

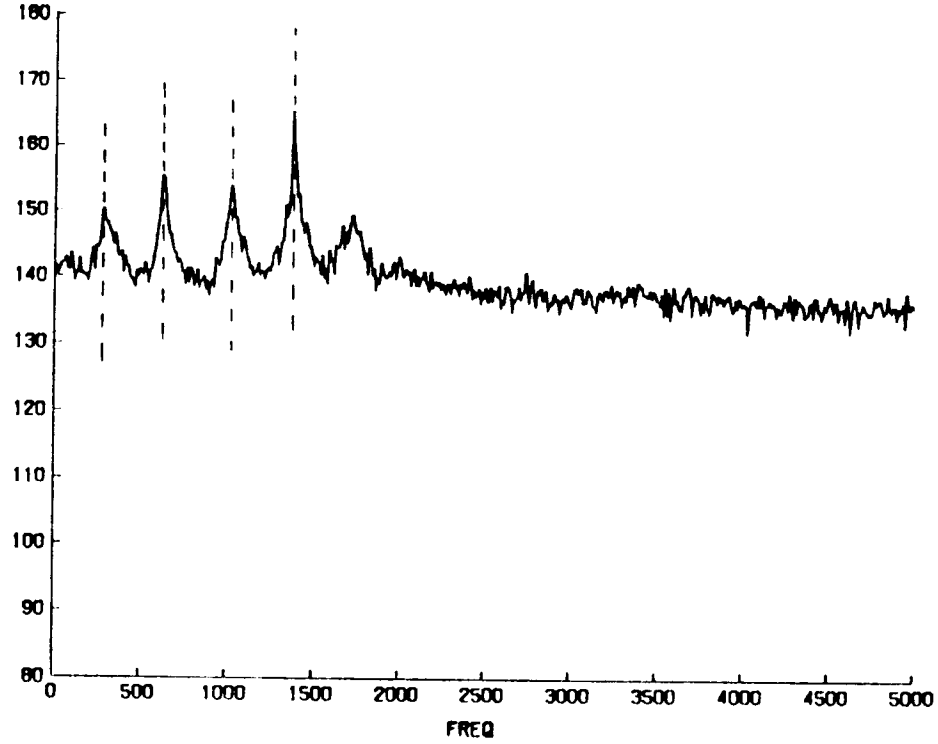
	MACH	UNIT RE, 1/FT.	V-INF	Q-INF	PT	TT
□	1.60	2.42E+6	1550.9	511.63	1213.6	553.7



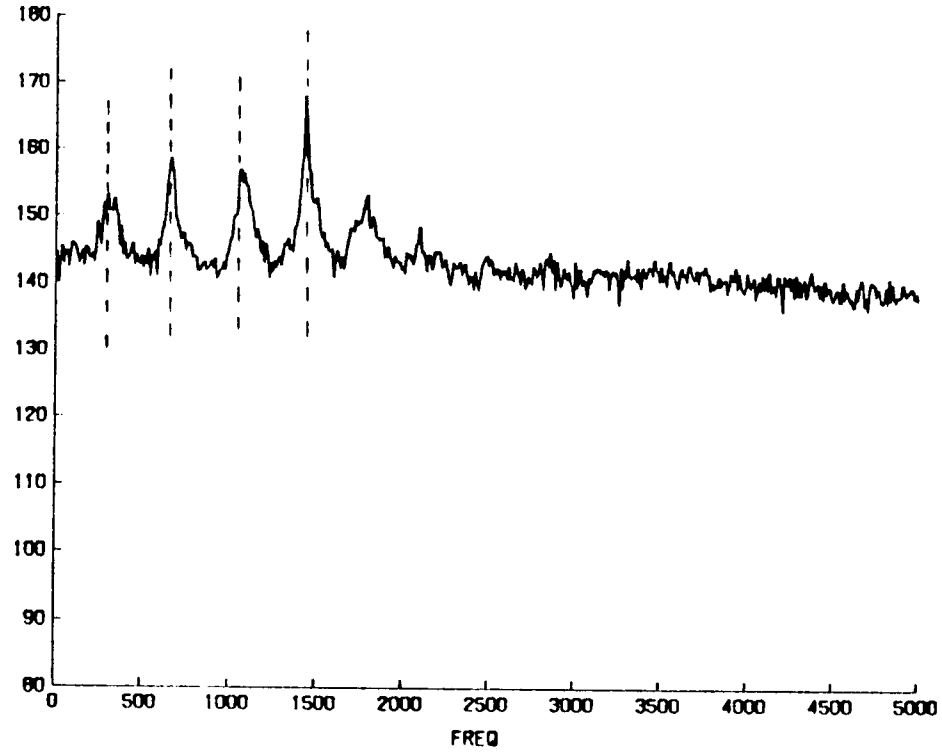
	MACH	UNIT RE, 1/FT.	V-INF	Q-INF	PT	TT
☐	1.75	2.31E+6	1588.9	487.5	1211.3	552.7



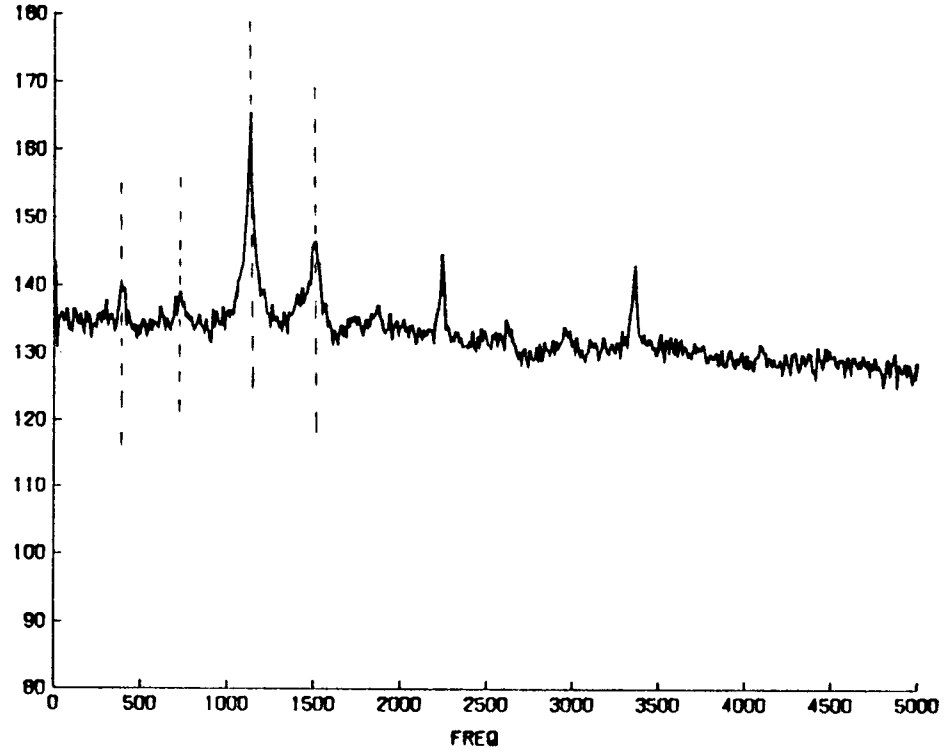
	MACH	UNIT RE, 1/FT.	V-INF	Q-INF	PT	TT
☐	1.90	2.18E+6	1667.4	456.5	1210.9	551.7



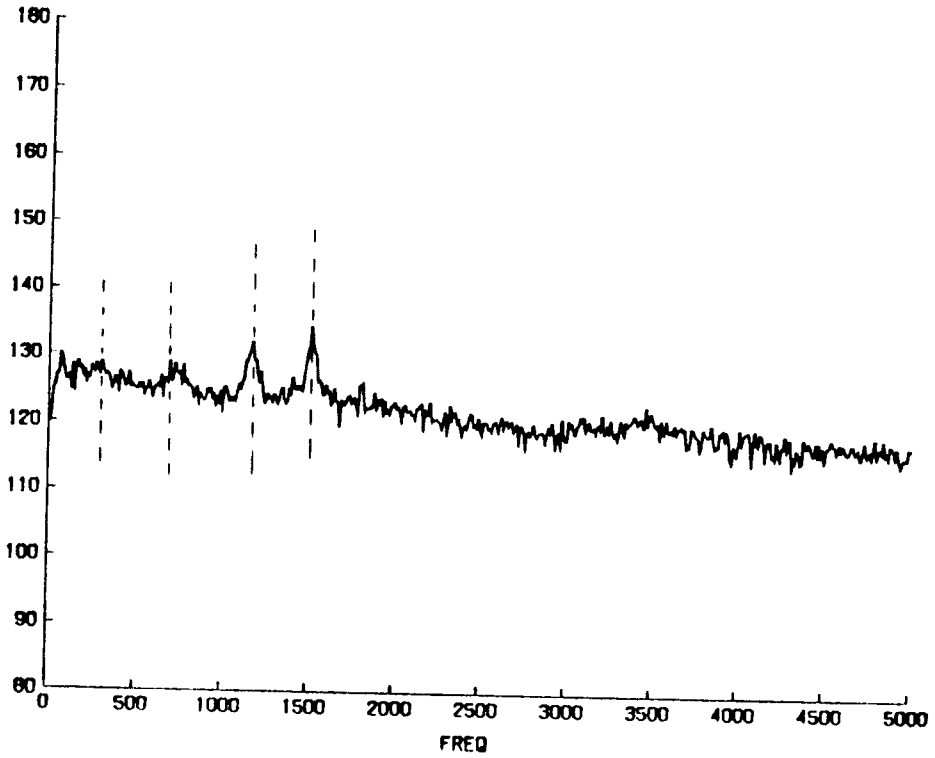
	MACH	UNIT RE. 1/FT.	V-INF	Q-INF	PT	TT
☐	2.00	3.01E+6	1762.4	670.7	1874.2	581.7



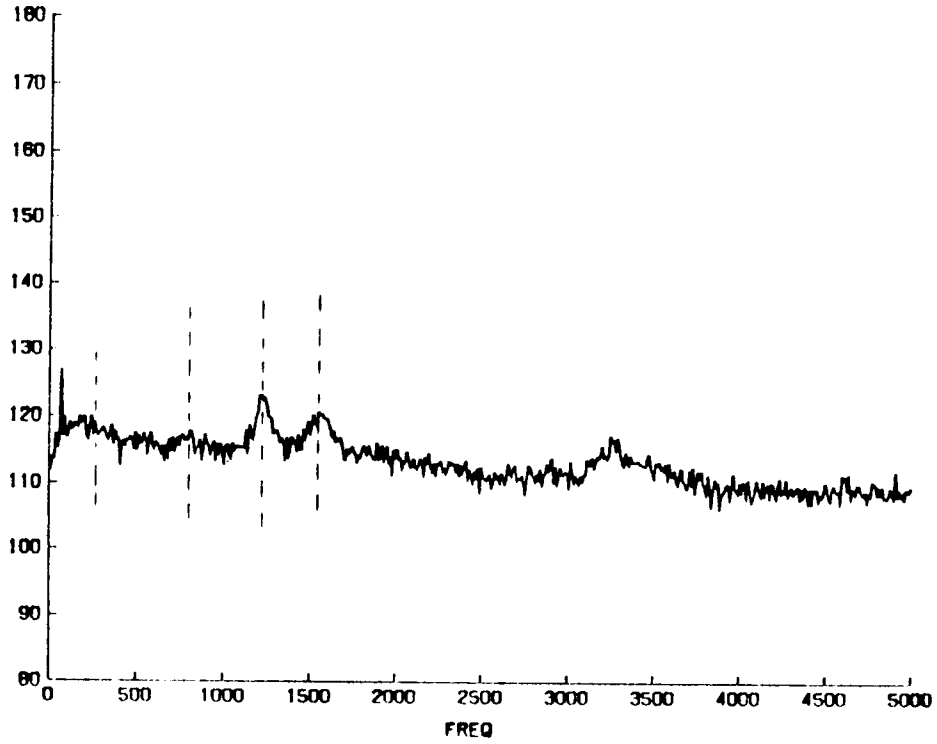
	MACH	UNIT RE, 1/FT.	V-INF	Q-INF	PT	TT
◻	2.75	2.90E+6	2049.4	551.2	2617.7	580.7



	MACH	UNIT RE, 1/FT.	V-INF	Q-INF	PT	TT
◻	3.51	2.97E+6	2227.7	446.3	4003.8	580.7

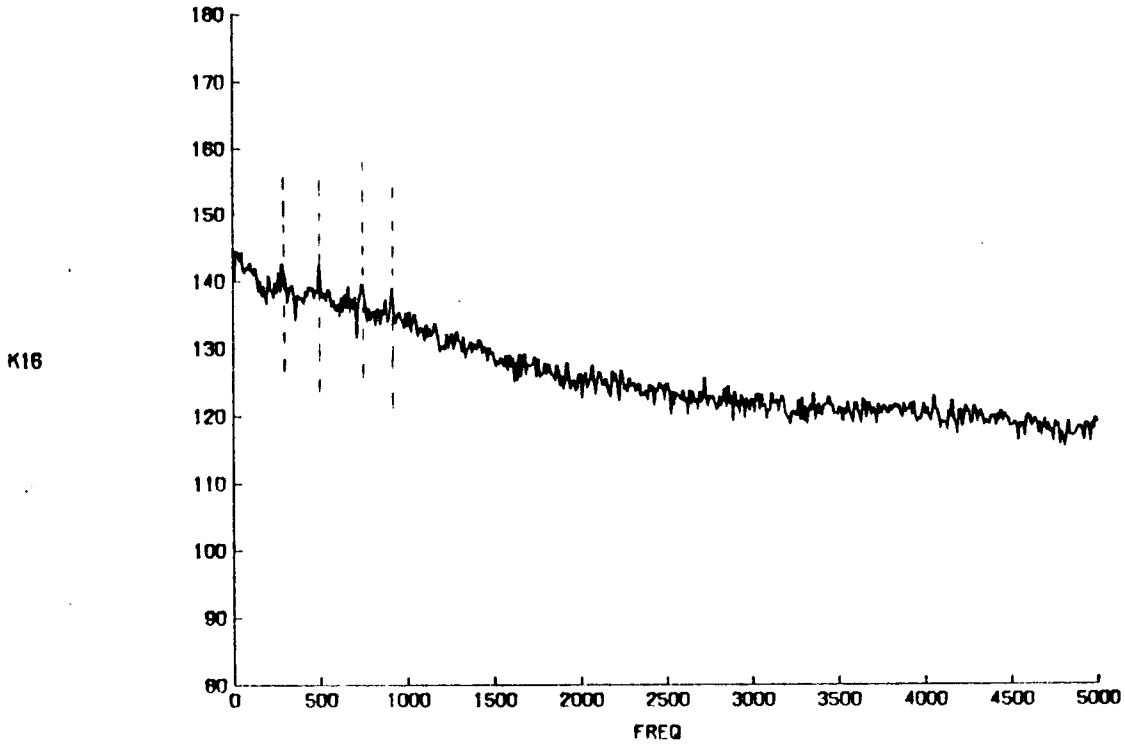


	MACH	UNIT RE. 1/FT.	V-INF	Q-INF	PT	TT
☐	5.04	3.00E+6	2455.6	292.5	9118.7	600.7

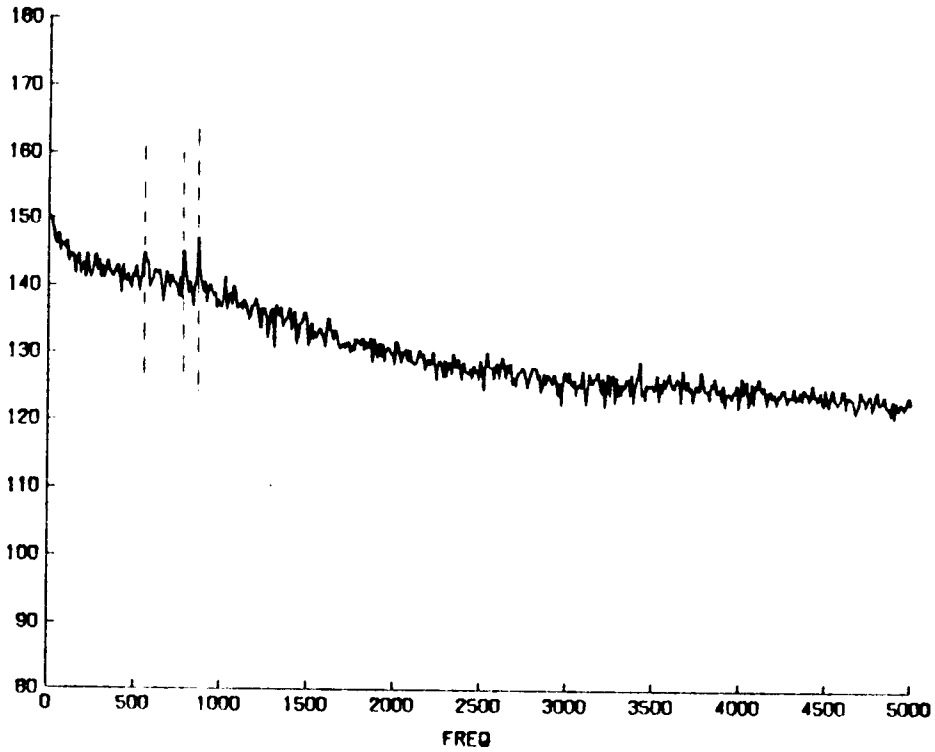


APPENDIX B. CAVITY RESPONSE PLOTS FOR A LENGTH-TO-DEPTH RATIO OF 9.0

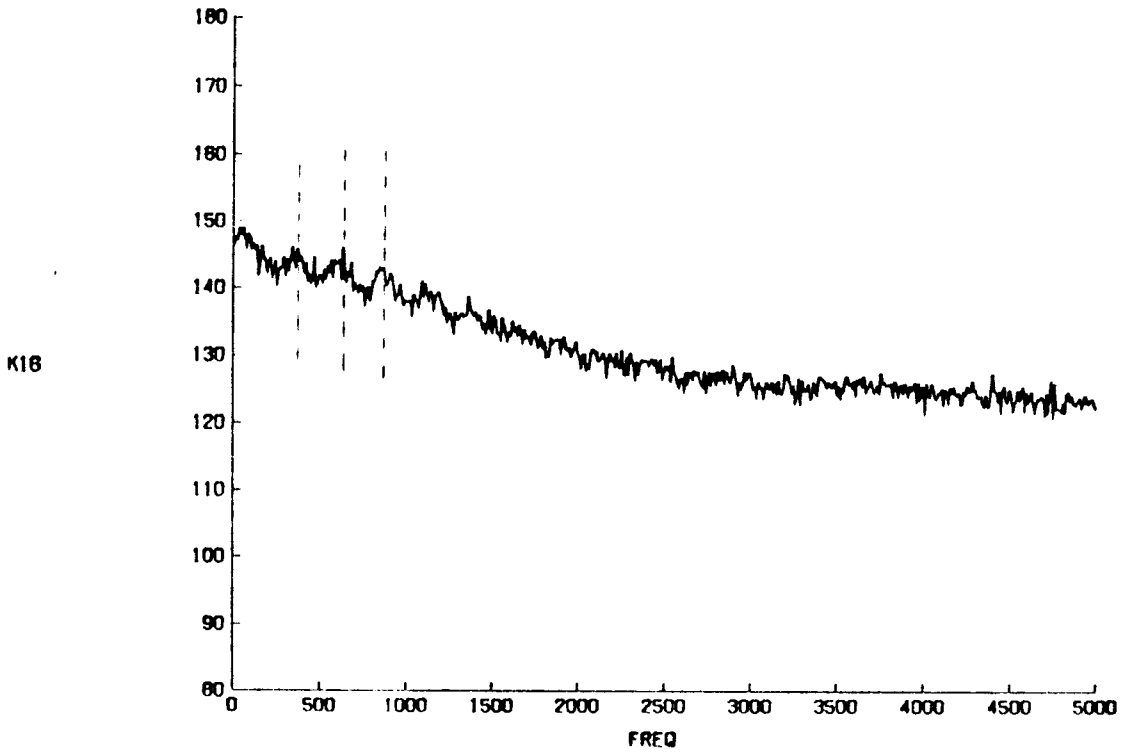
	MACH	UNIT RE. 1/FT.	V-INF	Q-INF	PT	TT
◻	0.60	1.97E+6	668.2	245.6	1243.6	553.7



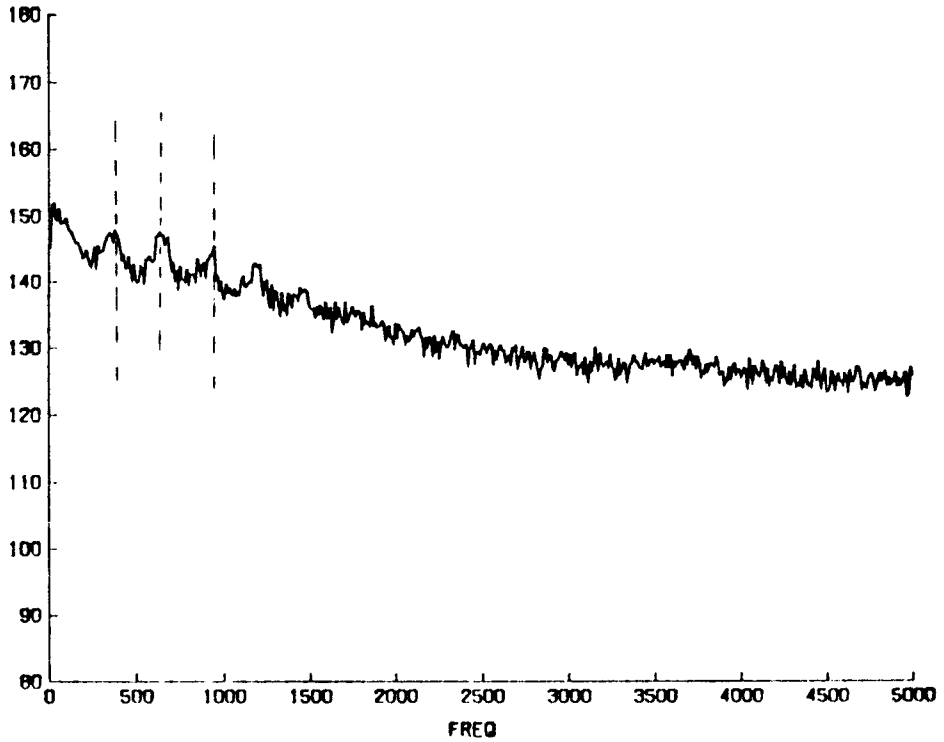
	MACH	UNIT RE. 1/FT.	V-INF	Q-INF	PT	TT
⊡	0.75	2.23E+6	823.8	329.9	1201.3	548.7



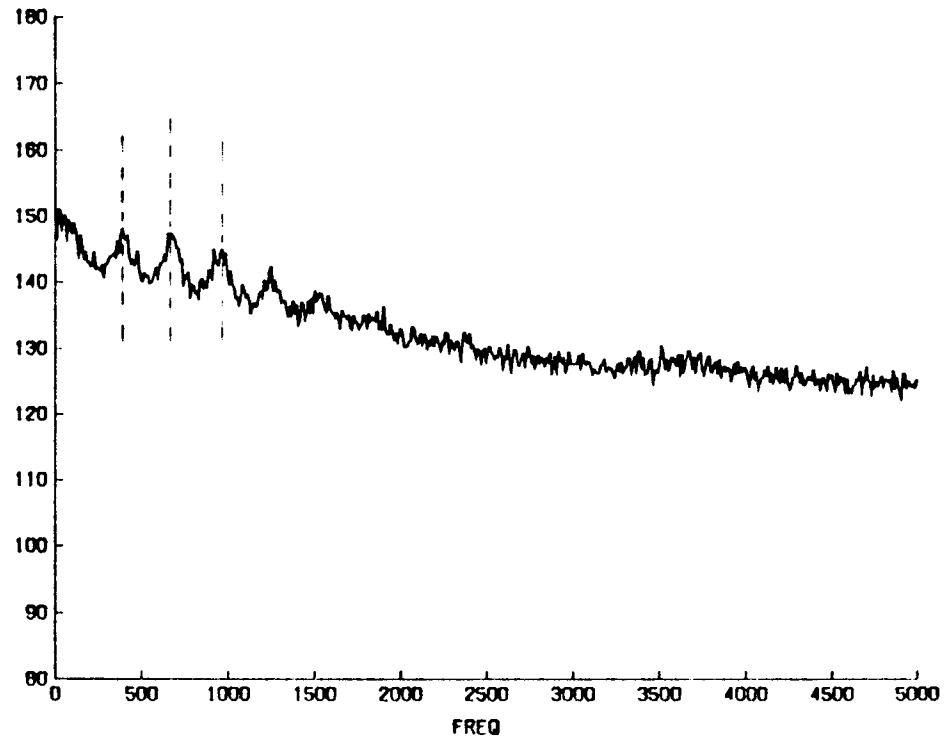
	MACH	UNIT RE. 1/FT.	V-INF	Q-INF	PT	TT
□	0.85	2.34E+6	911.8	375.0	1188.7	547.7



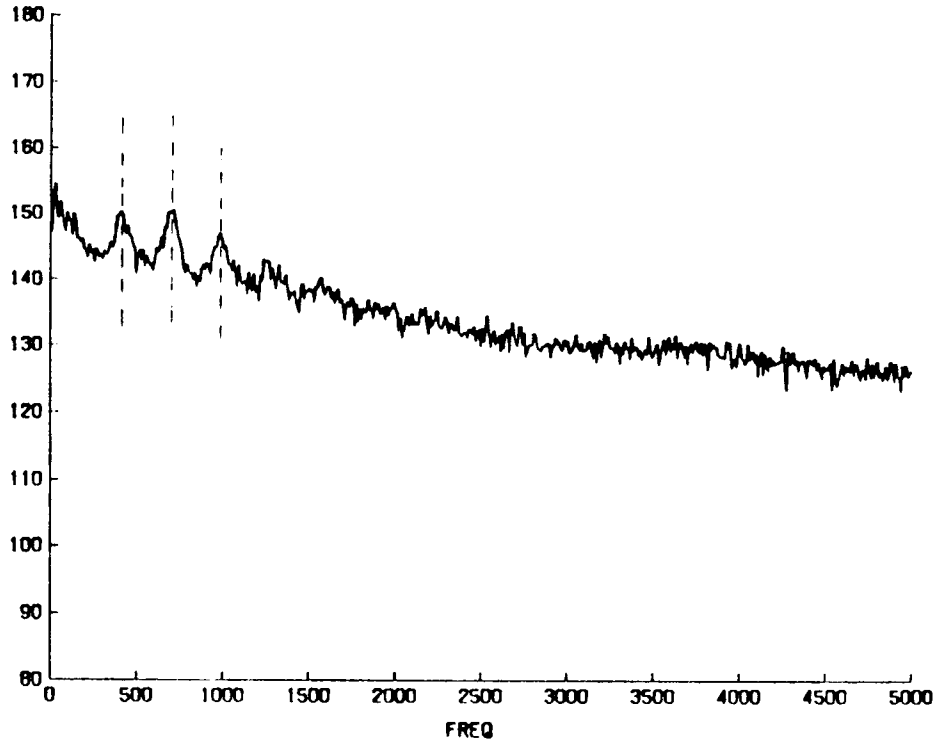
	MACH	UNIT RE. 1/FT.	V-INF	Q-INF	PT	TT
☐	0.90	2.41E+6	958.0	400.7	1196.3	548.7



	MACH	UNIT RE. 1/FT.	V-INF	Q-INF	PT	TT
◻	0.95	2.03E+6	1005.8	350.7	992.3	550.7



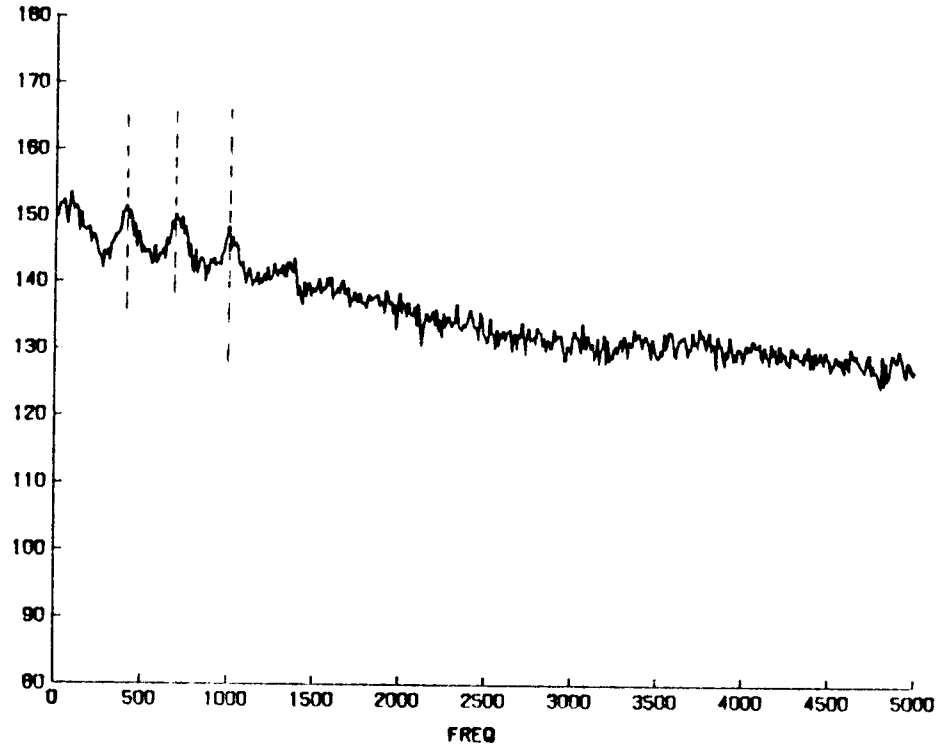
	MACH	UNIT RE, 1/FT.	V-INF	Q-INF	PT	TT
□	1.00	2.47E+6	1055.2	440.5	1184.5	549.7



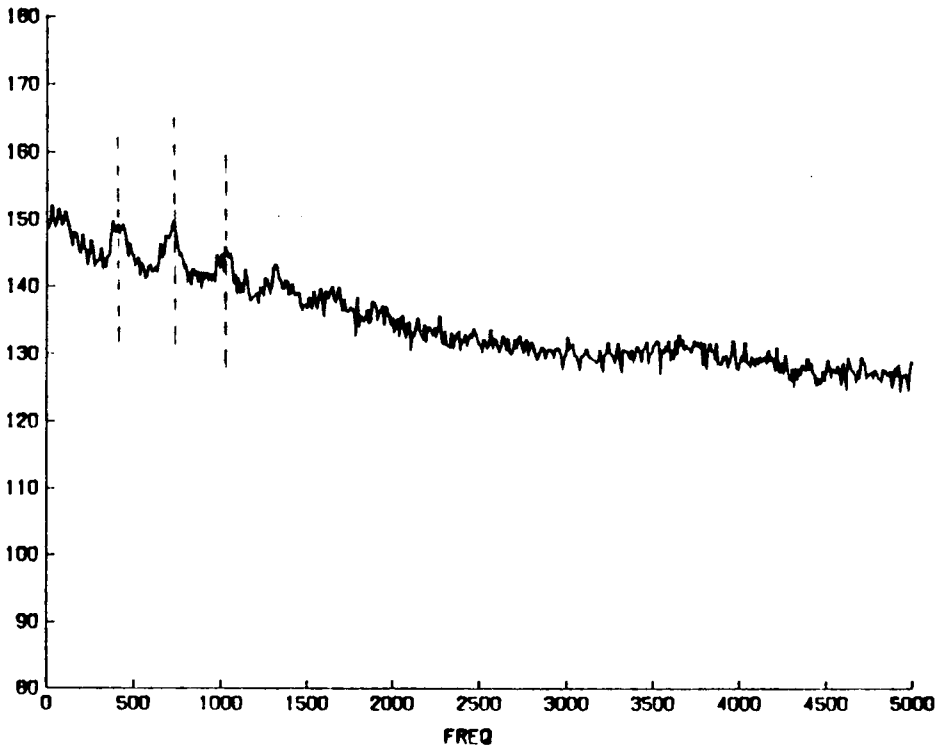
K18

	MACH	UNIT RE. 1/FT.	V-INF	Q-INF	PT	TT
☐	1.05	3.01E+6	1100.3	558.3	1451.7	556.7

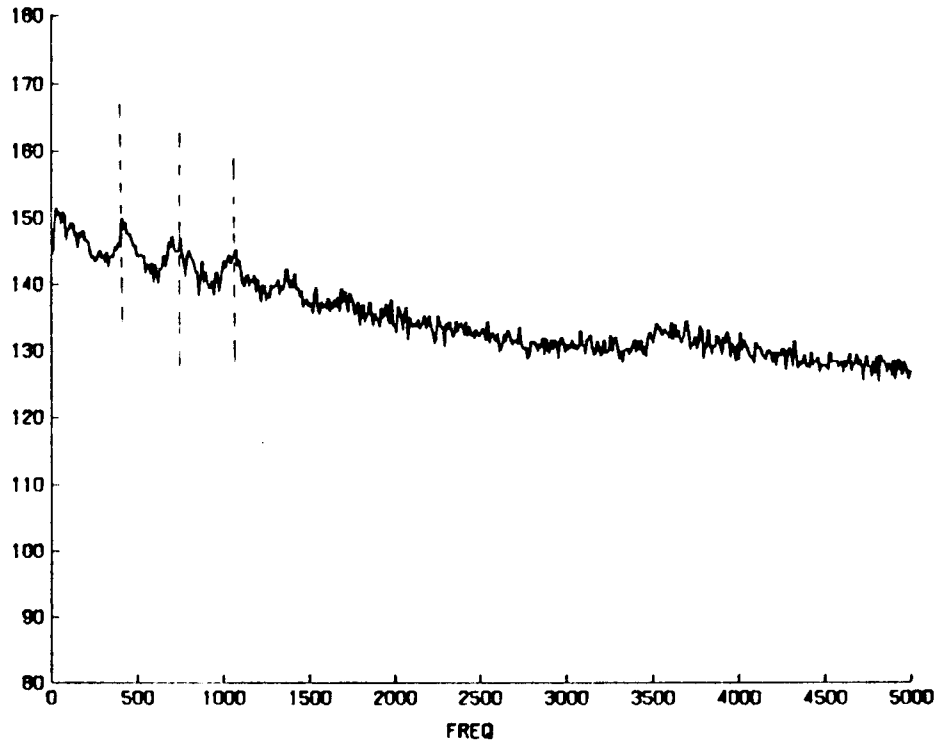
K16



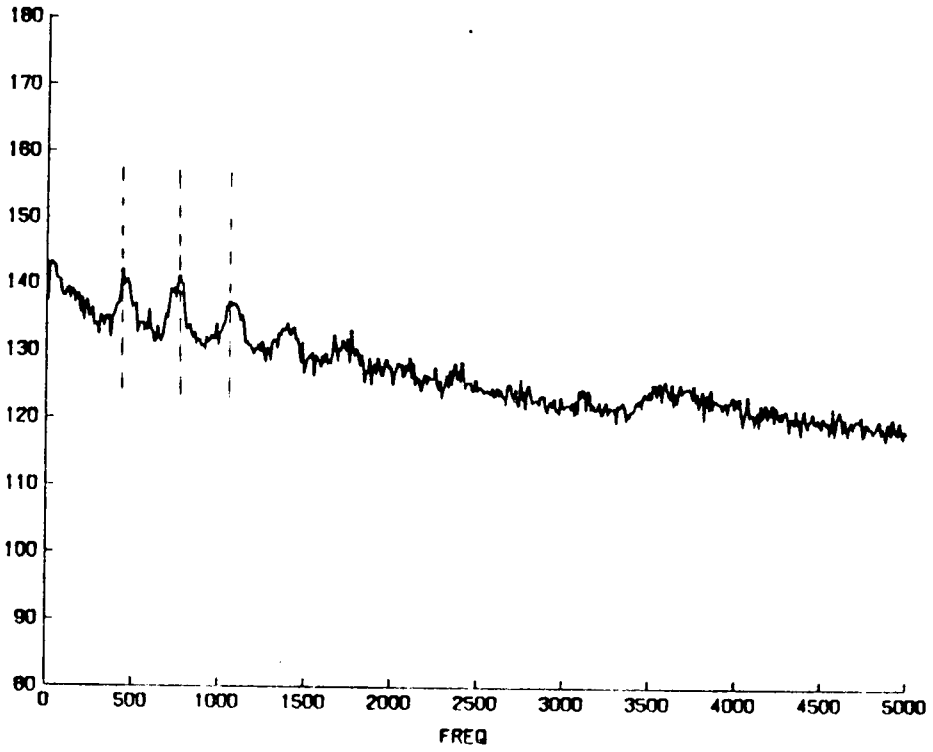
	MACH	UNIT RE, 1/FT.	V-INF	Q-INF	PT	TT
□	1.10	2.54E+6	1135.9	476.9	1201.7	550.7



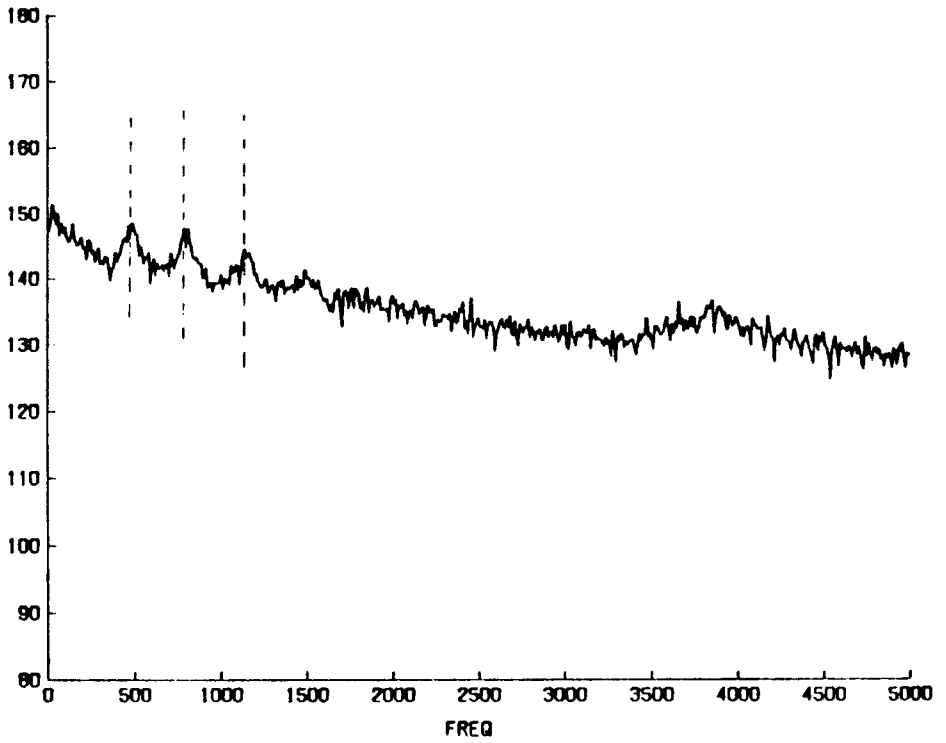
	MACH	UNIT RE. 1/FT.	V-INF	Q-INF	PT	TT
◻	1.15	2.53E+6	1181.1	489.4	1201.7	554.7



	MACH	UNIT RE. 1/FT.	V-INF	Q-INF	PT	TT
□	1.20	0.981E+6	1213.2	189.8	456.5	547.7



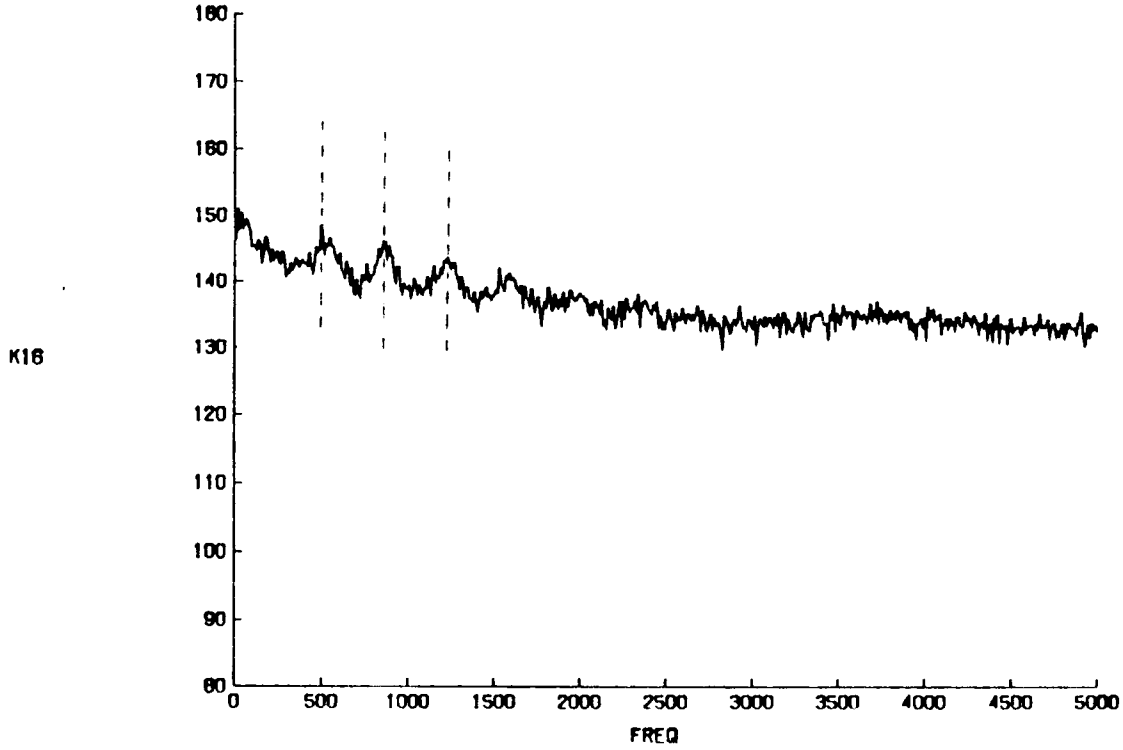
	MACH	UNIT RE, 1/FT.	V-INF	Q-INF	PT	TT
☐	1.30	2.52E+6	1300.8	511.3	1196.2	553.7



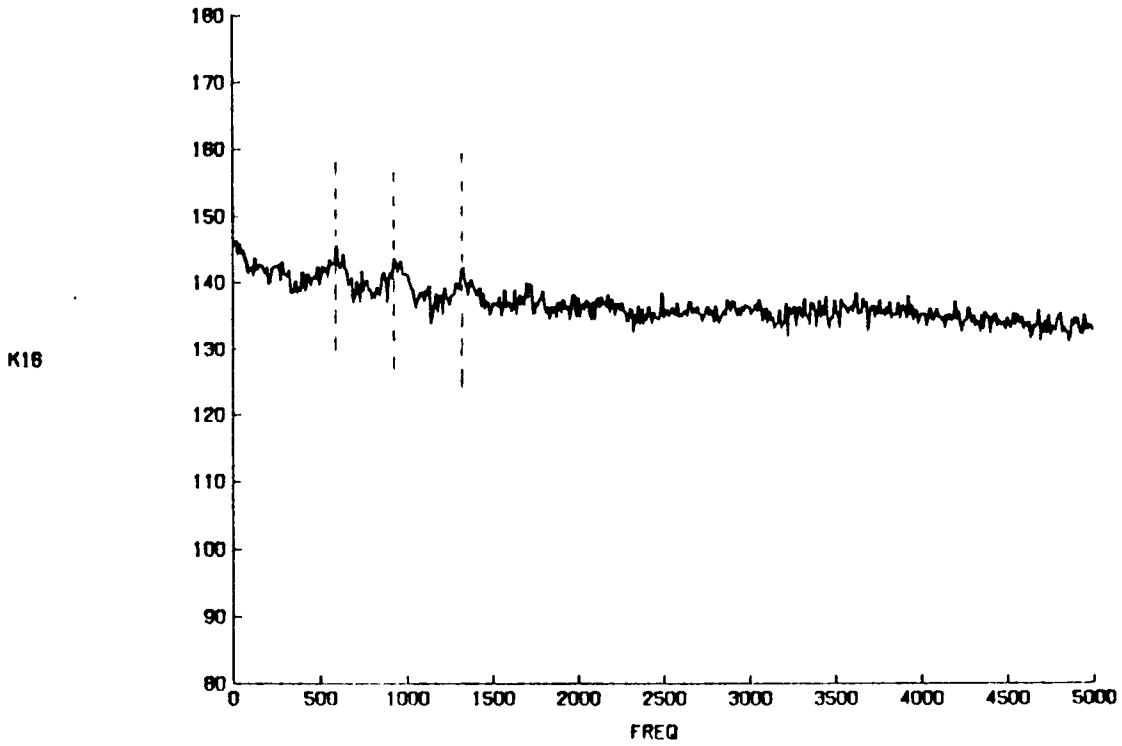
K16

06

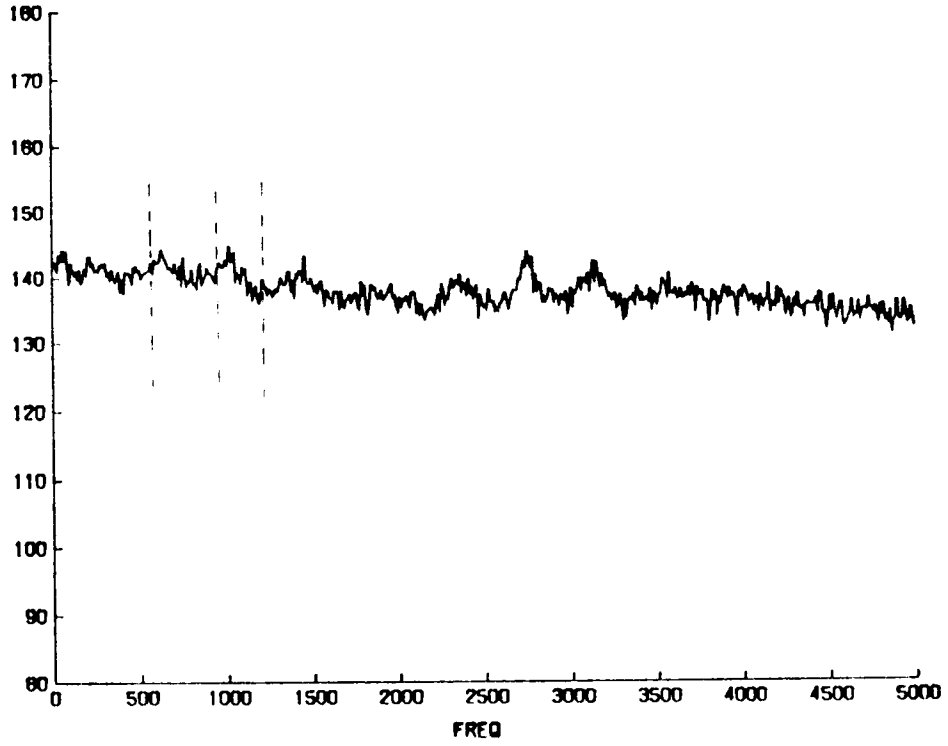
MACH	UNIT RE. 1/FT.	V-INF	Q-INF	PT	TT
⊡ 1.50	2.44E+6	1442.0	515.4	1201.3	557.7



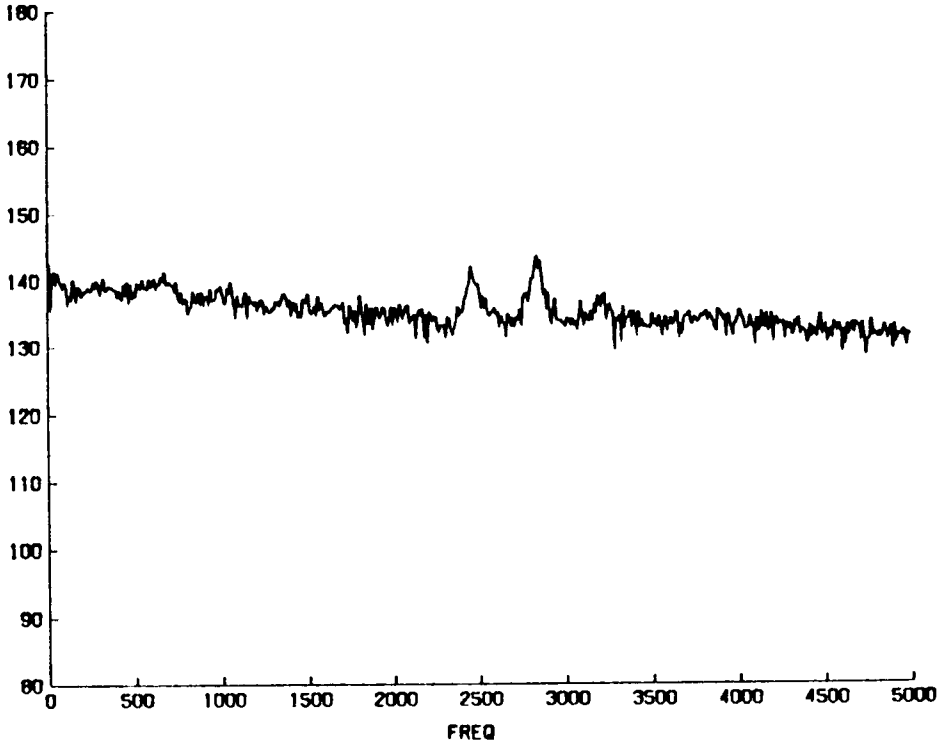
MACH	UNIT RE, 1/FT.	V-INF	Q-INF	PT	TT
⊡ 1.75	2.26E+6	1593.4	483.0	1199.1	556.7



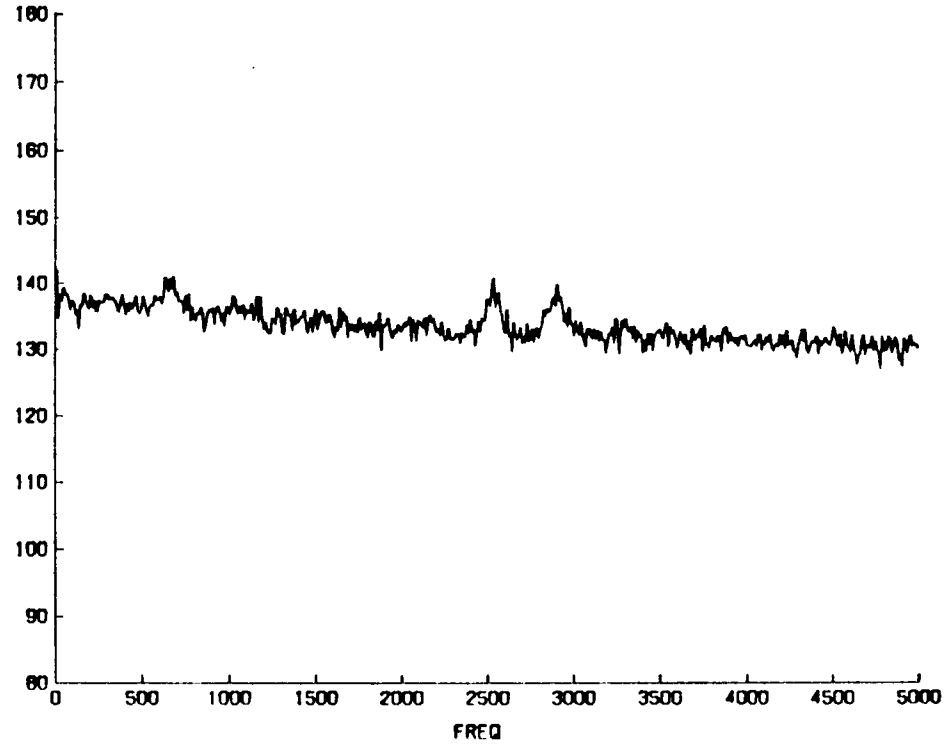
	MACH	UNIT RE, 1/FT.	V-INF	Q-INF	PT	TT
□	2.00	3.06E+6	1757.9	677.0	1891.8	578.7



	MACH	UNIT RE, 1/FT.	V-INF	Q-INF	PT	TT
□	2.25	3.02E+6	1873.6	646.7	2110.8	580.7

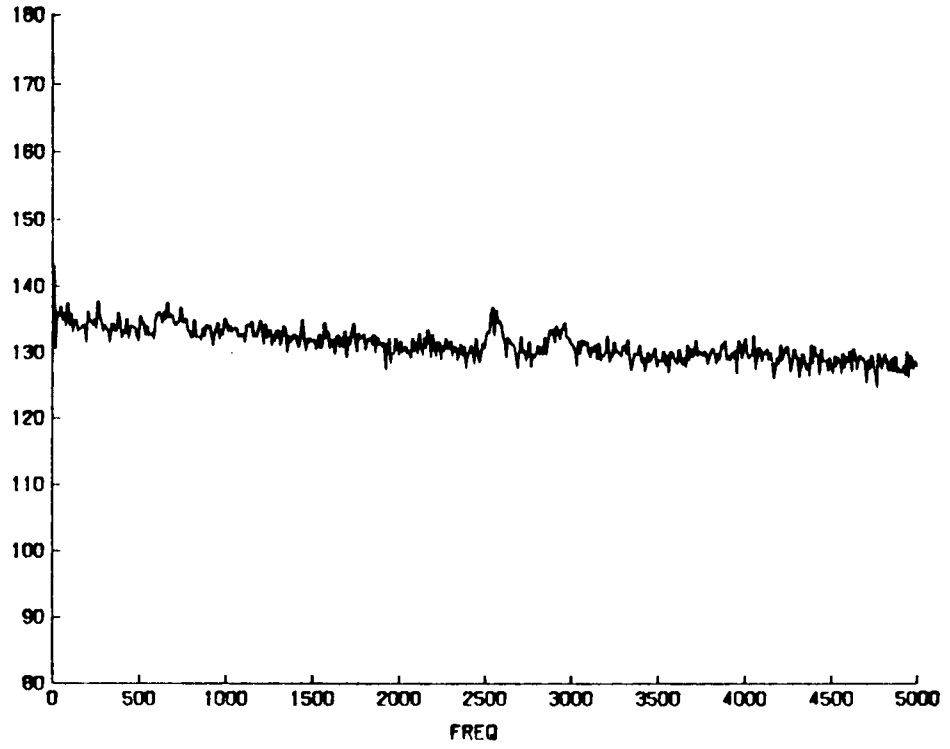


	MACH	UNIT RE, 1/FT.	V-INF	Q-INF	PT	TT
☐	2.50	3.00E+6	1968.8	608.4	2375.8	580.7



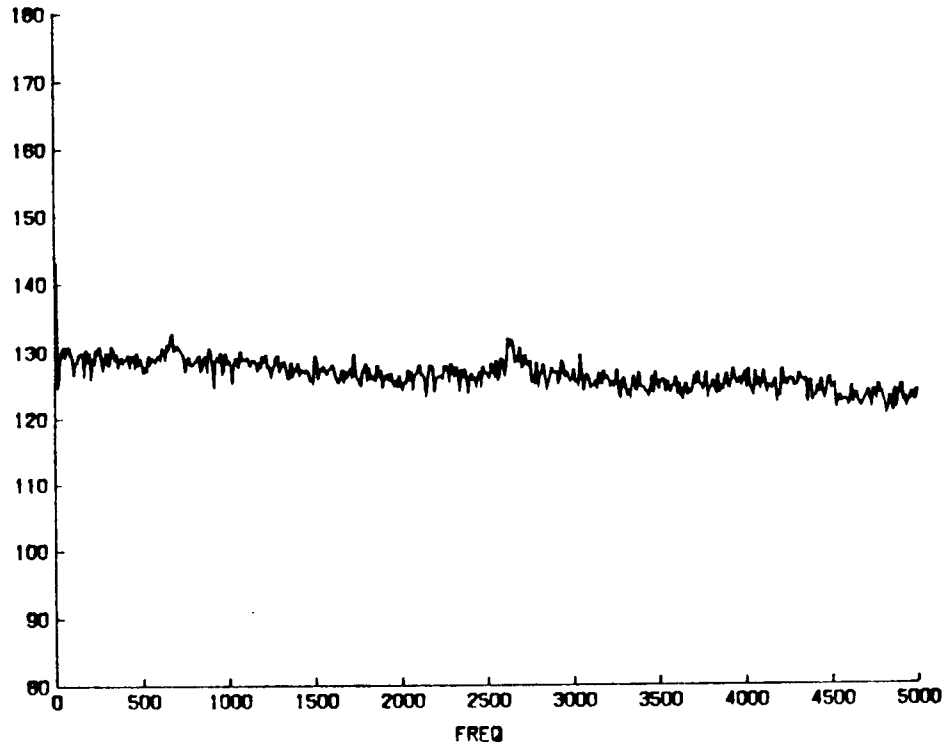
K18

	MACH	UNIT RE, 1/FT.	V-INF	Q-INF	PT	TT
☐	2.75	2.90E+6	2047.7	550.4	2613.8	579.7

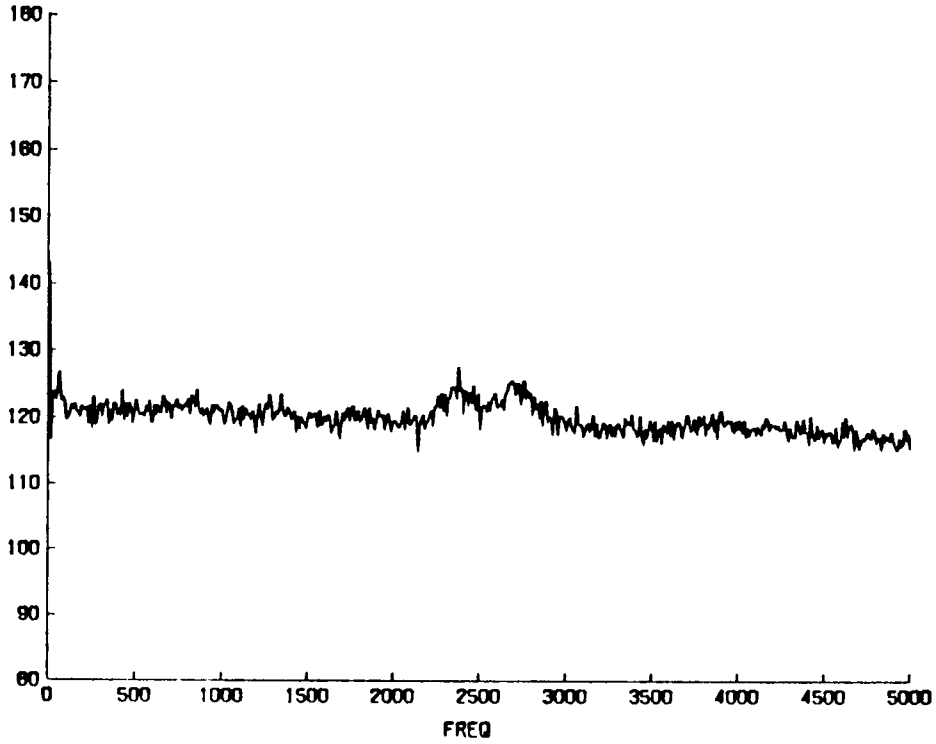


K16

	MACH	UNIT RE. 1/FT.	V-INF	Q-INF	PT	TT
☐	3.50	2.97E+6	2229.7	447.7	4015.8	581.7



	MACH	UNIT RE. 1/FT.	V-INF	Q-INF	PT	TT
☐	5.04	2.99E+6	2461.8	293.7	9156.4	603.7



VITA

Thomas Wyatt Dobson, Jr. was born in Jacksonville, Florida on December 15, 1958. He attended Beauclerc Elementary School in that city and graduated from Samuel W. Wolfson Senior High School in 1977. He attended David Lipscomb College in Nashville, Tennessee, and graduated in June 1981 with a Bachelor of Science in Biology. He then attended the Georgia Institute of Technology in Atlanta, Georgia, and graduated in September 1985 with a Bachelor of Mechanical Engineering. In September 1985, he started work with Calspan Corporation, a subcontractor at Arnold Engineering Development Center, as a Project Engineer. On October 10, 1989, he went to work as a Technology Applications Engineer for Calspan Corporation. He started attending graduate classes in January 1986 at The University of Tennessee Space Institute. He received the Master of Science degree with a major in Mechanical Engineering in December 1990. He is married to the former Leigh Ann Bumpas of Murfreesboro, Tennessee and they have one child, Joshua Thomas Dobson, born in Murfreesboro, Tennessee on November 19, 1987.